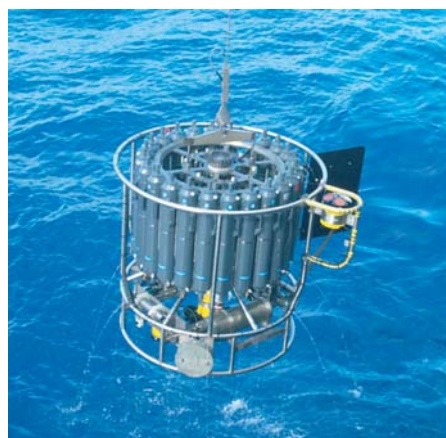




Early Holocene Eastern Mediterranean ocean climate and the stability of its overturning circulation

Fanny Adloff



Hinweis

Die Berichte zur Erdsystemforschung werden vom Max-Planck-Institut für Meteorologie in Hamburg in unregelmäßiger Abfolge herausgegeben.

Sie enthalten wissenschaftliche und technische Beiträge, inklusive Dissertationen.

Die Beiträge geben nicht notwendigerweise die Auffassung des Instituts wieder.

Die "Berichte zur Erdsystemforschung" führen die vorherigen Reihen "Reports" und "Examensarbeiten" weiter.



Notice

The Reports on Earth System Science are published by the Max Planck Institute for Meteorology in Hamburg. They appear in irregular intervals.

They contain scientific and technical contributions, including Ph. D. theses.

The Reports do not necessarily reflect the opinion of the Institute.

The "Reports on Earth System Science" continue the former "Reports" and "Examensarbeiten" of the Max Planck Institute.

Anschrift / Address

Max-Planck-Institut für Meteorologie
Bundesstrasse 53
20146 Hamburg
Deutschland

Tel.: +49-(0)40-4 11 73-0
Fax: +49-(0)40-4 11 73-298
Web: www.mpimet.mpg.de

Layout:

Bettina Diallo, PR & Grafik

Titelfotos:

vorne:

Christian Klepp - Jochem Marotzke - Christian Klepp

hinten:

Clotilde Dubois - Christian Klepp - Katsumasa Tanaka

Early Holocene Eastern Mediterranean
ocean climate and the stability
of its overturning circulation

Fanny Adloff

aus Aix-en-Provence, France

Hamburg 2011

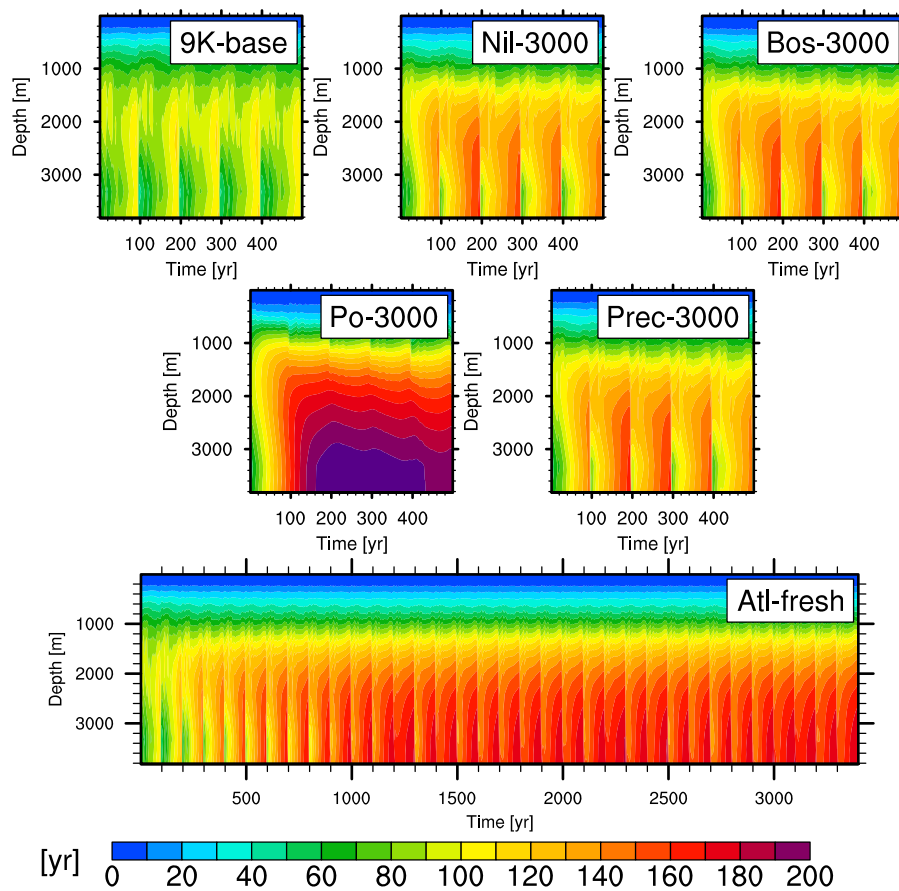
Fanny Adloff
Max-Planck-Institut für Meteorologie
Bundesstrasse 53
20146 Hamburg
Germany

Als Dissertation angenommen
vom Department Geowissenschaften der Universität Hamburg

auf Grund der Gutachten von
Prof. Dr. Gerhard Schmiedl
und
Dr. Uwe Mikolajewicz

Hamburg, den 6. Dezember 2011
Prof. Dr. Jürgen Oßenbrügge
Leiter des Departments für Geowissenschaften

Early Holocene Eastern Mediterranean ocean climate and the stability of its overturning circulation



Fanny Adloff

Hamburg 2011

Cover picture

The cover figure represents time series of the apparent age of the water averaged over the Eastern Mediterranean for different depths. 9K-base refers to the well-ventilated baseline experiment for the Early Holocene, and can be compared with the following freshwater perturbation experiments: Nil-3000, Bos-3000, Po-3000, Prec-3000 and Atl-fresh. The freshwater perturbations respectively correspond to an additional freshwater input of $3000 \text{ m}^3 \text{ s}^{-1}$ through the Nile river (Nil-3000), through the Strait of the Bosphorus (Bos-3000), through the Po river (Po-3000), and homogeneously distributed as additional precipitation (Prec-3000). The perturbation experiment Atl-fresh prescribes a freshening of the Atlantic water with a gradual decrease of 0.014 psu per century. Please, note that the 100-year periodicity is related to the repetition of the 100-year daily atmospheric data used in a loop to force the regional ocean model.

Contents

Abstract	1
List of Abbreviations	3
1 Introduction	5
1.1 The Mediterranean - present and past changes	5
1.2 Motivation and research questions	7
1.3 Thesis outline	8
2 Upper ocean climate of the Eastern Mediterranean Sea during the Holocene Insolation Maximum	11
2.1 Abstract	11
2.2 Introduction	12
2.3 Model, forcing and experiments	15
2.3.1 The regional OGCM	15
2.3.2 Atmospheric forcing and boundary conditions	16
2.3.2.1 Global model setup	17
2.3.2.2 Fresh water fluxes and restoring	18
2.3.3 Spin-up and initial conditions	19
2.4 The general features of the Eastern Mediterranean Sea for the control climate	19
2.4.1 Near-surface circulation and deep water formation	20
2.4.2 Surface temperature and salinity	22
2.4.3 Water budget	25
2.5 The Holocene Insolation Maximum	26
2.5.1 Stronger seasonal cycle	26
2.5.2 Salinity, stratification and deep water formation	28
2.5.3 The upper-ocean temperature	33
2.5.3.1 Seasonal cycle	33
2.5.3.2 The western Levantine subsurface warming pattern	33
2.5.4 Comparison to proxy data	42

2.5.4.1	The SST reconstructions	42
2.5.4.2	SST model-proxy comparison	43
2.5.4.3	A depth-integrated approach for model-proxy comparison of upper-ocean temperature . . .	47
2.6	Conclusion	52
3	Stability of the Eastern Mediterranean overturning cir- culation under freshwater perturbations during the Early Holocene	55
3.1	Introduction	55
3.2	Experimental design	57
3.3	State of the art of previous modelling studies	60
3.4	Sensitivity to enhanced Nile runoff	61
3.4.1	Circulation and hydrography changes	63
3.4.1.1	Changes at the surface	63
3.4.1.2	Changes at depth	66
3.4.2	Vertical stratification	71
3.4.3	Mixed layer depth and sources of dense water	74
3.4.4	Zonal and meridional overturning circulation	77
3.4.5	Water aging	81
3.4.6	Strait dynamics	84
3.4.7	Impact of extreme winters	86
3.5	Sensitivity to the magnitude of the perturbation	87
3.6	Sensitivity to the origin of the perturbation	91
3.6.1	Surface stratification	92
3.6.2	Vertical stratification	92
3.6.3	Mixed layer depth and sources of dense water	98
3.6.4	Water masses at intermediate depths	101
3.6.5	Water aging	101
3.7	Transient perturbation: a prerequisite to maintain the stag- nation	104
3.8	Synthesis and implications	106
3.9	Discussion	111
3.9.1	Limitations	111
3.9.2	Comparison to previous studies	113
3.9.2.1	Comparison to observations	113
3.9.2.2	Comparison to previous model studies	116
3.10	Summary and conclusion	118
3.11	Outlook	120
4	Summary and Conclusion	121

List of Figures	125
List of Tables	133
Bibliography	135
Acknowledgement	145

Abstract

The Mediterranean Sea is modelled at times of climate extremes in the Holocene in order to understand its sensitivity to high- and low-latitude climate forcings. The focus lies on the Holocene Insolation Maximum (HIM, 9000 years BP), which coincides with the beginning of the deposition of the sapropel S1, an organic rich marine sediment layer indicating low oxygen availability in the deep Eastern Mediterranean basin. One of the hypothesis for S1 formation is that both warming and freshening of the Mediterranean surface water induced a decrease in surface density and thus reduced/prevented the formation of dense deep water. A consequent abrupt change in the circulation occurred and led to a weakened ventilation of deeper water masses, promoting thus the preservation of the organic matter.

The main objective of this thesis is to investigate the sensitivity of both hydrography and circulation of the Eastern Mediterranean Sea to the HIM climate, to validate the simulated ocean climate with proxy data, and to assess plausible physical mechanisms responsible for deep Eastern Mediterranean Sea stagnation.

We set up a regional version of the ocean general circulation model MPIOM for the Mediterranean. The model is forced by atmospheric fluxes derived from global simulations. We first perform a HIM baseline simulation representing the pre-sapropel well-ventilated conditions. To assess the sensitivity of Eastern Mediterranean ventilation to increased freshwater input, we carry out a set of freshwater perturbation experiments, starting from the baseline simulation, and based on several assumptions discussed in the literature. We investigate the effect from sudden opening of the Strait of the Bosphorus, strong increase in Nile and Po runoff, freshening from the inflowing Atlantic water and increased precipitation, at various rates for each. From an age tracer incorporated in the model, we infer the strength and duration of the developing stagnation of Eastern Mediterranean deep water, consequent to each perturbation.

In the HIM baseline simulation, a stronger seasonal cycle is simulated with a homogeneous winter cooling and a summer warming with well-defined spatial patterns, in particular an enhanced subsurface warming in the Cretan/West Levantine region. The drivers of this warming are found to be a

combination of (i) enhanced downwelling (due to strong Ekman transport) and wind mixing, both caused by strengthened Etesian winds, and (ii) enhanced thermal forcing due to the stronger summer insolation. Together, these processes induce a stronger heat transfer from the surface to the subsurface during late summer in the western Levantine and are responsible for the anomalous heat accumulation simulated in this region. To validate the HIM baseline simulation, we use SST reconstructions from planktonic foraminifer and develop a depth-integrated approach to account for variable habitat depth of the species. This new approach, which vertically integrates the temperature signal over a wider depth range including the subsurface, leads to a better agreement between reconstructions and model results, which both display the main spatial patterns.

The sensitivity experiments show that all the freshwater perturbations lead to a reduction of the ventilation in the eastern basin, with an active vertical circulation restricted to the upper ~ 800 m of the water column and stagnant deep water in the open Eastern Mediterranean. However, none of the freshwater perturbations is sufficient to trigger a stagnation lasting long enough to produce sapropels (3000 years), nor to induce a surface salinity decrease as strong as suggested by paleoreconstructions. The increase of the Po runoff creates the strongest stagnation of Eastern Mediterranean deep waters, highly affecting the main production of dense water. In order to maintain stagnating deep water over thousands of years, our results indicate that a permanent source for the decrease in surface density is required in addition to the initial perturbation; e.g. a gradual freshening of incoming Atlantic water, as could result from ice sheet melt. In all the experiments prescribing a fixed perturbation, the vertical mixing/diffusion gradually reduces density differences between ventilated intermediate water and stagnant deep water, and the ventilation recovers after several centuries of stagnation. This raises the important role of the vertical mixing parameterization in the ocean model, which directly affects the time of recovery of the deep ventilation.

Our study suggests that the physical mechanisms often proposed in the literature are not sufficient to explain the sapropel S1 formation. Several of them need to be combined to achieve the surface density decrease recorded by the geological records and constrain the vertical circulation to the suggested upper 300 m.

List of Abbreviations

pCO ₂	partial pressure of carbon dioxide
ABW	Aegean Bottom Water
CTRL	control simulation
E	evaporation
ECHAM5	atmospheric general circulation model developed at the Max Planck Institute for Meteorology
ECMWF	European Centre for Medium-Range Weather Forecasts
EMDW	Eastern Mediterranean Deep Water
ERA-Interim	ECMWF reanalysis data set
ESM	Earth system model
HIM	Holocene Insolation Maximum
HOAPS	Hamburg Ocean Atmosphere Parameters and Fluxes from Satellite Data
IS	index of stratification
JAS	summer season
JFM	winter season
LGM	Last Glacial Maximum
LIW	Levantine Intermediate Water
LPJ	Lund-Potsdam-Jena dynamic global vegetation model
MOF	meridional overturning stream function
MPIOM	Max Planck Institute Ocean Model
MTHC	Mediterranean thermohaline circulation
OGCM	Ocean General Circulation Model
P	precipitation
P-E	precipitation minus evaporation
R	rivers
S	sea surface salinity
SST	sea surface temperature
WOA	World Ocean Atlas
ZOF	zonal overturning stream function

Chapter 1

Introduction

1.1 The Mediterranean - present and past changes

Enclosed between southern Europe, North Africa and Minor Asia, the Mediterranean Sea extends from the west to the east between $6^{\circ}W$ to $36^{\circ}E$, and from the north to the south between $46^{\circ}N$ and $30^{\circ}N$. Because of its warm and semi-arid climate, the Mediterranean is a concentration basin, where evaporation exceeds precipitation. This marginal sea has only a narrow connection with the Atlantic ocean via the shallow strait of Gibraltar. The basin is characterised by a buoyancy driven anti-estuarine circulation with low density Atlantic water flowing into the Mediterranean at the surface, and denser Mediterranean water flowing into the Atlantic ocean at depth.

Acting as a miniature ocean, the basin has its own thermohaline circulation, which is driven by deep water formation in some of the northern sub-basins. This unique configuration makes the Mediterranean basin an interesting region to study climatic changes, because its response is expected to be much quicker than in the world ocean.

Another deciding factor in favour of studying the Mediterranean climate is that this region has been referenced as one of the most responsive regions to climate change and defined as a primary “Hot-spot” by Giorgi (2006), based on the results from climate change projection scenarios. The context

of global warming stresses the necessity to assess the possible consequences of the ongoing climate change.

Whereas global and regional models are developed to simulate projections of the future climate, another way to improve our understanding of future climatic changes is to look at past climates. The investigation of past climatic changes provides some insight into how the climate responds to external forcings, and allows to understand better the evolution of the present climate. The Mediterranean is a suitable region for this purpose because it is particularly well-sampled for both present-day and the past, providing a deep understanding of the Mediterranean system, and its past changes.

The surface fluxes acting on the Mediterranean basin have considerably varied over long time scales, as inferred from paleoclimatic records (Myers, 2002). One climatic change in the Mediterranean Sea is particularly well-recorded by marine sediments, in form of black layers called sapropels. These layers have a high content in organic carbon ($> 2\%$) and reflect anoxic conditions of the deep waters in the eastern basin. The latest deposition of a sapropel layer is dated between approximately 9 ka BP and 6 ka BP (e.g. Mercone et al., 2000) and is called sapropel S1. Whereas the Mediterranean of today has low-productivity and is well-ventilated, the occurrence of sapropel layers indicates that strong changes of the Mediterranean behaviour arose.

Several hypotheses have been raised to explain the oxygen depletion. One of them argues that extra freshwater supply led to a surface density decrease, which strengthened the vertical stratification. According to this assumption, the formation of dense water was thus strongly weakened and the associated vertical circulation was restricted to the upper part of the water column. Below the ventilated intermediate water, the deep water was stagnating, inducing slowly the complete consumption of the deep oxygen, since no new oxygen was brought down through renewal of deep waters. The absence/depletion of deep oxygen promoted the preservation of organic matter in the sediment and built the sapropel layer.

In this thesis, we use a regional ocean general circulation model forced by atmospheric data derived from global simulations, to simulate and analyse the ocean climate of the Eastern Mediterranean Sea for the 9 ka BP time

period. Through perturbation experiments, we investigate the plausibility of various freshwater sources to have triggered the stagnation of Eastern Mediterranean deep water, and allow the formation of the sapropel S1.

1.2 Motivation and research questions

The investigation of warm climate periods is a particularly challenging test of our understanding of climate system processes (Huber et al., 2000). Here, we address the sensitivity of the Mediterranean Sea to high- and low-latitude climate forcings at times of climate extremes in the Holocene. Coinciding with the onset of the deposition of the sapropel S1, the Holocene Insolation Maximum or HIM (9 ka BP) represents a time period with warmer summers, which underwent important changes in thermohaline circulation. Despite an active scientific community working on the topic, the question about the mechanisms leading to the sapropel formation and the associated reduction of the vertical circulation remains unsolved.

The aim of this thesis is to test some of the mechanisms proposed in the literature for the origin of the sapropel S1 with a regional ocean model, and provide some insight into various mechanisms, which could have suppressed the ventilation of the Eastern Mediterranean deep water.

We address the following research questions:

- Is it possible to simulate states of the Mediterranean ocean climate adequately, using an atmospheric forcing derived from global simulations with a coarse resolution Earth system model?
- Can we simulate an Early Holocene ocean climate of the Eastern Mediterranean, which is consistent with the geological records?
- What causes the pronounced spatial temperature patterns recorded by reconstructions for the HIM?
- Which perturbations of fresh water fluxes are required in order to generate a stagnation of deep waters in the Eastern Mediterranean?

- What are the mechanisms governing the establishment of deep water stagnation?
- Can we simulate a stagnation of Eastern Mediterranean deep water, which lasts for several millennia?

1.3 Thesis outline

The Chapters 2 and 3 of this thesis are written in the style of journal publications. As a consequence, they contain their own introduction and conclusions, and can be read largely independently of one another. Chapter 2 is published in *Climate of the Past*¹, and is reproduced here with editorial adjustments. It deals with the analysis of the hydrographic changes of the Eastern Mediterranean simulated for the Holocene Insolation Maximum (9 ka BP), and the validation of model results with reconstructions. Chapter 3 is currently being prepared for submission, and deals with the investigation of some of the mechanisms, which could have triggered the deep water stagnation in the Eastern Mediterranean during the sapropel S1 period.

This thesis is structured as follows:

- In **Chapter 2**, we investigate the ocean climate of the Eastern Mediterranean Sea during the Holocene Insolation Maximum (HIM). After validating the regional ocean model for the present-day climate, we analyse the modelled changes in the upper-ocean during the HIM. The physical mechanisms responsible for strong regional contrasts of the simulated temperature signal are investigated. We validate our model results for the HIM using sea surface temperature reconstructions, and introduce a novel methodology to carry out the model/proxy comparison.

¹Adloff, F., Mikolajewicz, U., Kučera, M., Grimm, R., Maier-Reimer, E., Schmiedl, G., and Emeis, K.-C.: Upper ocean climate of the Eastern Mediterranean Sea during the Holocene Insolation Maximum – a model study, *Clim. Past*, 7, 1103-1122, doi:10.5194/cp-7-1103-2011, 2011.

- In **Chapter 3**, we discuss the possible sources which could have freshened the Mediterranean basin. We analyse, compare and quantify the mechanisms leading to a possible persistent strong stagnation of the deep water masses, as postulated for the sapropel S1 period. We isolate the effect of single well-identified freshwater perturbations, such as enhanced Nile and Po runoff, an opening of the Strait of the Bosphorus, increased precipitation and a gradual freshening of the Atlantic waters. We investigate how sensitive the deep ventilation is to (i) the magnitude, and (ii) the origin of the freshwater perturbation.

The thesis closes with a summary of our main findings in **Chapter 4**.

Chapter 2

Upper ocean climate of the Eastern Mediterranean Sea during the Holocene Insolation Maximum

2.1 Abstract

Nine thousand years ago (9 ka BP), the northern hemisphere experienced enhanced seasonality caused by an orbital configuration close to the minimum of the precession index. To assess the impact of this “Holocene Insolation Maximum” (HIM) on the Mediterranean Sea, we use a regional ocean general circulation model forced by atmospheric input derived from global simulations. A stronger seasonal cycle is simulated by the model, which shows a relatively homogeneous winter cooling and a summer warming with well-defined spatial patterns, in particular a subsurface warming in the Cretan and western Levantine areas.

The comparison between the SST simulated for the HIM and a reconstruction from planktonic foraminifera transfer functions shows a poor agreement, especially for summer, when the vertical temperature gradient is strong. As a novel approach, we propose a reinterpretation of the reconstruction, to consider the conditions throughout the upper water column rather than at a single depth. We claim that such a depth-integrated approach is more ade-

quate for surface temperature comparison purposes in a situation where the upper ocean structure in the past was different from the present-day. In this case, the depth-integrated interpretation of the proxy data strongly improves the agreement between modelled and reconstructed temperature signal with the subsurface summer warming being recorded by both model and proxies, with a small shift to the south in the model results.

The mechanisms responsible for the peculiar subsurface pattern are found to be a combination of enhanced downwelling and wind mixing due to strengthened Etesian winds, and enhanced thermal forcing due to the stronger summer insolation in the northern hemisphere. Together, these processes induce a stronger heat transfer from the surface to the subsurface during late summer in the western Levantine; this leads to an enhanced heat piracy in this region, a process never identified before, but potentially characteristic of time slices with enhanced insolation.

2.2 Introduction

During the Early Holocene, the northern hemisphere climate experienced an enhanced seasonality of insolation. This period is here referred to as the Holocene Insolation Maximum (HIM) because of the high insolation rate occurring in northern hemisphere summer. The stronger seasonality of the insolation was associated with a strengthening of the North African monsoon (e.g. Rossignol-Strick, 1983).

Coincident with the strengthened orbital forcing, sediment cores from the Eastern Mediterranean Sea display a dark sediment layer, rich in organic carbon, called sapropel S1, deposited between approximately 9 and 6 ka BP (e.g. Mercone et al., 2000). The sapropel S1 and earlier equivalents reflect low oxygen availability in the deep Eastern Mediterranean basin. One of the hypothesis for the sapropel formation is that a freshening of the Mediterranean surface water induced a decrease in surface density and thus prevented the ventilation of deeper layers through the reduced/absent formation of dense deep water, promoting the preservation of organic matter in the sediment (e.g. Rohling and Hilgen, 1991; Rohling, 1994; Cramp and O'Sullivan, 1999).

Because of its isolated configuration, the Mediterranean Sea, as a "mini-

ocean“, is thought to show a rapid and amplified response to past or future climate changes and can be used as a “laboratory” for modelling climate changes. However, only few paleo-modelling studies have investigated the effect of changes in atmospheric forcing on the Mediterranean. Both Bigg (1994) and Mikolajewicz (2011) used a regional ocean general circulation model (OGCM) forced by fluxes interactively calculated from bulk formulas with atmospheric input data from a coarse resolution atmospheric model to simulate the ocean climate of the Last Glacial Maximum (LGM) for the Mediterranean. Meijer and Tuenter (2007) forced their OGCM with present-day realistic climate, and adjusted the runoff and precipitation minus evaporation (P-E) values to precession minimum conditions; those adjustments were based on experiments performed with an Earth system model of intermediate complexity. Myers et al. (1998) and Myers and Rohling (2002) forced a regional OGCM with both modified sea surface temperature (SST) and salinity (SSS) according to reconstructions. Their studies focused on the LGM and the Early Holocene. Meijer and Dijkstra (2009) forced their regional OGCM with strongly idealized atmospheric forcing to mimic the effect of a past climate change. Finally, Myers (2002) forced their Mediterranean OGCM with artificial surface fluxes of heat and freshwater to investigate changes in excess evaporation.

Our modelling strategy aims at simulating the Mediterranean ocean climate of the HIM (9 ka BP). This time slice has been chosen for several reasons. First, the HIM represents a typical past climate with enhanced seasonality and particularly warmer summers, whose influence on the Mediterranean ocean climate is important to be assessed in a today’s context of global warming. Second, a newly compiled data set of upper-ocean temperature reconstructed from foraminifera has identified a significant warm anomalies pattern in summer SST around Crete for the time slice 8.5 – 9.5 ka BP (see Kucera et al., in prep.). Here, we would like to investigate the mechanisms driving this pattern through modelling. Third, we already have global simulations which represent a reasonable Early Holocene climate, so we can use them to force our Mediterranean ocean model. This exercise tests the adequacy of simulating a regional past climate state by using an atmospheric forcing extracted from global model simulations whose resolution is

more than one order of magnitude lower than the one of the regional ocean model. Finally, the HIM Mediterranean simulation can be used in a future stage as baseline to test the hypotheses for sapropel formation, through fresh water perturbation experiments.

For the above-detailed reasons, we carry out and validate simulations for the HIM climate. To assess the performance of the Mediterranean ocean model when it is forced by atmospheric input from coarse resolution global simulations, we perform a comparison with the data set of reconstructed upper-ocean temperature from Kucera et al. (in prep.). We investigate the changes in ocean climate that are simulated in response to an atmospheric forcing representing the HIM. The focus lies on the upper ocean of the Eastern Mediterranean.

To achieve a proper comparison of model output with reconstructed quantities, the model has to be free from any information from paleo-reconstructions. We therefore follow a similar approach as Bigg (1994) and Mikolajewicz (2011) by using a regional OGCM which is forced by fluxes calculated with bulk formulas from atmospheric input data derived from long-term simulations with a coupled global atmosphere-ocean-vegetation model. Not presented here, a future study will test the hypothesis for sapropel S1 formation by performing fresh water perturbation experiments against the validated baseline to assess the plausible physical mechanisms leading to a weakening/shutdown of the deep ventilation.

The goals of the present study are the following: (i) to analyse the modelled changes in the upper-ocean state during the “Holocene Insolation Maximum”, (ii) to investigate the physical mechanisms responsible for strong regional contrasts of the modelled temperature signal, (iii) to validate the modelling results with sea surface temperature reconstructions.

The chapter is organized as follows: in section 2.2 model, forcing and experiments are described. Key quantities of the obtained model control climate are compared to observations in section 2.3. The results for the HIM are described, analysed and compared to reconstructions in section 2.4.

2.3 Model, forcing and experiments

2.3.1 The regional OGCM

For this study, we use the Mediterranean configuration of the ocean general circulation model MPIOM (Max Planck Institute Ocean Model) which has been used by Mikolajewicz (2011). The three-dimensional primitive equation hydrostatic ocean model MPIOM is described in detail in Marsland et al. (2003). For the horizontal discretization, an orthogonal curvilinear Arakawa C-grid is used (Arakawa and Lamb, 1977). The treatment of subgridscale mixing is done with an isopycnal diffusion scheme; at the surface a simple mixed layer scheme is included to account for the effect of the wind mixing; in the interior, the Richardson number dependant mixing term follows the PP scheme (Pacanowski and Philander, 1981). Convective adjustment is treated by an enhanced vertical diffusion coefficient for tracers ($0.5 m^2 s^{-1}$). The model grid covers the entire Mediterranean Sea including the Black Sea and a small area of the Atlantic, west of Gibraltar (Fig. 2.1). The grid is curvilinear with an horizontal resolution of roughly 20 km. We use a 29-level z-coordinates system, with 5 levels within the upper 54 m. The thickness of the first ocean layer is 12 m plus sea level, the model SST is thus centered at 6 m depth. The time step is 36 minutes.

The topography is realistic, the Strait of Gibraltar and the Bosphorus are both represented by one grid point and their sills have depths of 256 and 21 m respectively in the topography used for the pre-industrial climate simulation. During the Early Holocene, the sea level was approximatively 20 m lower than today. To account for this in the paleo-simulations, we reduced the depth by modifying the Mediterranean Sea topography according to the ICE-5G reconstruction from Peltier (2004) (Fig. 2.1). Moreover, we assume the Bosphorus to be closed at this time, so that there is no outflow of fresher water from the Black Sea into the Marmara Sea. We base this assumption on the study from Ryan et al. (1997) who consider a catastrophic inflow of water from Mediterranean into Black Sea happening around 8.4 ka BP, and the study from Sperling et al. (2003) who reconstructed high salinities in the Marmara Sea for S1 sapropel time. However, other studies contradict this statement; Aksu et al. (2002), for instance, suggests an overflow from

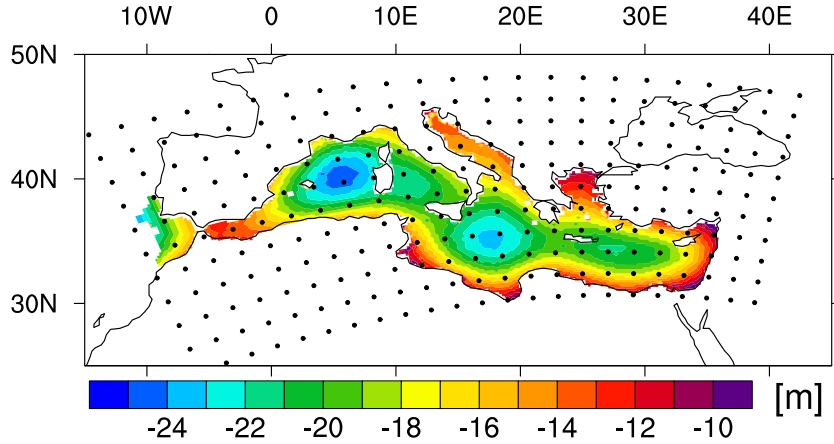


Figure 2.1: Topography changes between 9K and CTRL. The superimposed dots represent 1 of each 10 grid box center of the model in each direction.

Black Sea into the Marmara Sea from 10.5 ka BP onwards with low salinities found in the Marmara Sea. A recent study by Soulet et al. (2011) suggests a reconnection at around 9 ka BP.

2.3.2 Atmospheric forcing and boundary conditions

At the surface, the Mediterranean regional OGCM is forced by air-sea fluxes of heat, momentum and water. The heat fluxes are calculated from daily atmospheric data with bulk formulas according to da Silva et al. (1994).

The atmospheric forcing is derived from long-term simulations performed with the coupled global circulation model ECHAM5/MPIOM/LPJ in a global setup (Mikolajewicz et al., 2007). The atmosphere component ECHAM5 (Roeckner et al., 2003) has a T31 horizontal resolution and 19 vertical levels; the ocean component MPIOM has a curvilinear grid with poles over Greenland and Antarctica. The horizontal resolution of MPIOM is roughly 3° , and there are 40 vertical levels. The dynamical vegetation component LPJ has the same horizontal resolution as the atmosphere component.

2.3.2.1 Global model setup

The simulations with the global model have been carried out until equilibrium for the pre-industrial climate and for two different simulations of the HIM. The reference simulation refers to a pre-industrial type climate. Following the PMIP2 protocol (Braconnot et al., 2007), the atmospheric partial pressure of CO₂ (pCO₂) is set to 280 ppm and the insolation corresponds to 1950 (changes in the orbital parameters lead to negligible insolation differences between 1750 and 1950). For the HIM (9 ka BP), the global simulation used to force the “9K1” regional simulation only considers changes in insolation. In the HIM global simulation used to force the “9K2” regional simulation, besides the changes in earth orbital parameters, the atmospheric pCO₂ is set to 260 ppm instead of 280 ppm and the topography is modified using ice sheet distributions and topography changes according to the ICE-5G reconstruction (Peltier, 2004).

From these global simulations, we derived three different sets of atmospheric forcing input: one for the pre-industrial climate used as control climate (CTRL) and two for the HIM climate (9K1 and 9K2).

We extracted a 100-year daily atmospheric forcing data set with the following variables: precipitation, incoming short wave radiation, cloud cover, near-surface air temperature, dew point temperature, 10-m wind speed and sea level pressure. Due to the coarse resolution of the global coupled model, simulated wind stress patterns are too smooth over the Mediterranean Sea. Therefore, we applied a statistical downscaling to calculate the wind stress from the sea level pressure (SLP) of the global model. For the statistical downscaling, we used the SLP and wind stress from NCEP reanalysis data for the period 1978-2002 (Kalnay et al., 1996). We considered daily data of SLP of the Mediterranean and adjacent regions (truncated on the T31-grid of the global model), and wind stress interpolated onto the ocean model grid. First, we subtracted the long-term mean from the data to obtain anomalies of the NCEP data. Then we calculated a linear regression between principal component time series of empirical orthogonal functions (EOFs, von Storch and Zwiers, 1999) of (i) the anomalies of SLP data from NCEP and (ii) the anomalies of wind stress data from NCEP. Afterward, SLP anomalies from the coarse resolution global model were projected onto the EOFs. Wind

stress anomalies were estimated from the obtained loadings using the regression matrix obtained from the NCEP reanalysis. Finally, the wind stress anomalies were added to the long-term mean of NCEP reanalysis data.

As the global model has a cold bias over the Mediterranean, the systematic bias between the model and the NCEP climatology was added to the actual model values for near-surface air temperature and dew point temperature.

2.3.2.2 Fresh water fluxes and restoring

The components of the water fluxes are the monthly prescribed river runoff (R), the precipitation (P) from the atmospheric data derived from the global model, and the evaporation (E) calculated from the latent heat flux using model SST. For the river discharge, we use a 1-year monthly climatology from the UNESCO RivDis database (Vörösmarty et al., 1998). The seasonal cycle is taken into account only for the major rivers (Danube, Nile, Dniepr, Rhone, Po and Ebro). For the Nile and the Ebro rivers, we consider discharge rates prior to the damming, with a yearly averaged runoff of $2930 \text{ m}^3\text{s}^{-1}$ for the Nile and $410 \text{ m}^3\text{s}^{-1}$ for the Ebro. For the HIM simulations, the anomalies (9K vs. CTRL) of the river discharge simulated by the coupled model are superimposed on the monthly climatology of river runoff used for the CTRL experiment.

At the surface, there is no restoring to SST and SSS. At the western margin of the Atlantic box, a restoring to climatological monthly temperature and salinity from World Ocean Atlas (WOA, Levitus et al., 1998) is applied over 5 grid cells. For the paleo-simulations, the same procedure is applied as for the runoff: the anomalies (9K vs. CTRL) of the Atlantic hydrography from the global model experiments are superimposed to the values used in CTRL.

The evaporation is varying, depending on the latent heat flux, which is a function of the SST. As the freshwater fluxes also affect sea level due to the mass flux boundary condition, the net evaporation of the Mediterranean would lead to continuously decreasing sea level. To account for this, we perform a sea level restoring in the 5 most western grid cells of the Atlantic buffer zone, thus ensuring that the net water transport through the Strait of Gibraltar corresponds to the net water loss in the Mediterranean and the Black Sea.

2.3.3 Spin-up and initial conditions

The integration time strongly differs between the already existing studies: 25 years for Bigg (1994), 20 years for Meijer and Tuentner (2007), 100 years for Myers et al. (1998) and Myers and Rohling (2002), 1000 years for Meijer and Dijkstra (2009) and 1999 years for Mikolajewicz (2011). A long spinup is essential to reach an ocean state which is no longer drifting from the surface to intermediate depths and we therefore perform 700 years simulations with the Mediterranean OGCM.

We start the three simulations from an initial state with homogeneous low density water (38 psu and 20°C for the Mediterranean and the Atlantic box; 20 psu and 20°C for the Black Sea) and let the model run in a free mode for 700 years, forced by the 100-year daily atmospheric dataset repeated in a loop. Such initial conditions allow the model to form its own water masses without being under the influence of starting hydrographic conditions derived from a climatology. Because these experiments were started from homogeneous light water and the forcing is not transient, our simulations can only lead to an ocean state with an active deep circulation as stationary solution, because cross-isopycnic mixing would prevent a state with stagnant deep water to be maintained, through the slow erosion of the stratification.

The results presented in this study correspond to an annual climatology based on the last 100 years (years 601 to 700).

2.4 The general features of the Eastern Mediterranean Sea for the control climate

For convenience, Fig. 2.2 names and locates the sub-basins of the Mediterranean, as well as the main straits.

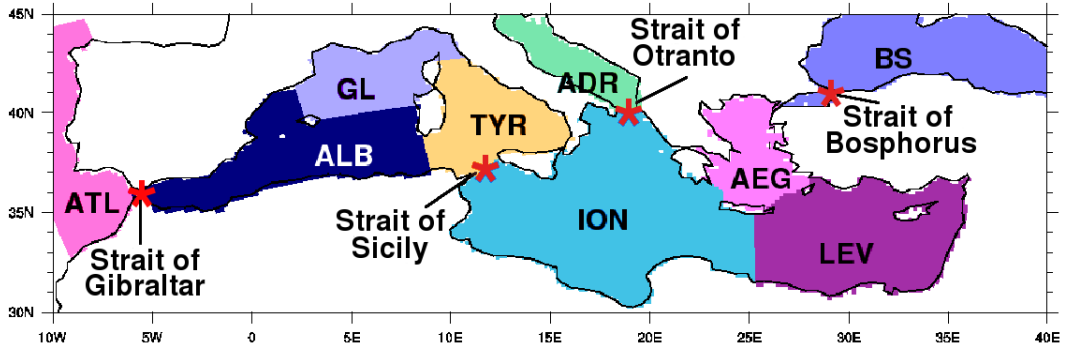


Figure 2.2: Sub-basins of the Mediterranean: Gulf of Lion (GL), Alboran Sea (ALB), Tyrrhenian Sea (TYR), Adriatic Sea (ADR), Ionian Sea (ION), Aegean Sea (AEG), Levantine Sea (LEV). The Atlantic box (ATL) and the Black Sea (BS) are shown as well. The main straits are marked with a red star.

2.4.1 Near-surface circulation and deep water formation

The circulation features of the Eastern Mediterranean Sea for the CTRL climate are illustrated in Fig. 2.3 by the near-surface currents field at 27 m depth. Two intense cyclonic gyres are represented in the Adriatic and in the North Levantine basin (Rhodes Gyre). These gyres correspond to the location of dense water formation. Consistently with the description of the horizontal circulation structure summarized by Pinardi and Masetti (2000), the Atlantic-Ionian Stream coming from the Atlantic Ocean and entering through the Strait of Sicily into the central Ionian is well-simulated, as are the Mid-Mediterranean Jet flowing between Crete and the North African coast and the Asia Minor Current flowing along the Turkish coasts.

Linked to this general circulation, the winter mixed layer depth is an indicator widely used to assess the ability of a model to form the different Mediterranean water masses. In our model, the mixed layer depth is a purely diagnosed quantity which is calculated from a density criterion of 0.125, whose value has been originally motivated by the Levitus Atlas (Levitus,

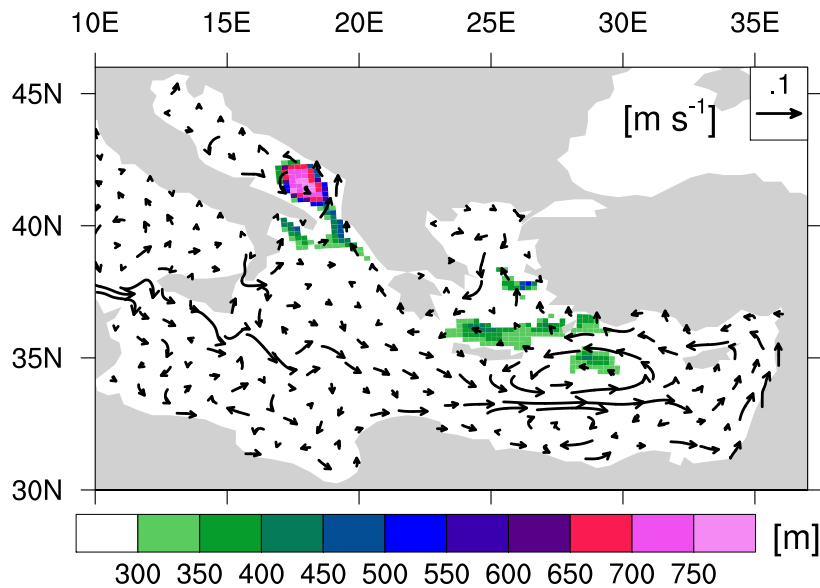


Figure 2.3: Modelled March mixed layer depth (colours) and near-surface currents field (arrows) at 27 m depth for CTRL. Only a subset of vectors has been plotted. The mixed layer depth is reached when the density difference between this depth and the surface exceeds 0.125. Note that such a calculation can only give an approximative estimate of the depth of the mixed layer.

1982).

Fig. 2.3 shows that deep mixed layer patterns are modelled in the Adriatic, where the Adriatic Bottom Water (ABW) is formed and flows out of the Strait of Otranto, in the South Aegean Sea and in the North Levantine where the Levantine Intermediate Water (LIW) is formed. In the Ionian Sea, the mixing of transformed LIW with outflowing ABW forms the Eastern Mediterranean Deep Water (EMDW). The modelled mixed layer patterns are realistic and consistent with the climatology of D’Ortenzio et al. (2005) based on observations and calculated with a temperature difference criterion.

The model simulates an averaged net water transport at Gibraltar of 0.051 Sv ($1 \text{ Sv} = 10^6 \text{ m}^3 \text{ s}^{-1}$), with a surface inflow of 0.84 Sv and a deep outflow of 0.79 Sv. Those values are in agreement with observations by Bryden and Kinder (1991); Bryden et al. (1994); Tsimplis and Bryden (2000) and Baschek

et al. (2001), who suggest values between 0.72 and 0.92 Sv for the inflow and between 0.68 and 0.88 Sv for the outflow. The modelled LIW transport at the Strait of Sicily from the eastern basin to the western basin occurs below 120 m depth and has a mean value around 1.04 Sv which is very close to the observed value of 1.1 Sv (Garzoli and Maillard, 1979; Astraldi et al., 1996).

2.4.2 Surface temperature and salinity

To assess the ability of the model to reproduce observed SST and SSS patterns, we compare our results from the CTRL simulation with the climatologies from WOA 1998 (Levitus et al., 1998) and MEDATLAS (MEDAR-Group, 2002). Because the temperature point in our model vertical discretization is at 6 m depth, we consider the climatological temperature interpolated to 6 m depth to make a consistent comparison.

Fig. 2.4 shows the comparison between the modelled and both climatological SSTs. The model exhibits SST gradient from west to east and from north to south, consistently with the climatologies. For the annual mean as well as for winter (JFM) SSTs, the deviations remain below 1 K. The winter modelled SST values are in between the values of both climatologies, MEDATLAS showing slightly warmer SST than WOA in the Levantine Sea and in the southern Ionian Sea. Both the Aegean and Adriatic Seas have too cold simulated temperatures during winter time. These regions are almost land-locked, with narrow connections to the wider part of the Eastern Mediterranean, through the Strait of Otranto for the Adriatic Sea and three straits of the Cretan Arc for the Aegean Sea. Small-scale atmospheric processes are acting over both areas, so that accurate wind patterns are difficult to simulate adequately at the resolution we are using. For summer (JAS), WOA displays SST 1 to 2 K warmer than MEDATLAS. The modelled summer SST shows warm biases in comparison with both climatologies. In the southern Ionian Sea and in the eastern Levantine Sea, biases up to 3 K are simulated by the model (in comparison with MEDATLAS, the coldest climatology). These biases could be due to the Atlantic-Ionian jet travelling slightly too far north in the model (compared to Pinardi and Masetti, 2000), thus reducing the import of cooler water from the western basin into the

southern Ionian Sea.

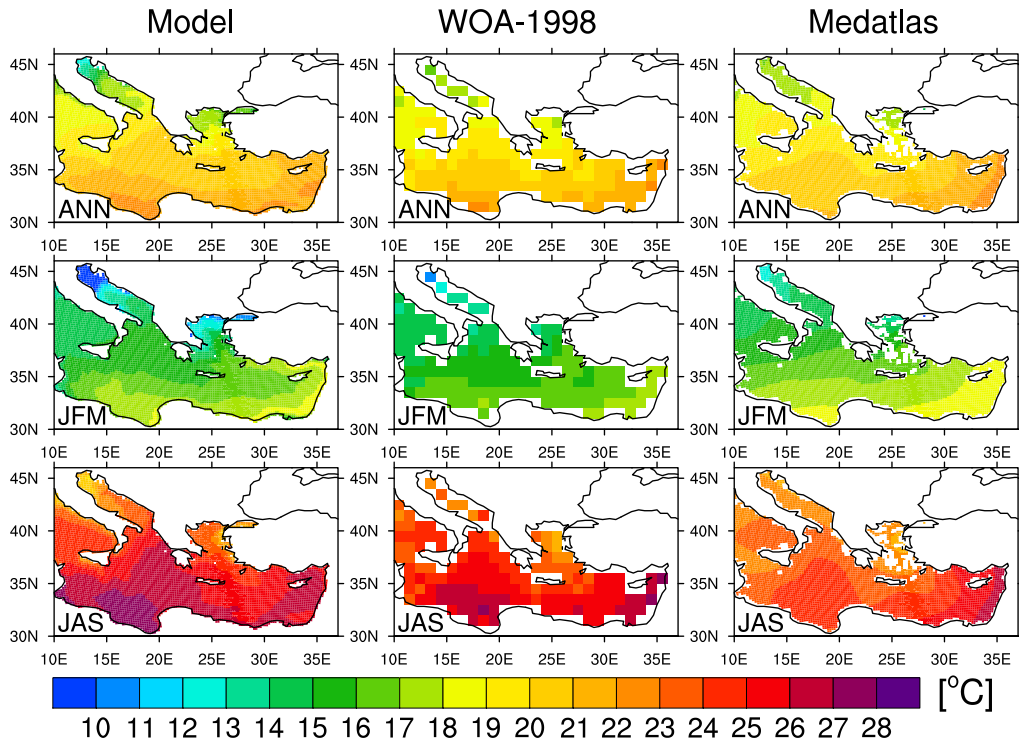


Figure 2.4: Annual, winter (JFM) and summer (JAS) SSTs at 6 m for CTRL (left), World Ocean Data 1998 climatology (middle) and MEDATLAS climatology (right).

Fig. 2.5 displays the deviations of the annual mean modelled SSS from both MEDATLAS and WOA climatologies. The comparison of model results with each climatology exhibits similar discrepancies, which are found in the Levantine and in the Cretan region with a salty bias around 0.3 psu. The fresh bias in the northern Aegean indicates that the model overestimates the fresh water input in this region. The northern part of the Adriatic Sea has a strong negative salinity anomaly corresponding to the fresh tongue from the Po river runoff that flows along the western coast. Nevertheless, the central and South Adriatic show a strong salty bias up to 0.5 psu which can be linked to the underestimation of the mean fresh water input from the Adriatic rivers as well as the overestimation of the penetration of salty Ionian water into the Adriatic. However, part of this discrepancy is probably artificial, as it can be

attributed to the smoothing of the observational data, which has been introduced in the generation of the observational climatologies. Finally, the model has a positive salinity bias all along the North African coast. There are several contributors to this bias: first, this area has a warm SST bias (probably linked to the inability of the model to represent small scale atmospheric processes at the coasts, as explained before), leading to a stronger evaporation and consequently higher salinities. Second, the regional river discharge may be underestimated; third, the Atlantic-Ionian jet, which brings fresher water to the eastern basin, is located slightly too far north in the model. Thus, the southern Ionian remains somewhat isolated and is not significantly impacted by this fresher current. Most of the discrepancies do not reflect the inadequacy of the model to correctly simulate consistent SSS, but they can be directly linked to some discrepancies in the fresh water components of our forcing, mainly the too low precipitation (explained hereafter) as well as missing river discharge. On average, this induces an averaged positive salinity bias of 0.25 psu in the eastern basin.

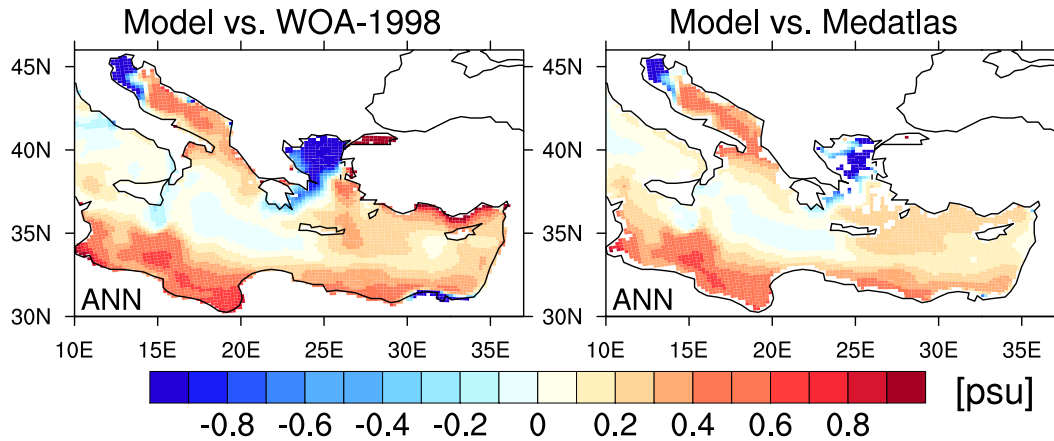


Figure 2.5: Annual mean SSS deviations at 6 m, CTRL vs. World Ocean Data 1998 climatology (left) and CTRL vs. MEDATLAS climatology (right).

2.4.3 Water budget

Table 2.1 summarizes the different components of the fresh water budget for the Mediterranean. The averaged precipitation prescribed over the Mediterranean Sea from the global models is only 0.59 mm/day and the averaged calculated evaporation is 2.83 mm/day. The rivers contribute to the fresh water input by adding 0.35 mm/day. The input from the rivers is close to the data from Ludwig et al. (2009), who indicate a value of 0.39 mm/day. Nevertheless, the amount of prescribed precipitation is relatively low in comparison with both observations and reanalysis (0.7 mm/day for HOAPS, Andersson et al. (2007); and 1.07 mm/day for ERA-Interim Reanalysis, Simmons et al. (2007)). The interactively calculated evaporation is also lower than values from reanalysis (3.34 mm/day for ERA-Interim Reanalysis and observations (3.12 mm/day for HOAPS)).

The resulting water deficit of 1.89 mm/day is compensated by the positive net fresh water transport from the Black Sea into the Mediterranean through the Strait of the Dardanelles (0.18 mm/day or 0.0055 Sv) and from the Atlantic Ocean through the Strait of Gibraltar (1.71 mm/day or 0.051 Sv). The net water transport through both straits is consistent with the observations. Bryden et al. (1994), Bryden and Kinder (1991) and Béthoux (1979) suggest the values of 1.42 mm/day, 1.37-1.64 mm/day and 2.74 mm/day respectively for the estimation of the net water transport at Gibraltar. Concerning the net water transport from the Black Sea through the Strait of the Dardanelles, the data from Stanev and Peneva (2002) indicate a value of 0.22 mm/day.

In Table 2.1, we compare the mean values of each component of the water budget averaged for the full Mediterranean with those averaged for the eastern basin only (from the Strait of Sicily until the Bosphorus). This shows how much the eastern basin differs from the western in terms of E-P balance. We observe that the mean precipitation rate in the eastern basin is around 20% lower than for the full basin, the mean river input is 6% lower and the mean evaporation is 6% higher. The Nile is responsible for 44% of the river input of the eastern basin.

Table 2.1: Fresh water budget for the Mediterranean and the Eastern Mediterranean for CTRL, 9K1 and 9K2.

	Mediterranean			Eastern Mediterranean		
	CTRL	9K1	9K2	CTRL	9K1	9K2
P (mm d ⁻¹)	0.59	0.66	0.60	0.51	0.58	0.52
E (mm d ⁻¹)	2.83	2.87	2.83	2.99	3.03	2.98
R total (mm d ⁻¹)	0.35	0.53	0.45	0.33	0.61	0.49
R total (m ³ s ⁻¹)	10 443	15 535	13 070	6630	11697	9319
R Nile (m ³ s ⁻¹)	2930	7494	5401	2930	7494	5401
$P + R - E$ (mm d ⁻¹)	-1.89	-1.68	-1.78	-2.15	-1.84	-1.97
Net Gib (mm d ⁻¹)	1.71	1.68	1.78			
(10 ⁶ m ³ s ⁻¹)	0.051	0.049	0.052			
Net Bos (mm d ⁻¹)	0.18			0.28		
(m ³ s ⁻¹)	5621			5621		

2.5 The Holocene Insolation Maximum

2.5.1 Stronger seasonal cycle

In the HIM global simulations, the changes in the Earth’s orbital parameters lead to stronger amplitude of the seasonal cycle of insolation. The averaged downward short wave radiation at the top of the atmosphere over the Mediterranean Sea is increased by about 15 Wm⁻² during the summer season and is decreased by about 15.5 Wm⁻² during the winter season for both 9K1 and 9K2 experiments in comparison with the CTRL experiment. This leads to an increased summer warming and an enhanced winter cooling as shown by the near-surface air temperature anomalies signal displayed in Fig. 2.6. The more realistic set up in 9K2 (presence of the decaying Laurentide ice sheet and lower atmospheric pCO₂) leads to a generally slightly colder climate in 9K2. This decreases the summer warming and increases the winter cooling in comparison with the 9K1 simulation.

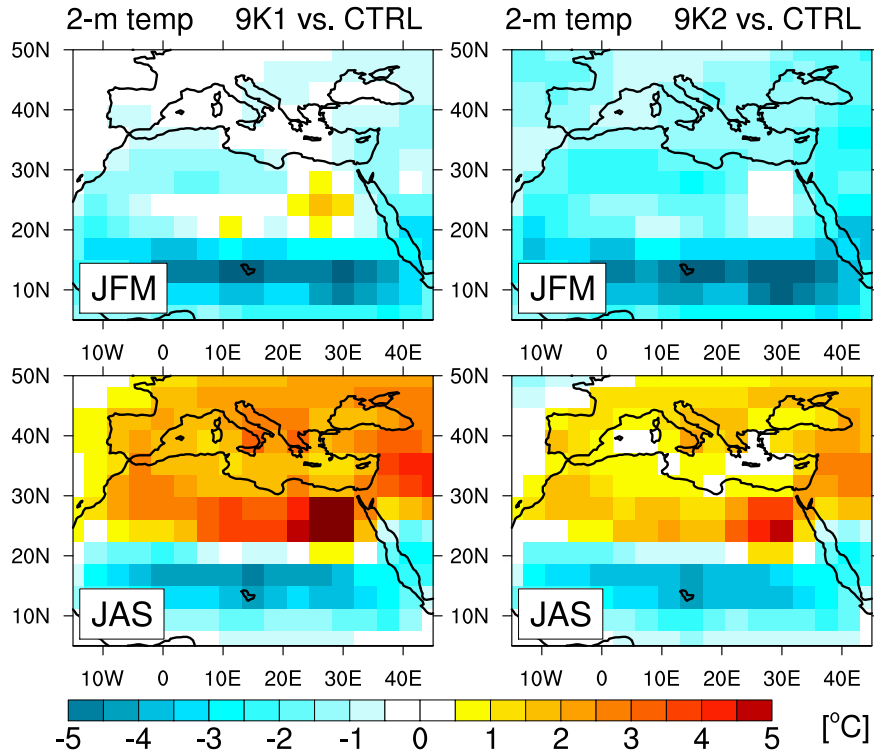


Figure 2.6: Anomalies of 2-m temperature for winter (JFM) and summer (JAS) from global simulations, 9K1 vs. CTRL (left) and 9K2 vs. CTRL (right).

In the global simulations, the increase in the amplitude of the seasonal cycle of solar forcing during the HIM is associated with an intensification of the Northern Hemisphere summer monsoon. The gradient of atmospheric pressure between land and sea being amplified, the monsoonal circulation is strengthened. The enhanced North African monsoon signal is well caught by the model and leads to an increased evaporation (Fig. 2.7). Over sea, the Mediterranean region is characterised by a precipitation increase in 9K1 whereas this is only true for some part of the Eastern Mediterranean basin in 9K2. This increase in P is related to the more southerly propagation of cyclones in winter. In summer, the increase in P is related to an enhanced water recycling. Over sea, the increased evaporation prevails, leading to negative P-E anomalies, except for the eastern Levantine which shows a reduced evaporation (thus positive P-E anomalies) in both simulations (Fig.

2.7). The Nile has a larger water discharge for the HIM with runoff surplus of $4564 \text{ m}^3\text{s}^{-1}$ for the 9K1 simulation and $2471 \text{ m}^3\text{s}^{-1}$ for the 9K2 simulation in comparison with the CTRL experiment.

Table 2.1 summarizes each component of the water budget from the ocean model (over sea only), for the CTRL and the two HIM simulations. Values are averaged for (i) the entire Mediterranean and (ii) the Eastern Mediterranean (the western boundary at the Strait of Sicily). If we consider the entire Mediterranean, the precipitation over sea remains almost constant for the 9K2 simulation but we see an increase by 12% for the 9K1 simulation. In average, the evaporation is almost unchanged. The total riverine fresh water input is increased by more than 50% for the 9K1 simulation and more than 28% for the 9K2 simulation. In both cases, the increase is mainly due to the enhanced discharge from the Nile river which is fed by the increased North African monsoon. If we consider the eastern basin only, the increase in precipitation is higher with a value of 14% for the 9K1 simulation and can be neglected for 9K2. The averaged changes in evaporation are small for both simulations. The fresh water input from the river runoff into the Eastern Mediterranean is almost doubled in the 9K1 simulation and enhanced by 48% in the 9K2 simulation; in both cases the enhanced Nile runoff is the main contributor to this increase. Mainly because of the enhanced riverine input, the P+R-E value over the Eastern Mediterranean increases slightly during the HIM.

In general, the fresh water budget does not show strong changes because the enhanced Nile runoff partially compensates the missing water from the Black Sea.

2.5.2 Salinity, stratification and deep water formation

As a consequence of the missing outflow from the Black Sea due to the closure of the Bosphorus in the HIM simulations, the salinity of the Aegean Sea increases in 9K1 and 9K2 (Fig. 2.8). This results in a shift of the location of intermediate water formation from the North Levantine/South Aegean towards the North Aegean (Fig. 2.8) as it has been recently suggested by the proxy-based study of Schmiedl et al. (2010) which implies a persistent deep

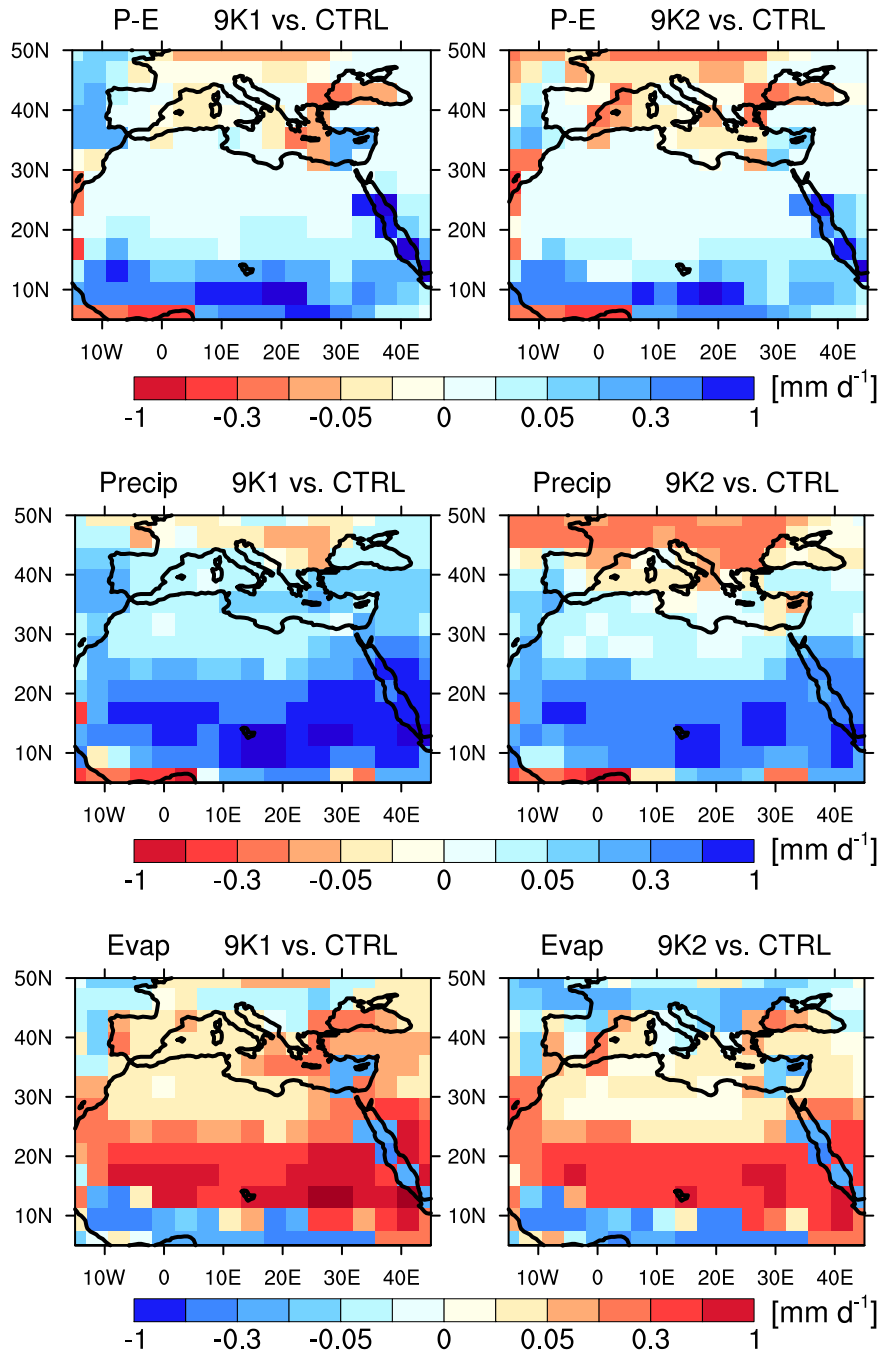


Figure 2.7: Annual mean anomalies of P-E, P and E from global simulations, 9K1 vs. CTRL (left) and 9K2 vs. CTRL (right).

water ventilation in the northern Aegean Sea during the HIM. In our simulations, the salty and relatively dense water formed in this region flows out of the Aegean Sea through the Strait of Antikithira and follows the western Greek coast towards the Adriatic. Along the trajectory following western Greece, a mixed layer pattern of intermediate depth appears due to the fact that the dense salty water flowing from the Aegean entrains the surrounding lighter water on its way to the Adriatic. During the HIM, the deep outflow of Mediterranean water through the Strait of Gibraltar decreases with values of 0.72 and 0.77 Sv respectively for 9K1 and 9K2 (vs. 0.79 Sv in CTRL).

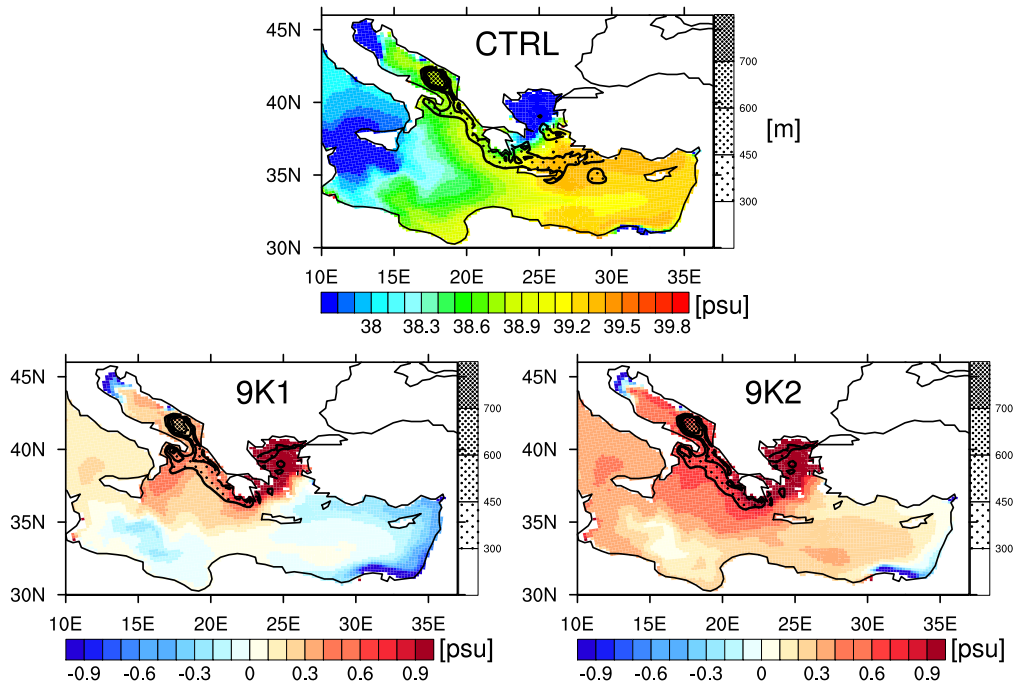


Figure 2.8: Annual mean SSS (CTRL, top) and SSS anomalies vs. CTRL (9K1, middle; 9K2, bottom) at 6 m depth (colours). March mixed layer depth is overlaid as fill patterns.

In both HIM simulations, the modelled SSSs averaged over the eastern basin are higher than in CTRL, with positive anomalies of 0.17 (9K1) and 0.48 (9K2). The rough difference of 0.3 psu between 9K1 and 9K2 is mainly caused by changes in the properties of the inflowing Atlantic water. In 9K2, the salinity prescribed at the western Atlantic boundary is higher because the

corresponding global simulation has a lower sea level, which is not the case in the 9K1 global simulation. Acting in the opposite direction, the enhanced discharge of the Nile tends to reduce the salinity. The latter effect is stronger in 9K1 than in 9K2. Despite their differences in SSS anomalies, the modelled winter mixed layer depth patterns remain similar in both HIM simulations.

The simulated SSS anomalies display a signal which is not too far from the one reconstructed for 9 ka BP. In the Tyrrhenian Sea, Kallel et al. (1997b) reconstruct SSS around 1 psu saltier than today, the model simulates positive anomalies of 0.1 (9K1) and 0.35 psu (9K2). In the Ionian Sea, Emeis et al. (2000) reconstruct SSS anomalies 1 psu higher than present-day, the model exhibits SSS anomalies of +0.35 (9K1) and +0.5 psu (9K2). Finally the SSS signal reconstructed in the Levantine by Emeis et al. (2000) is 2 psu fresher than today whereas the model shows SSS anomalies of -0.15 (9K1) and +0.2 psu (9K2). The inconsistency between model and reconstruction in the Levantine is probably related to the Nile runoff which could be underestimated by the global model (particularly in the 9K2 simulation), thus leading to too salty SSS.

To assess the impact of the salinity changes on the ventilation of the deeper layers, we focus on the vertical stratification of the water column and calculate an Index of Stratification (IS) (in $m^2.s^{-2}$, see Beuvier et al., 2010; Herrmann et al., 2008; Somot, 2005; Lascaratos, 1993). This index has been used in previous studies to investigate the preconditioning of the convection by looking at the changes in the vertical stratification. It corresponds to the loss of buoyancy which must be provided to the stratified water to induce a convection event up to the bottom of the sea. The lower the index, the more likely is the convection to occur, inducing thus the ventilation of deeper water. IS is calculated on a 100-year mean basis, for each model grid point (i, j) using the following formula:

$$IS(i, j, h_{bot}) = \int_0^{h_{bot}(i,j)} N^2(i, j, z) z dz, \quad (2.1)$$

where z is the depth, h_{bot} is the depth at the bottom and N is the local Brunt-Vaisala frequency: $N^2 = \frac{g}{\rho} \frac{\partial \rho}{\partial z}$.

This calculation is performed for each grid point (i, j) characterised by its

local maximal depth h_{bot} .

Table 2.2 compiles IS values averaged over the main convective areas for the three simulations. In the Adriatic, the most active location for deep water formation, low IS values are displayed for the three simulations, reflecting a weak stratification. From these similarities, we infer that the deep water production in the Adriatic remains identical during the HIM with formation rates comparable to CTRL. This happens because the changes in surface salinity have reached the deeper layers and the state has become quasi-stationary with a stable density gradient similar to CTRL. During the HIM, both past experiments simulate a decreased IS in the North Aegean and an increased IS in the South Aegean in comparison with CTRL, consistently with the shift of winter mixed layer depth pattern from the south to the north displayed in Fig. 2.8.

Table 2.2: Index of Stratification (IS , in $m^2.s^{-2}$).

	CTRL	9K1	9K2
Adriatic	0.95	1.00	0.98
South Aegean	1.07	1.27	1.27
North Aegean	1.25	0.92	0.89

We thus obtain 3 simulations, each representing a well-ventilated state. Winter convection occurs in different sub-basins and forms intermediate and deep water in the Adriatic, the South Aegean and the Northeastern Levantine in CTRL; and in the Adriatic and the North Aegean in the HIM simulations. Despite these small shifts between past and present, the zonal overturning stream function remains almost identical, with a deep counter-clockwise cell in the eastern Mediterranean, displaying a maximum value of 0.2 Sv. These simulated past climate states aim at representing a stable and stationary environment before entering into the transition phase which triggered the sapropels through weakened/prevented ventilation of the deep water.

2.5.3 The upper-ocean temperature

2.5.3.1 Seasonal cycle

As a direct effect of the changes in incoming short wave radiation at the surface, an increase in the amplitude of the seasonal cycle of the water temperature (Fig. 2.9) is simulated. The enhanced cooling during winter spreads over the entire water column through mixing and convective processes. The enhanced seasonal cycle leads to warmer surface temperatures in both 9K simulations in summer. During spring and summer, stable stratification prevents a deep penetration of the warming signal. The region with temperatures warmer than in the control run is thus restricted to the upper 30 and 20 m respectively for the 9K1 and 9K2 simulations. Since the 9K1 simulation is in general warmer than the 9K2 simulation (due to the presence of rest of the Laurentide ice sheet and reduced atmospheric $p\text{CO}_2$ in 9K2), the summer warming relative to the CTRL run is more intense (up to + 1.5 K for the surface water of the 9K1 experiment vs. + 0.8 K for 9K2) and spreads slightly deeper than for the 9K2. Below, the water shows cold anomalies during summer, which is a remainder from the cold winter signal.

2.5.3.2 The western Levantine subsurface warming pattern

In this section, we analyse the patterns of the spread of the surface summer warming signal into the subsurface layers. Fig. 2.10 displays the anomalies between 9K1/9K2 and the CTRL, for 6 m depth (the modelled SST), 17 m depth and 27 m depth. The surface warming is relatively homogeneous for both paleo-simulations, but the subsurface temperature anomaly signal shows strong regional contrasts with a well-defined pattern. At 17 m depth, the region around Crete and the western Levantine still show a warming signal, whereas the central Ionian, the Tyrrhenian and, only for 9K1, the eastern Levantine, experience a cooling. At 27 m depth, cooling is mainly observed over the Eastern Mediterranean, but is strongly reduced around Crete and western Levantine, and even absent for the 9K1 simulation.

The pattern of subsurface temperature anomalies is quite similar to the present-day pattern of subsurface spread of the summer SST in the Eastern Mediterranean (Fig. 2.11). The model shows weaker vertical gradients of

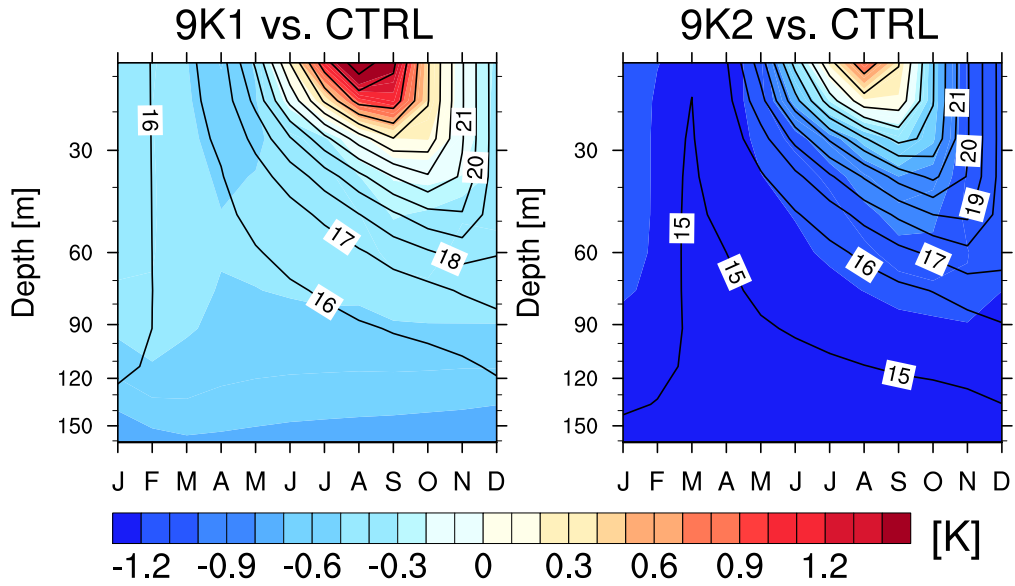


Figure 2.9: Anomalies in monthly seasonal cycle of upper ocean temperature averaged over the Eastern Mediterranean, 9K1 vs. CTRL (left) and 9K2 vs. CTRL (right); isolines represent the absolute values in $^{\circ}\text{C}$ for 9K1 (left) and 9K2 (right).

the near-surface temperature in the western Levantine (and thus a deeper penetration of the summer warming signal) than in the eastern Levantine and the Ionian; the same pattern is also obvious in the MEDATLAS climatology.

The reduced vertical near-surface temperature gradient in the western Levantine is caused by the Etesian winds. The Etesian winds are dry northerly winds blowing over the Aegean Sea and the Levantine Sea from about mid-May to mid-September, mainly because of the monsoon effect leading to a thermal low pressure trough over Turkey, with higher pressure over southern Balkans; and the passage of cold fronts over the Balkans and the associated cold-air circulation behind them (e.g. Meteorological-Office, 1962; Brody and Nestor, 1985). In the model derived forcing used for CTRL, Etesian winds are acting from mid-May until mid-October (Fig. 2.12, black line) and are essentially a north-south blowing wind (Fig. 2.12 and 2.13). The westward Ekman transport induced by this wind pattern involves upwelling of cold subsurface water in the eastern Levantine (resulting in a strong vertical near-surface temperature gradient) and downwelling of warm surface

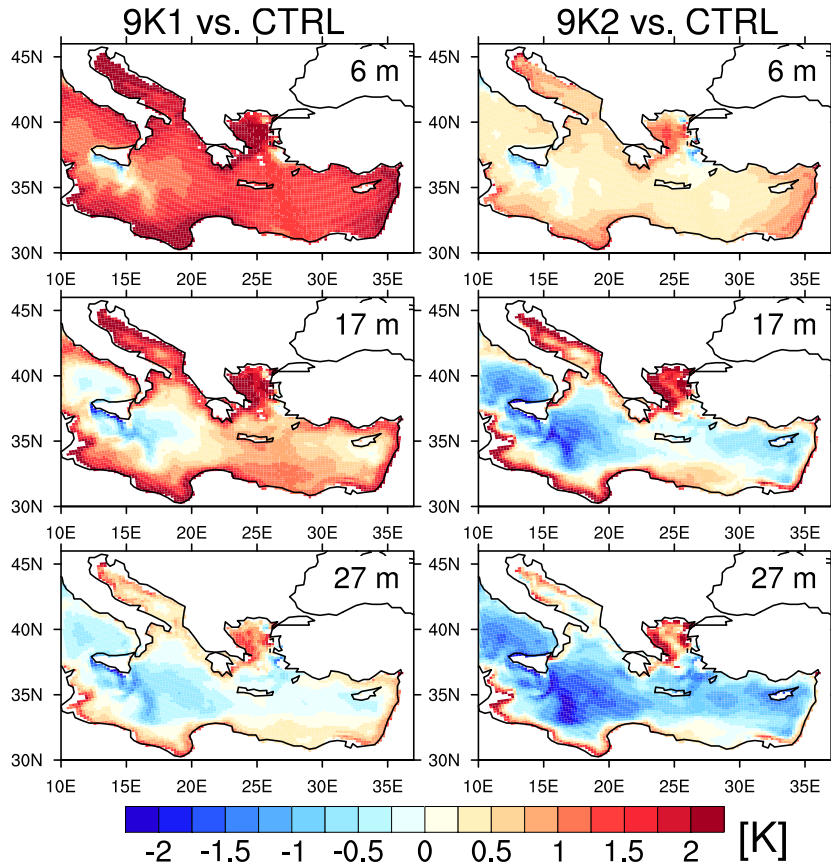


Figure 2.10: Anomalies of summer (JAS) temperature at different levels, 9K1 vs. CTRL (left column) and 9K2 vs. CTRL (right column).

water west of the core of the Etesian winds with reduced vertical near-surface temperature gradient. As an example, the vertical velocities and the associated subsurface heating rates are displayed in Fig. 2.14. The westward Ekman transport leads to a substantial heat transport from the eastern to the western Levantine. This becomes evident when comparing the atmospheric heat input with the actually observed changes in ocean heat content for the period from May to September, when the Etesian winds are present (Fig. 2.15, left). In the western Levantine, an additional heat source of up to 60 Wm^{-2} working for 5 months is required to explain the changes in ocean temperature. In the eastern Levantine, a similar heat sink is required (up to 65 Wm^{-2}). In the centers of action, these heat source/sink correspond

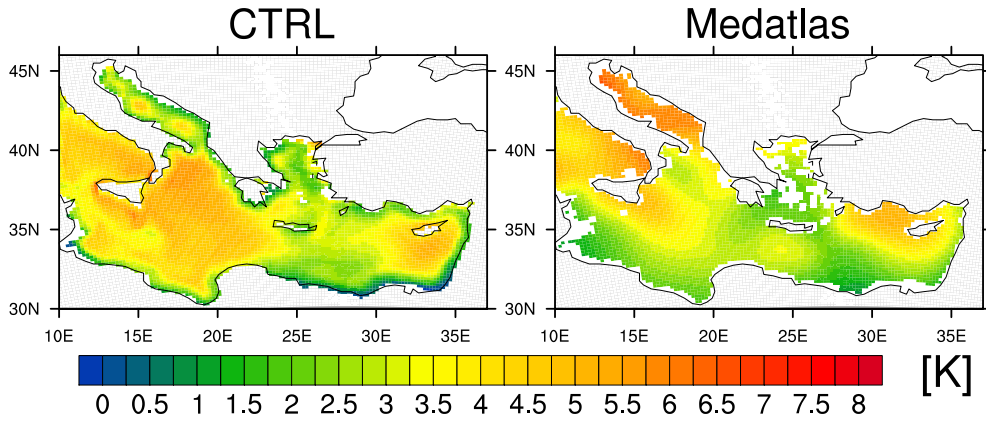


Figure 2.11: Summer (JAS) temperature difference between 6 m and 27 m for CTRL and MEDATLAS climatology.

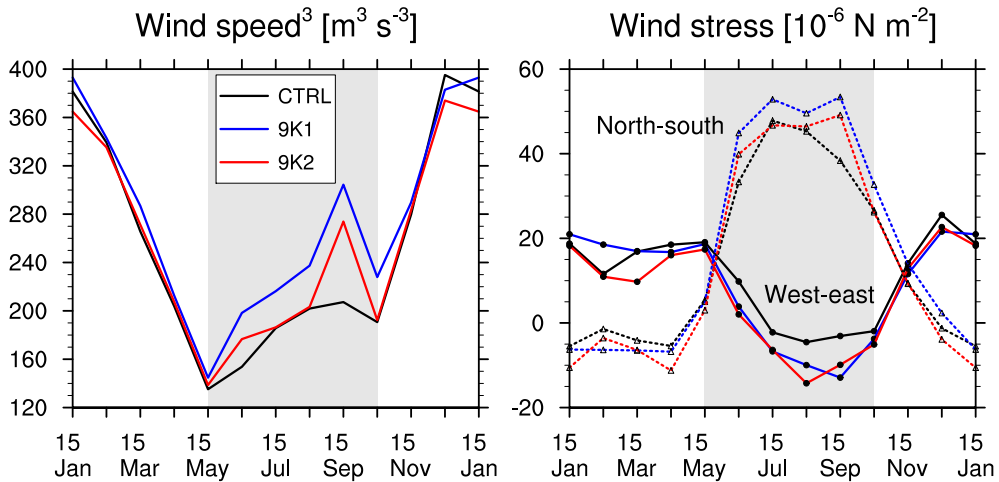


Figure 2.12: Monthly climatology of wind components averaged over the Aegean/West Levantine regions for CTRL (black), 9K1 (blue) and 9K2 (red). Left panel shows 10-m wind speed cubed, the cubed value is considered because it is proportional to mixing strength. Right panel shows both west-east and north-south wind stress components. The shading represents the time period, when modelled Etesian winds are active.

to more than 40% of the atmospheric heat input for this time of the year. The obvious connection are the westward Ekman transport of warm surface water and the compensation flow of colder subsurface water. This pattern is

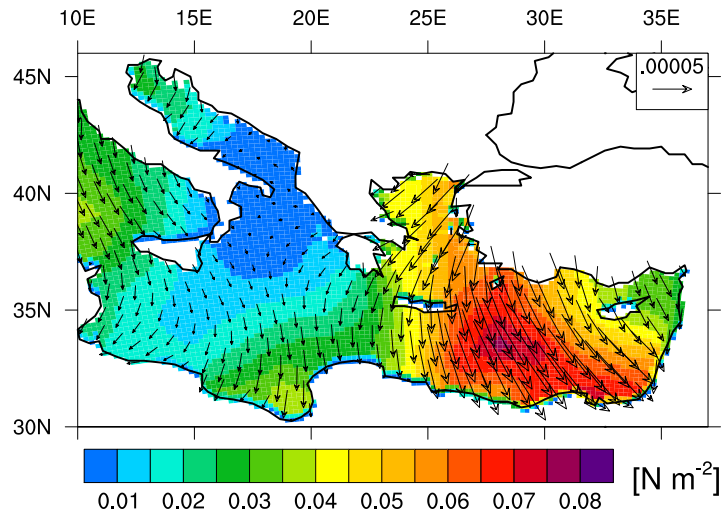


Figure 2.13: Mean summer (JAS) wind stress for CTRL.

restricted to the period, when the Etesian winds are blowing. In the other months, westerly winds are prevailing. The annual mean climatological net air-sea heat exchange shows only a very weak annual mean heat loss in the western Levantine (Fig. 2.16), indicating that the heat “piracy” of the western Levantine is restricted to late spring and summer. In the other months of the year, the western Levantine is actually exporting heat.

In order to determine, whether the summer heat piracy is a model artefact, we performed the same calculation using net atmospheric heat input from the ERA-Interim Reanalysis averaged over the years 1989-2005 (Berrisford et al., 2009) and the ocean heat content changes calculated from the MEDATLAS temperatures (Fig. 2.15, right). The results show an even stronger heat piracy (up to 150 Wm^{-2}) around Crete and in the southeastern Levantine. Additional simulations performed with our ocean model forced with ERA-Interim derived atmospheric forcing have produced similar results (not shown). The difference between modelled and observation derived-estimates can be explained by differences in the Etesian winds. The Etesian winds derived from the global model are essentially blowing from the north (Fig. 2.12 and 2.13). In the present-day observations, they also have a westerly component over the Levantine, thus causing the west-east dipole of the model to be

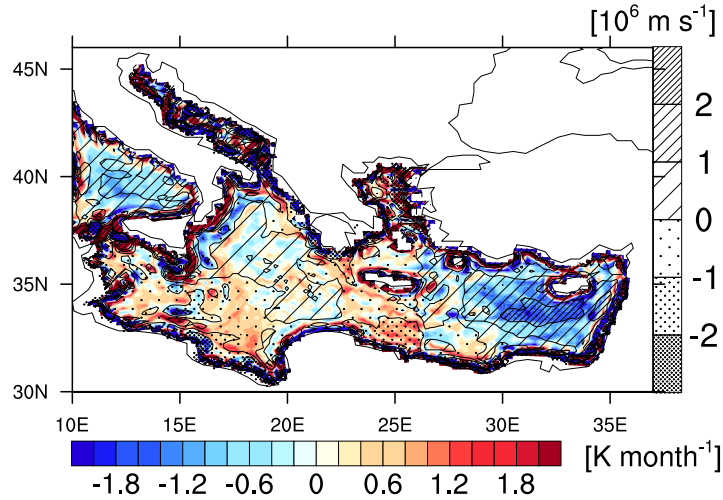


Figure 2.14: Temperature change through vertical advection averaged between 12 and 42 m (colours) and vertical velocities (fill patterns, positive values for upward velocities) in July for CTRL.

somewhat rotated with the strongest part of the upwelling shifted more to the southeast, and the strongest part of the downwelling shifted more to the south. The observed Etesian winds are also slightly stronger, which explains the stronger heat piracy in the observation-based estimate.

During the HIM, the amplified seasonal cycle of surface temperature (which is a direct effect of the insolation forcing) enhances the vertical gradients in near-surface ocean temperature. Together with the Ekman-induced circulation, this stronger seasonality of the insolation cycle could explain the pattern of subsurface temperature changes displayed by the anomalies 9K vs. CTRL (Fig. 2.10). In the upwelling region of eastern Levantine, colder subsurface water is upwelled, in the western Levantine warmer surface water is downwelled, thus causing a positive anomaly of subsurface temperatures. Additionally, the modelled Etesian winds are found to be increased for both HIM experiments (Fig. 2.12): a further strengthening of the temperature dipole is thus expected through enhanced Ekman transport.

In the following, the respective contributions of increased Etesian winds and enhanced seasonal cycle of insolation, to the subsurface temperature anomaly in Cretan and south Levantine regions are analysed. For this pur-

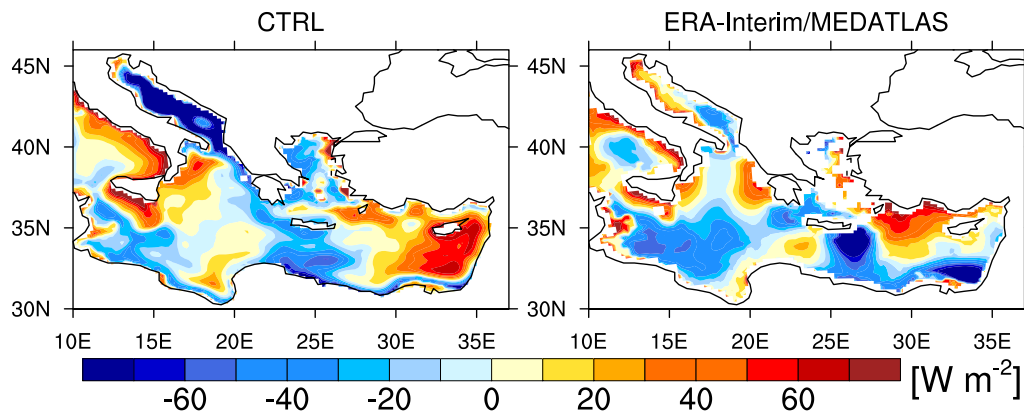


Figure 2.15: Difference between the net atmospheric heat input and changes in ocean heat content from May 1st until September 30th. Left panel shows CTRL. Right panel shows differences between net atmospheric heat input from ERA-Interim Reanalysis (averaged over 1989/2005) and changes in ocean heat content from MEDATLAS climatology. Positive values indicate that the atmospheric input is higher than the temperature change in the water column, reflecting an export of heat from this region. Negative values reflect an heat accumulation.

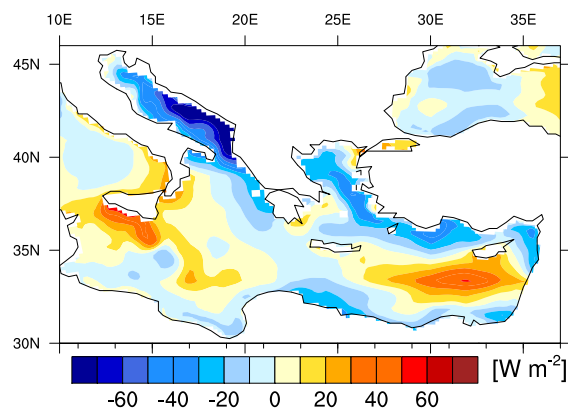


Figure 2.16: Annual mean net heat flux at the surface for CTRL.

pose, two different 100-year sensitivity experiments are set up, all starting in year 600 of experiment 9K2:

- 9K2-W0 uses the same setup as the 9K2 simulation, but both wind

speed and wind stress from CTRL (weaker Etesian winds) are prescribed. With this simulation, the effect from the “full“ wind (speed and stress) on the 9K2 climate can be assessed when compared with 9K2, and the effect of the increased thermal forcing alone can be assessed when compared to CTRL.

- CTRL-W9 is similar to CTRL simulation, but we prescribe both wind speed and wind stress from the 9K2 experiment (enhanced Etesian winds). This simulation enlightens the effect of the “full” wind signal (speed and stress) on the CTRL climate when compared with CTRL.

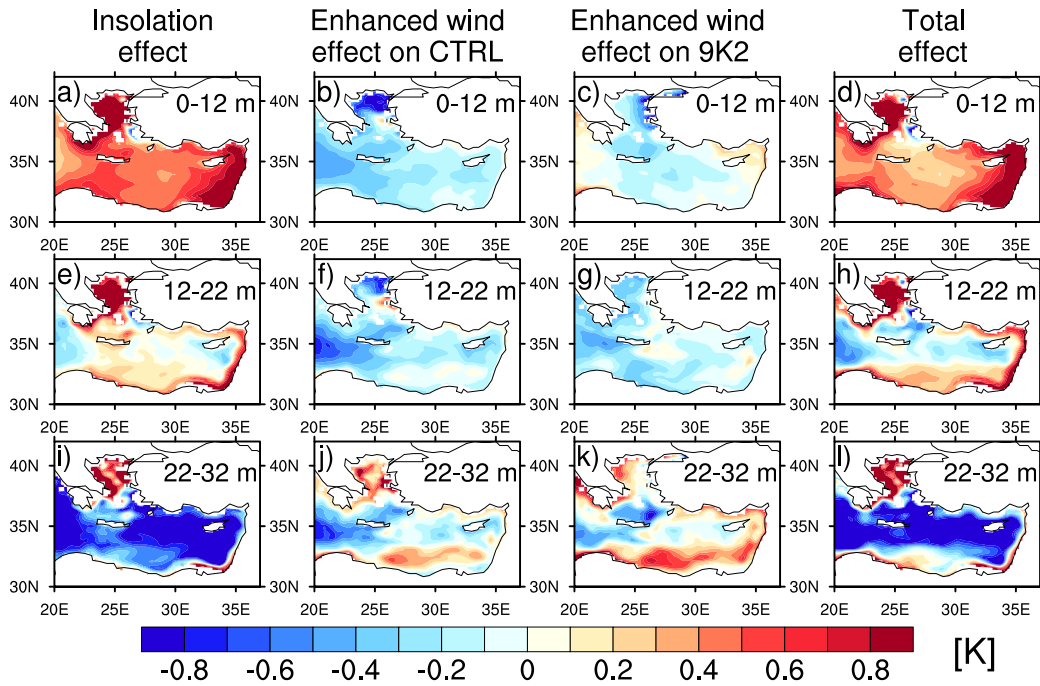


Figure 2.17: Anomalies of temperature for different model layers for summer (JAS). The columns show the isolated effect of insolation forcing (9K2-W0 vs. CTRL), enhanced Etesian winds on CTRL climate (CTRL-W9 vs. CTRL) and on 9K2 climate (9K2 vs. 9K2-W0), as well as the total effect of both factors (9K2 vs. CTRL).

Fig. 2.17 displays the contribution of different factors to temperature anomalies at different levels of the subsurface. Factors analysed are (i) the enhanced insolation forcing (9K2-W0 vs. CTRL), (ii) the increased Etesian

winds on CTRL climate (CTRL-W9 vs. CTRL), and (iii) the increased Etesian winds on 9K2 climate (9K2 vs. 9K2-W0). Separate contributions are compared to the total effect from both increased winds and enhanced seasonal cycle of insolation (9K2 vs. CTRL).

The pure effect of the insolation in the 9K2 simulation is dominant in the first model layer (0-12 m), and is responsible for a mean warming of 0.5 K (Fig. 2.17a). The contribution of enhanced winds induces a mean cold bias of 0.3 K on a CTRL climate (Fig. 2.17b) and 0.2 K on a 9K2 climate (Fig. 2.17c). The wind-induced cooling is almost entirely a consequence of the enhanced wind speed which induces a stronger mixing at the top of the water column; this leads to stronger heat transfer from the sea surface toward subsurface, explaining the cold anomalies in the first ocean layer. The wind stress effect is small at the surface.

In the second layer (12-22 m), the insolation effect is strongly reduced with a warming around 0.2 K in the Cretan and southwestern Levantine regions and a cooling in eastern Levantine (Fig. 2.17e). These patterns are expected in this case, which combines enhanced summer insolation signal and present-day winds: the water downwelled in southwestern Levantine is warmer, leading to warmer pattern, and the subsurface water upwelled in eastern Levantine is colder, leading to cooler pattern. In this second layer, the main effect of stronger Etesian winds is still a cooling (Fig. 2.17f and 2.17g), however, a warming up to 0.2 K becomes noticeable in the south Levantine area on 9K2 climate (Fig. 2.17g).

From the third ocean layer (22-32 m) toward greater depth, the remaining cooling from the winter is prevailing, explaining the cold anomalies displayed for the insolation effect (Fig. 2.17i and 2.17m). The effect from the increased wind becomes strong from 22 m on: on CTRL climate, southwestern Levantine shows warm anomalies up to 0.5 K in 22-32 m layer (Fig. 2.17j) and up to 0.8 K in 32-42 m layer, whereas the eastern Levantine cooling reached the value of 0.6 K in both layer. On 9K2 climate, the warming induced by increased winds in southwestern Levantine is 0.2 K stronger than on CTRL climate (Fig. 2.17k vs. 2.17j). This warm/cold dipole is triggered by the enhanced wind stress which leads to enhanced Ekman transport, namely stronger downwelling of surface warm water in southwestern Levantine and

stronger upwelling of deeper cold water in eastern Levantine. Both patterns persist down to 250 m depth. The increased wind speed is responsible for warm anomalies southeast of Crete at that depth (heat gain through higher transfer to subsurface).

In general the wind effects become stronger when acting on a temperature distribution with enhanced vertical gradients. This becomes obvious when comparing the respective panels with wind effects on CTRL and 9K2 basis state. Thus the nonlinear effects between the two mechanisms (stronger seasonal cycle and stronger Etesian winds) are amplifying the temperature signal.

When all effects are combined, the total results to a subsurface warming pattern around Crete and in southwestern Levantine in the 12-22 layer (Fig. 2.17h). The warming around Crete vanishes for the 22-32 m layer (Fig. 2.17l), because of the prevailing cooling from the insolation signal (Fig. 2.17i). Only the warming in southwestern Levantine (induced by enhanced downwelling of warm water) is strong enough to prevail in the layers 22-32 m (Fig. 2.17l) and 32-42 m (Fig. 2.17p).

From this analysis, we conclude that general anomalous heat accumulation happens in the region south of Crete for both CTRL (Fig. 2.15) and paleo-simulations in summer, and can be attributed to Ekman transport. However, during the HIM, the combination of (i) enhanced downwelling in southwestern Levantine, (ii) enhanced mixing around Crete; both related to increased Etesian winds; and (iii) enhanced thermal forcing, are driving together stronger surface heat transfer to the subsurface during summer in the Cretan/southwestern Levantine region and are thus responsible for the simulated warm subsurface anomaly pattern.

2.5.4 Comparison to proxy data

2.5.4.1 The SST reconstructions

The transfer function used to reconstruct the paleo-SST is based on census counts of 23 species of planktonic foraminiferal species in 274 core tops, 145 from the Mediterranean and 129 from the Atlantic (Hayes et al., 2005). The data are calibrated to seasonal (JFM and JAS) and annual mean SST values

at 10 m water depth from the observational dataset WOA (Levitus et al., 1998). The transfer function method based on “artificial neural networks” is described in Hayes et al. (2005).

Based on ^{14}C data, oxygen isotope stratigraphy, biostratigraphy or a combination of those, the Holocene Insolation Maximum interval has been identified in 33 Mediterranean sediment cores as an interval between approximately 9.5 and 8.5 ka BP. Only samples occurring within this interval as identified by the individual age models were considered. Faunal counts were collated with the same procedure as for the core-top samples. SST reconstructions were averaged throughout each Holocene Insolation Maximum Interval for each core.

The full data and discussion of the proxy resulted are presented in a companion paper by Kucera et al. (in prep.).

2.5.4.2 SST model-proxy comparison

In this section, we compare the SST modelled in 9K1 and 9K2 with the SST reconstructed from foraminifera for 9.5 - 8.5 ka BP. We first consider absolute values and analyse annual, summer (JAS) and winter (JFM) temperatures.

Fig. 2.18 displays for each experiment the fit between the SST reconstructions and the modelled SST at each core location; for annual mean, winter (JFM) and summer (JAS). In general, the 9K1 simulation, which only considers the change in solar forcing, yields too warm SST in comparison with the reconstructions. In contrast, the SST predicted by the model in the 9K2 simulation show a better match with the reconstructions because the 9K2 simulation takes also into account the cooling effect of the glaciers and the reduced atmospheric CO_2 concentration, which leads to SST around 1 K colder than for the 9K1 simulation. The model-data discrepancies of the 9K1 simulation are mainly located in the central Ionian, with a warm SST bias of 1 K for annual mean and 3 K for summer (Fig. 2.19). As for the CTRL simulation, this bias may be linked to the Atlantic-Ionian jet travelling too far north in the model.

The two strongest deviations displayed in Fig. 2.18 refer to data located in the Adriatic and in the Aegean (Fig. 2.19). These two regions are difficult

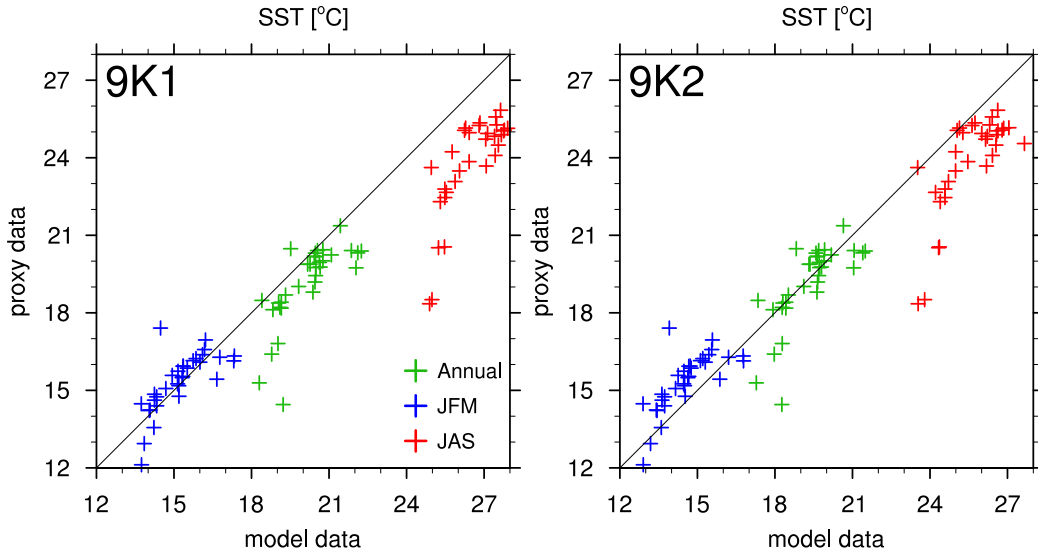


Figure 2.18: Comparison of modelled SST with SST reconstructed from proxy data (Kucera et al. (in prep.)) for 9K1 (left) and 9K2 (right). Annual mean, winter (JFM) and summer (JAS) are considered.

to simulate at our resolution due to their size and small-scale processes acting over these areas, among these are katabatic winds, which are not resolved adequately by the coarse global model. This may explain the strong disagreement encountered in these locations with discrepancies up to 6 K and 5 K in summer, respectively for 9K1 and 9K2 (Fig. 2.19). Furthermore, the two temperature reconstructions available for the Adriatic differ strongly so that it is difficult to extract a clear signal from the observations for this region. For the two simulations, the modelled SST fall between both reconstructed SST values. For both simulations, the simulated winter SST matches well with the reconstructed signal (Fig. 2.18, blue): the biases do not exceed 1 K except for the Aegean. The major disagreement between model and proxy data is restricted to summer SST (Fig. 2.18, red): both HIM experiments show a warm bias with summer SST errors in excess of 3 K in average for the 9K1 simulation and 2 K for the 9K2 simulation. Again, except for the enclosed Aegean and Adriatic Seas, the major discrepancies are found in the central Ionian and in the Tyrrhenian Sea (Fig. 2.19).

To evaluate how model and reconstructions depict differences between the

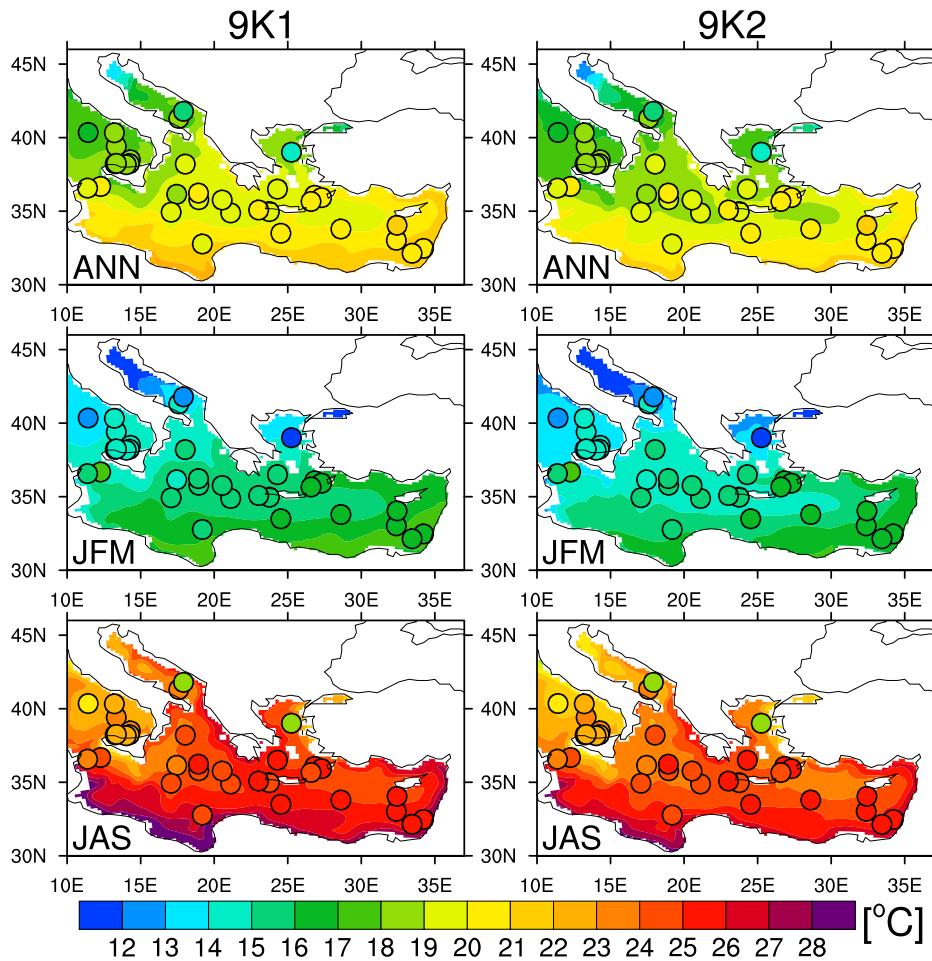


Figure 2.19: Annual, winter (JFM) and summer (JAS) SST, reconstructed from proxy data (dots, Kucera et al. (in prep.)) vs. modelled one (background colour) for 9K1 (left) and 9K2 (right). 1st row displays annual SST, 2nd row displays winter SST, 3rd row displays summer SST.

HIM and the present-day, we compare the 9K1/9K2 simulations with the CTRL simulation, and the time slice 9.5 - 8.5 ka BP of reconstructed SST with pre-1998 instrumental mean SST. The differences allow us to check the ability of the model to reproduce the changes between the HIM and the present-day ocean state, without being affected by the internal model discrepancies that may have an impact on the absolute values. The reconstructed SST anomalies (Fig. 2.20) reveal strong spatial patterns of the signal. The annual and summer reconstructed SST anomalies (Fig. 2.20, 1st

and 3rd rows) show a strong warming around the Cretan region and a cooling of the middle Ionian, the Tyrrhenian and the eastern Levantine. We refer to this alternance of cold / warm / cold anomaly patterns from the west to the east as the “tripole”. In summer, this reconstructed SST anomaly signal is much stronger than for annual mean. In fact, the reconstructed winter SST anomalies (Fig. 2.20, 2nd row) generally show a cooling, except for the Cretan and Sicilian regions which display a small warming: this winter signal dampens the stronger summer signal and explains the smoother gradient for the annual SST reconstructions. Concerning the model ability to reproduce these spatial anomaly patterns, the model results are not consistent with the reconstructions. Whereas the tripole pattern is somewhat imaged by the 9K1 simulation for the annual SST anomalies, the 9K2 simulation is again consistently too cold. For the summer SST anomalies, the 9K1 experiment shows a rather homogeneous warming but hardly any cooling of the middle Ionian and the Tyrrhenian. The 9K2 experiment shows a much weaker warming and is able to reproduce an enhanced warming pattern around Crete. The modelled winter SST anomalies do not show the warming around Sicily, and the 9K2 experiment simulates a far too strong cooling over the entire basin.

Two points are important to notice at this stage of the analysis: the simulated temperature signal decreases very strongly with depth in the upper part of the water column during the summer season, due to strong stratification (Fig. 2.9). Moreover, the foraminifera used for the SST reconstructions are not limited to the 10-m depth of the calibration, but inhabit the entire mixed layer and some live even below it (Bé et al., 1977; Schiebel and Hemleben, 2005). They are thus likely to record subsurface temperatures as well, which are colder than the surface temperature in summer.

To account for this, we decide to consider subsurface temperature for our comparison. The strong depth dependency of both annual and summer temperature signals leads us to propose a new depth-integrated approach of interpreting SSTs derived from foraminifera census data. Moreover, the temperature anomaly patterns recorded by the reconstruction closely resemble the patterns recorded at subsurface depth in our simulation, as shown in the section 2.4.3.2. This strengthens our motivation to test an approach which integrates subsurface temperature to validate model data with temperature

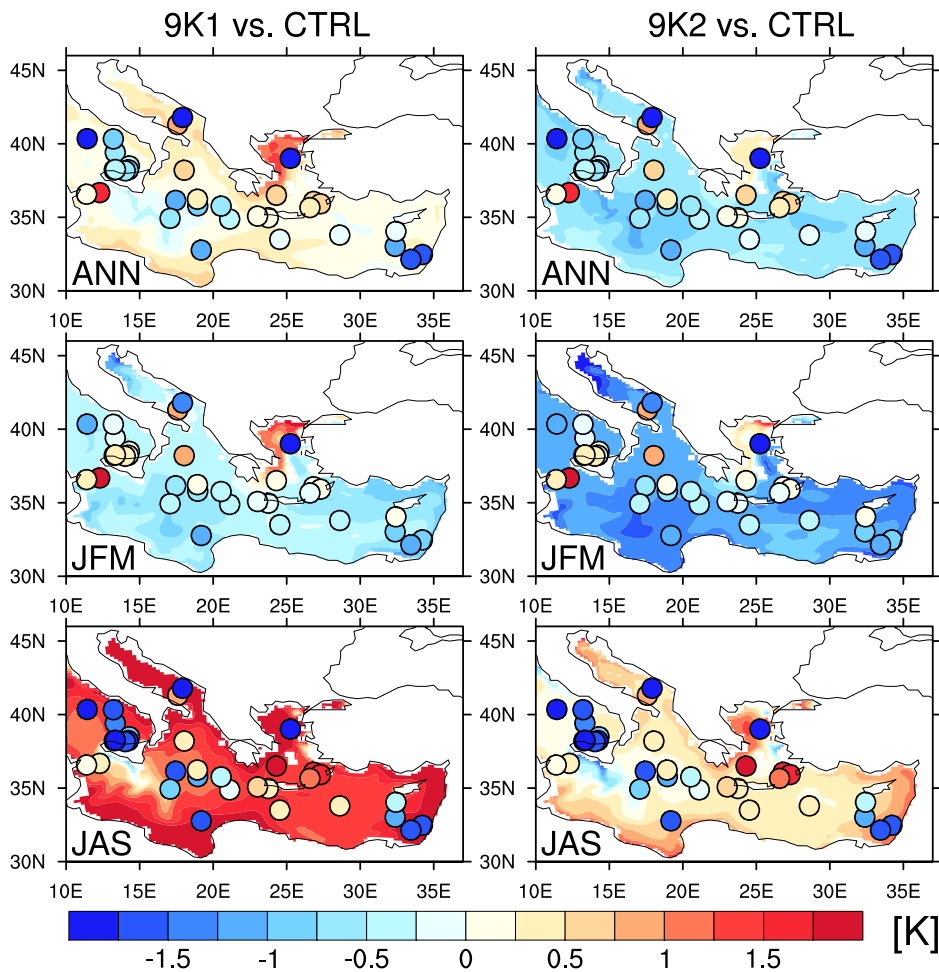


Figure 2.20: Annual, winter (JFM) and summer (JAS) SST anomalies, reconstructed from proxy data (dots, Kucera et al. (in prep.)) vs. modelled one (background colour) for 9K1 vs. 0K (left) and 9K2 vs. 0K (right). 1st row displays annual SST anomalies, 2nd row displays winter SST anomalies, 3rd row displays summer SST anomalies.

reconstructions from proxy data.

2.5.4.3 A depth-integrated approach for model-proxy comparison of upper-ocean temperature

In this section, we propose an alternative approach to perform a comparison of surface temperature signal between output from model simulations and

reconstructions based on planktonic foraminifera.

We consider temperatures averaged over a larger depth interval for our model-proxy comparison instead of restricting it to a narrowly defined SST signal. As an example, we choose to integrate the temperature over the depth interval between 0 and 30 m (henceforth T_{0-30}), where the vertical temperature gradient is strongest. We do not claim that 0-30 m is the range of depth which should be always chosen but we rather aim to highlight the need to consider a broader interval of depth which depends of the living depth of the foraminifera. The present section is an example of how the comparison could be led. However, the interval of depth chosen to integrate the temperature signal should be informed by the oceanographic conditions of a given region and the ecology of the planktonic species used.

The proxy temperatures are in a strict sense only valid for 10 m depth. As for many of the core locations, no core top estimates of the pre-industrial climate are available, anomalies versus climatologies for this depth have been used. However, this approach is not adequate to obtain reconstructed anomalies of T_{0-30} signal: the present-day climatology for T_{0-30} can easily be calculated from the same climatology, but the proxy data should have been estimated with T_{0-30} as base too, which is beyond the scope of this chapter. As a simple approximation, we calculate a linear regression between T_{10} , which has been originally used to fit the proxy data, and T_{0-30} from the World Ocean Atlas dataset. Only data from the Mediterranean and the North Atlantic have been used (box selected between 30° and 50° North and -20° and 37° East). We subsequently apply this relation to the reconstructed data and get a new set of reconstructions for T_{0-30} . The following functions are applied: $T_{0-30} = 0.97 T_{10} + 0.29$ for annual temperatures, $T_{0-30} = 0.99 T_{10} + 0.015$ for winter and $T_{0-30} = 0.9 T_{10} + 1.45$ for summer. The R^2 is higher than 0.977 for all three scalings. The root mean square deviation (RMSD) of the obtained T_{0-30} is 0.41 K for summer, 0.02 for winter and 0.17 for annual mean. In winter, the mixed layer depth is in general deeper than 30 m and the vertical temperature gradient is small. For this season, the results for T_{0-30} are not substantially different from the results for T_{10} . Thus the discussion will rather focus on summer and annual mean.

The new model-proxy comparison for the absolute T_{0-30} is displayed in

Fig. 2.21. It exhibits the fit between the reconstructions and the model data at each core location; for annual mean, winter (JFM) and summer (JAS). The new comparison shows a great improvement, especially for the summer season where the strongest discrepancies were found in the previous strict SST comparison (Fig. 2.18). For both simulations, the biases between modelled and reconstructed T_{0-30} are generally below ± 1 K, except for the data located in the Adriatic and in the Aegean Seas (Fig. 2.22).

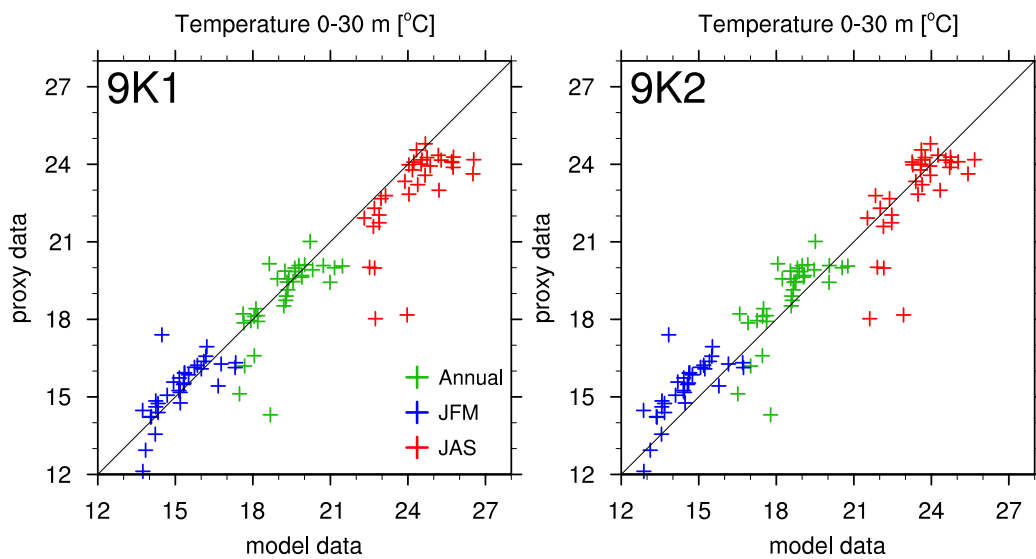


Figure 2.21: Comparison of modelled T_{0-30} with T_{0-30} reconstructed from proxy data (Kucera et al. (in prep.)) for 9K1 (left) and 9K2 (right). Annual mean, winter (JFM) and summer (JAS) are considered.

Fig. 2.23 displays the new comparison for the T_{0-30} anomalies (9 ka BP vs. CTRL) simulated by the model and the one recorded by the proxy indicators. The reconstructed summer T_{0-30} anomalies do show the west-east tripole (Fig. 2.23, 2nd row). However, in the Tyrrhenian, the central Ionian and the eastern Levantine, the cooling signal is less pronounced than with the strict SST reconstructions; this is in agreement with the modelled signal of the 9K2 simulation. The cold anomalies simulated by 9K1 in these regions are weak and even missing for the eastern Levantine. The new T_{0-30} reconstructions show a more homogeneous warming around Crete. This warming is simulated in the 9K1 experiment but the warmest anomalies are located in

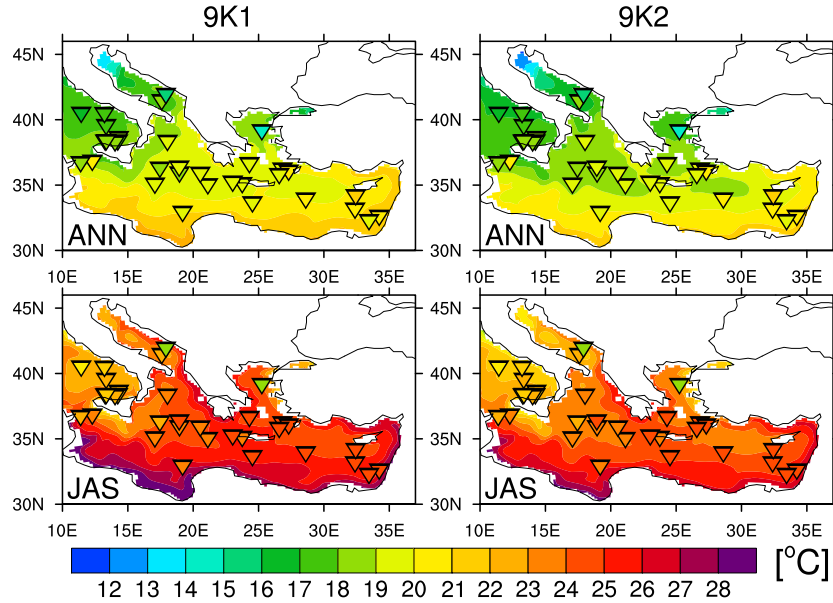


Figure 2.22: Annual and summer (JAS) T_{0-30} , calculated from SST reconstructions from proxy data (triangles, Kucera et al. (in prep.)) vs. modelled one (background colour) for 9K1 (left) and 9K2 (right). 1st row displays annual T_{0-30} , 2nd row displays summer T_{0-30} .

the southwestern Levantine. The 9K2 experiment displays a small cooling in the Cretan region and a small warming in the southwestern Levantine. The model produces the warmest anomalies in the southwestern Levantine rather than in the Cretan region because the downwelling of warm surface water is simulated too far south. Nevertheless, in few locations, the anomalies (9 ka BP vs. present-day) of estimated T_{0-30} reconstructions show a signal which is lower than the RMSD of the estimated summer T_{0-30} signal (0.41 K). These results should thus be interpreted cautiously.

It is worth mentioning that if the modelled Etesian winds had a stronger westerly component, and had their core centered over the east Aegean (as it is recorded by the observations), the downwelling of warm surface water would occur around Crete, leading to warm subsurface anomalies there rather than in the southwestern Levantine (as shown in Fig 2.15, right). This would also improve the agreement between model and proxies, showing a modelled warming more centered around Crete, consistently with the reconstructed

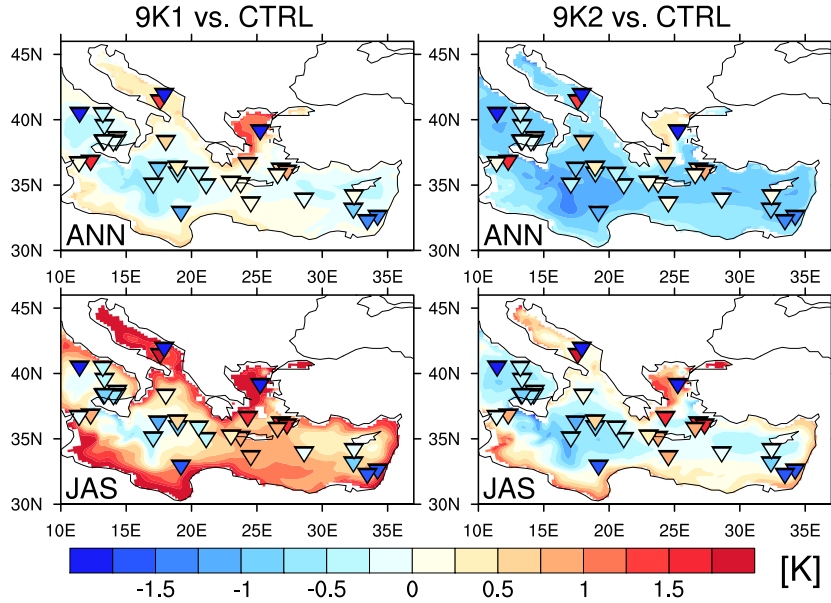


Figure 2.23: Annual and summer (JAS) T_{0-30} anomalies, calculated from SST reconstructions from proxy data (triangles, Kucera et al. (in prep.)) vs. modelled one (background colour) for 9K1 vs. 0K (left) and 9K2 vs. 0K (right). 1st row displays annual T_{0-30} anomalies, 2nd row displays summer T_{0-30} anomalies.

signal.

To summarize the results from the model-proxy comparison and to highlight the added value from the novel integrated approach, Table 2.3 compiles the mean bias and the mean standard error (RMSD) for (i) the SST comparison and (ii) the T_{0-30} comparison. The most obvious improvement is for summer, when both 9K1 and 9K2 simulations reach a much lower mean bias with the T_{0-30} comparison. The RMSD is also clearly improved. As expected, there is hardly any difference between the SST and T_{0-30} comparisons for winter, because the small temperature gradient during this season leads to similar results. If we average the mean bias and the RMSD for the three considered periods (winter, summer and annual mean), it is clear that the T_{0-30} comparison leads to a better match. To our point of view, the experiment 9K2 fits the reconstructions the best. Although the mean bias is slightly higher than for 9K1 (-0.59 vs. 0.55), the RMSD value of 9K2 is

lower (1.23 vs. 1.37).

Table 2.3: Mean error and mean biases.

		<i>SST</i>		<i>T</i> _{0–30}	
		9K1	9K2	9K1	9K2
Annual mean	Error (RMSD)	1.46	1.04	1.11	1.10
	Mean bias	1.02	0.19	0.35	-0.38
Winter (JFM)	Error (RMSD)	1.03	1.20	1.03	1.23
	Mean bias	0.00	-0.66	0.00	-0.71
Summer (JAS)	Error (RMSD)	3.10	2.16	1.83	1.34
	Mean bias	2.81	1.73	1.29	0.50
Averaged	Error (RMSD)	2.06	1.55	1.37	1.23
	Mean bias	1.27	0.42	0.55	-0.59

These results confirm the hypothesis that the model-proxy comparison should involve a temperature signal integrated over a wider range of sub-surface depth, consistent with the range of living depths of the planktonic foraminifera used, instead of restricting the comparison to the SST. Ideally, a new transfer function should be used to perform the reconstructions, taking into account an integrated temperature signal whose depth range should be previously determined.

The simulation 9K2 seems to represent an upper-ocean climate somewhat more realistic than the 9K1 simulation which simulates in general a too warm climate, due to the fact that the forcing used for this simulation does neither include the cooling effect from the melting glaciers nor from the lower pCO₂.

2.6 Conclusion

We have modelled the upper ocean climate of the Eastern Mediterranean for the Holocene Insolation Maximum (9 ka BP) with a regional OGCM forced by daily atmospheric data derived from global simulations. Two experiments have been carried out: 9K1 with changes in solar forcing only and 9K2 with

changes in solar forcing, atmospheric pCO₂ and topography (presence of major ice sheets).

We analysed the mechanisms responsible for the enhanced subsurface summer warming observed in the Cretan/West Levantine region during the HIM, which is recorded by both the model and proxy data. The drivers of this warming are found to be a combination of (i) enhanced downwelling (due to stronger Ekman transport) and wind mixing, both due to strengthened Etesian winds, and (ii) enhanced vertical temperature gradient due to the stronger seasonal cycle in the northern hemisphere. Together, these processes induce a stronger heat transfer from the surface to the subsurface during late summer in the western Levantine and are responsible for the heat piracy simulated in this region.

We used SST reconstructed from planktonic foraminifera assemblages to validate our HIM simulations, but found it necessary to integrate modelled SST over a wider depth range to account for variable habitat depth. We believe that this is how surface temperature comparisons between model data and reconstructions from foraminifera should be performed. This novel depth-integrated approach strongly improved the agreement between the reconstructions and the modelling results. The currently used technique to reconstruct temperature from planktonic foraminifera is likely inadequate for time periods when the vertical temperature gradient was different from today, which is likely to have been the case in the isolated Mediterranean Sea for periods with changing insolation. Ideally, the transfer function should be newly calculated for the temperature integrated over the considered depth range including subsurface.

We believe that the dipole in summer temperature anomalies identified in the Levantine by both simulations and reconstructions is a general feature of time periods with enhanced insolation. Such a characteristic response is thus expected for other past time slices like e.g. the Eemian.

Chapter 3

Stability of the Eastern Mediterranean overturning circulation under freshwater perturbations during the Early Holocene

3.1 Introduction

Since the discovery of the sapropel layers in sediment cores from the Eastern Mediterranean (Kullenberg, 1952; Olausson, 1961), the mechanisms which cause their formation have been discussed in the literature without reaching a strong agreement. Three main schools are driving the debate. The first proposes the following explanation: a freshening and/or a warming of the surface water of the Eastern Mediterranean led to a decrease in surface density, thus preventing the deep water formation in the Adriatic and/or Aegean Seas. The circulation cell would then be restricted to the upper part of the water column and the deep water masses would be stagnating, inducing slowly the complete consumption of the deep oxygen, since no new oxygen is brought down through convection. The second school of thoughts relates the sapropel formation to an increase in primary production due to higher nutrient input through the rivers. This would increase the pool of organic

matter sinking to the sea floor and form a sapropelic layer. The third school suggests a combination of both previously described mechanisms.

The first hypothesis, which relates the formation of sapropels to the stagnation of deep water masses of the eastern basin, is also subject to an internal debate. Which climatic and environmental changes might have triggered these circulation changes? Where does the additional freshwater come from to induce a dilution of the basin and thus strengthen the stratification?

Several mechanisms have been proposed to explain the development of the deep water stagnation. The main concepts suggested by previous studies are:

- Enhanced fluvial discharge (e.g. Rossignol-Strick et al., 1982; Rossignol-Strick, 1985, 1987; Rohling and Hilgen, 1991; Emeis et al., 2000; Freydier et al., 2001; Ducassou et al., 2008). These studies mainly propose an increase of the Nile runoff linked to the enhanced North African monsoon. However, the modelling study by Tuenter (2004) suggests that the enhanced Nile runoff was not sufficient to maintain a long stagnation of the deep water.
- Increased freshwater flux from the Black Sea caused by the opening of the strait (Lane-Serff et al., 1997). However, this hypothesis is refuted by Sperling et al. (2003), who reconstructed high salinities in the Marmara Sea for S1 sapropel time. Matthiesen and Haines (2003) modelled the effect of a gradual (Lane-Serff et al., 1997) and a catastrophic opening (Ryan et al., 1997) of the Bosphorus with an hydraulic box model; they found that the vertical stratification would be enhanced by respectively 13 % and 43 %.
- Enhanced precipitation over the Mediterranean region and/or the northern borderlands of the Eastern Mediterranean due to increased activity of Mediterranean depressions (e.g. Cramp et al., 1988; Rohling and Hilgen, 1991; Rohling, 1994; Kallel et al., 1997a; Schmiedl et al., 2010).
- Ice sheet melt from the Black Sea catchment, via the Black Sea (e.g. Olausson, 1961)

- Deglacial sea level rise and surface Atlantic water freshening induced by deglacial meltwater (e.g. Rohling, 1994; Béthoux and Pierre, 1999). Again, Matthiesen and Haines (2003) modelled the effect of strong meltwater events (Fairbanks, 1989) on the Mediterranean stratification and found that the Meltwater pulses 1A (12 000 years BP) and 1B (9500 years BP) would increase the vertical stratification by respectively 21 % and 14 %.
- Warming of surface water, which would enhance the stratification of the water, increase the evaporation, and make more water available for precipitation over the Eastern Mediterranean catchment (e.g. Rohling and Hilgen, 1991; Rohling, 1994; Emeis et al., 2003; Tüenter, 2004).

The simulations performed in the present study are carried out with a regional ocean model that represents physical processes only, and does not account for the biogeochemical processes. Thus, this chapter only investigates the physical hypothesis, addressing the question about the relevant mechanisms responsible for the formation and persistence of deep water stagnation.

3.2 Experimental design

As detailed in Chapter 2, the simulation 9K2, which includes the cooling effect from the melting glaciers and lower $p\text{CO}_2$, reproduced a realistic ocean climate for the Holocene Insolation Maximum (HIM). We thus chose this simulation as baseline to compare with our sensitivity experiments. In this chapter, this baseline simulation will be called “9K-base”. The abbreviation “CTRL” stands for the preindustrial present-day climate simulation.

In order to test the plausibility of the diverse mechanisms proposed in the literature to explain the stagnation of Eastern Mediterranean deep water and the consequent formation of the sapropel S1, a set of sensitivity experiments is carried out. The effect of various freshwater perturbations is investigated: (i) a sudden opening of the Strait of the Bosphorus, (ii) an increase of freshwater discharge from the Nile or from the Po, (iii) a homogeneous increase in precipitation over the eastern basin, and (iv) a freshening of the surface

Atlantic waters entering at Gibraltar. This set of experiments allows to assess if the origin of the perturbation plays a big role to reach a stagnation of the deep circulation. In order to quantify the strict effect of the amount of the freshwater input, some of the perturbations are tested for various input magnitudes for the same origin.

A short description of the experiments is given in Table 3.1.

Table 3.1: Description of the experiments.

<i>Short name</i>	<i>Description of the experiments</i>
CTRL	Control simulation representing the preindustrial climate
9K-base	Baseline simulation representing the climate of the 9 ka BP time slice
<i>Perturbation experiments based on 9K-base setup</i>	
Po-3000	Runoff from the Po enhanced by $3000 \text{ m}^3 \text{ s}^{-1}$
Nil-3000	Runoff from the Nile enhanced by $3000 \text{ m}^3 \text{ s}^{-1}$
Nil-6000	Runoff from the Nile enhanced by $6000 \text{ m}^3 \text{ s}^{-1}$
Nil-9000	Runoff from the Nile enhanced by $9000 \text{ m}^3 \text{ s}^{-1}$
Bos-3000	Opening of the Bosphorus with an outflow of $3000 \text{ m}^3 \text{ s}^{-1}$
Bos-6000	Opening of the Bosphorus with an outflow of $6000 \text{ m}^3 \text{ s}^{-1}$
Prec-3000	Increase in precipitation rate by $3000 \text{ m}^3 \text{ s}^{-1}$ homogeneously distributed over the eastern basin
Atl-fresh	Freshening of the Atlantic inflowing water of 0.014 psu per century
Nil-9000-Atl-fresh	Freshening of the Atlantic inflowing water of 0.014 psu per century and Runoff from the Nile enhanced by $9000 \text{ m}^3 \text{ s}^{-1}$

The aim of this chapter is to discuss the possible sources which could have freshened the Mediterranean basin; to understand, compare and quantify the mechanisms leading to a possible persistent strong stratification of the deep water masses. This modelling approach aims to move forward the debate about the origin of the sapropel S1 formation, by testing the assumptions proposed in the literature.

3.3 State of the art of previous modelling studies

Previous modelling studies have investigated the impact of changes in buoyancy forcing on the Mediterranean thermohaline circulation (MTHC). Myers and Haines (2002) determined the change in buoyancy forcing required to modify the qualitative nature of the MTHC. They found that a small increase in P-E fluxes yields a linear decrease of the overturning circulation whereas the deep water formation collapses in their model when P-E is increased by 20%. Myers et al. (1998) showed that atmospheric conditions corresponding to the time period of Sapropel S1 lead to the establishment of a deep stagnant layer below 400-500 m in the eastern basin and 100-150 m in the Aegean. Meijer and Dijkstra (2009) suggested that a decrease in evaporation yields a stable reduction of the zonal overturning stream function below 300 m in the eastern basin, when combined with a reduction of the vertical diffusivity.

All the above-mentioned studies applied a uniform modification of the surface fluxes over the Mediterranean. However, the most favoured hypothesis for the sapropel formation suggest a precise origin of the additional freshwater input (e.g. Nile, Black Sea, Atlantic, precipitation). Distributing the additional freshwater uniformly over the Mediterranean surface is likely to have a different impact on the circulation cell than having a precise source of additional freshwater. Following this idea, Meijer and Tuenter (2007) investigated the respective effect of changes in P-E, river discharge from the south and from the north, by adjusting their values to precession minimum conditions. The required adjustment was taken from a global climate model. They

found that an increase of the discharge from the north or enhanced precipitation were equally or more effective in triggering a more stable stratification than an increased river discharge from the south. In one of his experiments, Myers (2002) enhanced the Nile runoff to 2.5 times the pre-Aswan values and found similar results to that if the freshening was uniformly distributed over the basin; both changes led to a small decrease of the deep water formation. However, in both studies, the extremely short duration of the experiments (20 years for Meijer and Tuentner (2007); 100 years for Myers (2002)), as well as the absence of interannual variability in their atmospheric forcing, considerably weaken the robustness of their findings.

In this chapter, we isolate the effect of single well-identified freshwater perturbations and test different hypotheses concerning the origin of the additional freshwater input. The chapter is organized as follows: in section 3.4 we analyse the response of the Eastern Mediterranean vertical circulation to an increase Nile runoff with $9000 \text{ m}^3 \text{ s}^{-1}$ of additional freshwater input. We investigate how sensitive the deep ventilation of the basin is to (i) the magnitude of the freshwater perturbation in section 3.5, and (ii) the origin of the freshwater perturbation in section 3.6. The effectiveness of a transient perturbation is discussed in section 3.7. Finally, the results are synthesized, debated and compared to former findings in section 3.8, before we conclude in section 3.9.

3.4 Sensitivity to enhanced Nile runoff

In this section, we analyse the most debated hypothesis for the establishment of the stagnation, which is the increase of the Nile runoff, often considered as crucial for sapropel formation and directly related to the strengthening of the North African summer monsoon during this period (e.g. Rossignol-Strick, 1985, 1987). The focus is directed on the Nil-9000 experiment, with is the strongest perturbation of our experimental setup with an additional runoff of $9000 \text{ m}^3 \text{ s}^{-1}$. This big disturbance corresponds to a rough increase of the Nile runoff by a factor 2.7 in comparison with the baseline simulation for the Holocene Insolation Maximum (9 ka BP). This leads to a mean runoff of $14358 \text{ m}^3 \text{ s}^{-1}$, with a maximum water discharge of $20011 \text{ m}^3 \text{ s}^{-1}$ in September

and a minimum water discharge of $9876 \text{ m}^3 \text{ s}^{-1}$ in May. We analyse the development of the stratification involving the quantification of the time needed to reach a stagnation.

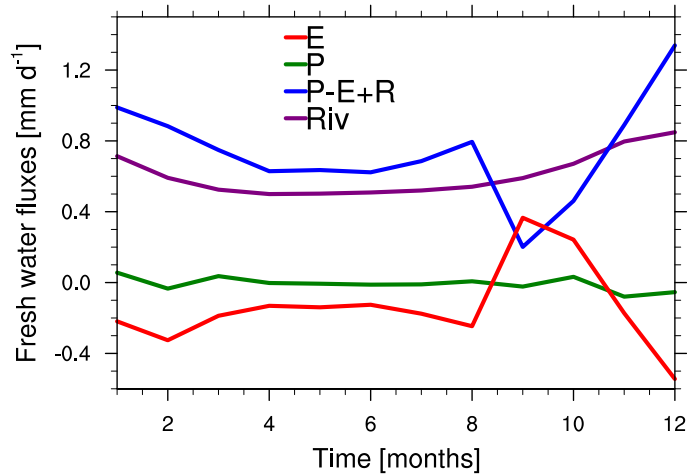


Figure 3.1: Monthly climatology of the freshwater fluxes anomalies, Nil-9000 vs. CTRL in mm d^{-1} .

To make our results comparable with those from the existing modelling studies, we first analyse the freshwater fluxes of our simulation. The addition of $9000 \text{ m}^3 \text{ s}^{-1}$ causes a strong disturbance of the freshwater budget of the Eastern Mediterranean which reaches the value of -1.5 mm d^{-1} against -1.97 mm d^{-1} in the baseline simulation and -2.15 mm d^{-1} in the CTRL simulation (present-day climate). Fig. 3.1 displays the anomalies for each component of the freshwater fluxes over sea averaged for the eastern basin, in comparison with the CTRL simulation. The precipitation changes compared to the present-day climate are negligible. The strengthening of the precipitation over the northern borderlands of the Eastern Mediterranean, which has been postulated in previous studies based on proxy data (e.g. Rohling, 1994; Schmiedl et al., 2010), is not simulated by the global model as it does not display substantial changes in runoff from the northern rivers.

The mean evaporation is reduced by 0.04 mm d^{-1} (2.95 mm d^{-1} in Nil-9000 vs. 2.99 mm d^{-1} in CTRL), but this signal displays a strong seasonality with a winter decrease of up to 0.5 mm d^{-1} , and an increase in late summer and autumn up to 0.4 mm d^{-1} , reflecting the effect of the changes in insolation.

The freshwater flux from the rivers increases by 0.62 mm d^{-1} and 78 % of the increase is due to the artificial increase of the Nile runoff with a contribution of 0.47 mm d^{-1} . The simulated net freshwater fluxes (P-E+R) increases by 0.67 mm d^{-1} .

To compare the amplitude of our perturbation with the changes prescribed in the studies from Myers and Haines (2002), Myers et al. (1998) and Meijer and Dijkstra (2009), we convert the additional freshwater input in terms of percentage of changes in the P-E+R flux with the 9K-base as reference. The artificial addition of $9000 \text{ m}^3 \text{ s}^{-1}$ through the Nile is equivalent to a mean increase by 24 % of the P-E+R flux with a maximum increase by 54 % occurring in spring and a minimum increase by 13 % occurring in autumn. This change in P-E+R flux is larger than the change required to obtain a collapse of the deep circulation according to Myers and Haines (2002).

3.4.1 Circulation and hydrography changes

3.4.1.1 Changes at the surface

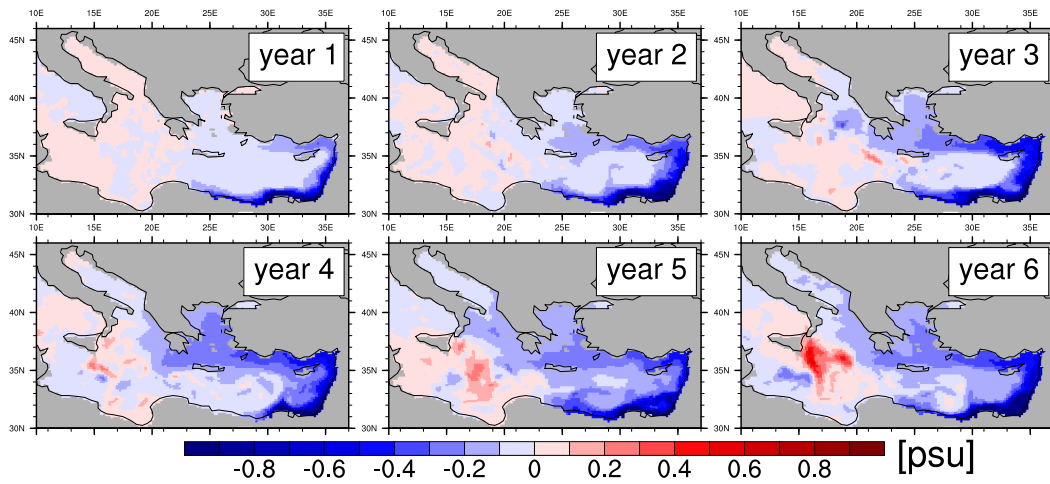


Figure 3.2: Yearly mean surface salinity anomalies (Nile-9000 vs. 9K-base) of the first six years of the perturbation experiment.

The development of the surface salinity anomalies for the first six years of the perturbation experiment is displayed in Fig. 3.2. Due to the addition of

freshwater from the Nile, a decrease in salinity is simulated along the main stream path. The modified Atlantic water coming from the west is joining the freshwater discharged by the Nile. This water mass flows counterclockwise along the Levantine coast until the Aegean inducing fresh anomalies along the way. In the first years, a spread of the fresh anomaly is also simulated westward, due to an intensification of the clockwise gyre in the extreme South Levantine, which entrains a part of the fresh outflow along the coast toward the west. From the third year on, the freshening starts affecting the Adriatic. Although the general circulation at the surface remains mainly unchanged, little shifts of some gyres might explain the salty anomalies. These are particularly found in the western Ionian, where a tiny displacement of the main Atlantic jet can induce an interface of positive/negative salinity anomaly. The presence of such anomalies due to a small shift of the currents is only obvious in regions with strong gradients. This is the case in the western Ionian, where a strong front is established between the incoming modified surface Atlantic water, which is relatively fresh, and the Ionian water, which displays a much higher salinity. Taking into account that the Atlantic water keeps unmodified hydrographic properties in Nil-9000 (vs. 9K-base), and that Ionian water becomes fresher, a shift of the front towards the south leads to positive salinity anomalies between the new and the former front.

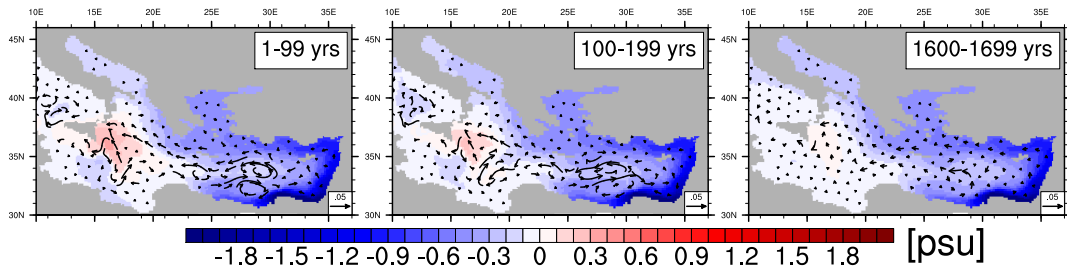


Figure 3.3: Anomalies (Nile-9000 vs. 9K-base) of the surface salinity (colours) and the near-surface circulation field (arrows) at 27 m depth averaged over 1-99 years, 100-199 years and 1600-1699 years after the start of the perturbation. Only a subset of vectors has been plotted.

Fig. 3.3 depicts the same quantity as 3.2 but for later periods. The mean anomalies of the circulation at 27 m depth is overlaid. The salinity anomalies

at 27 m depth averaged over the second century of perturbation (time period 100-199 years) do not differ much from those in the 17th century after the start of the perturbation (time period 1600-1699 years), an equilibrium is thus reached within 100 years for that depth. However, this is not true for both the Ionian and Tyrrhenian Seas, where the surface salinity is still drifting after 2 centuries. Concerning the sub-surface circulation at 27 m, we can infer from the anomalies that the circulation is almost identical to that of the baseline after 17 centuries of perturbation, except for the Rhodes Gyre feature, which becomes stronger in the perturbation experiment Nil-9000.

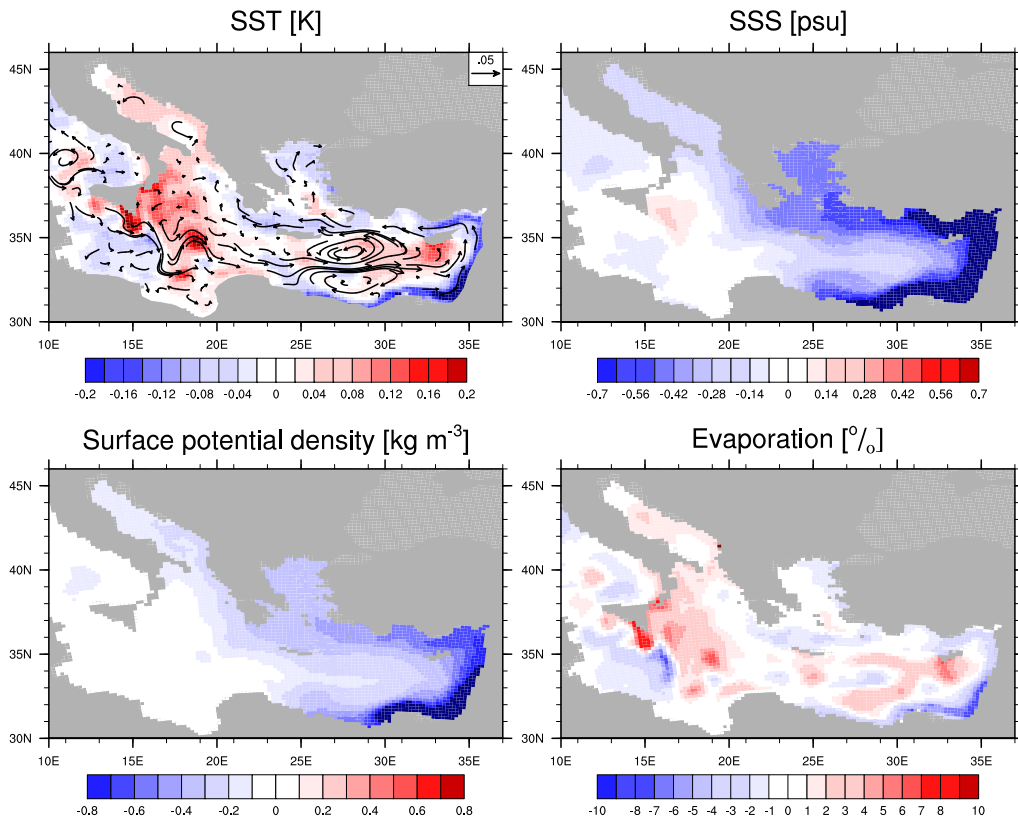


Figure 3.4: SST, SSS and surface potential density anomalies (Nil-9000 vs. 9K-base) averaged over the years 400-499. The near-surface circulation field at 27 m depth for Nil-9000 is overlaid as arrows on the SST anomalies. Only a subset of vectors has been plotted.

To analyse the changes in surface stratification, Fig. 3.4 displays anomalies of SST, SSS, surface potential density and evaporation after 5 centuries of perturbation. Differences in SST between Nil-9000 and 9K-base correlate well with the variation of freshwater input: colder surface waters are modelled along the eastern Mediterranean coast, on the path of the fresher flow. The warmer Adriatic water is feeding the central Ionian where it joins the Atlantic water and enters the Levantine basin, being trapped by the gyre west from the mouth of the Nile. The warm anomalies found in the Ionian are responsible for an increased evaporation and thus partly contribute to the positive salinity anomalies in this region, whereas the rest of the basin shows surface water fresher than the baseline. A complementary explanation for the low anomalies in surface salinity simulated in the western Ionian Sea is that this part of the basin is dominated by the Atlantic water, which enters the eastern basin with unmodified salinity properties in comparison to the baseline. As mentioned before, the positive bias close to Sicily is also related to a small shift of the salinity front. The surface density does not change in the Ionian Sea because the changes in surface salinity compensate the changes in surface temperature. Everywhere else, the potential density decreases at the surface, mainly related to the freshening; this leads to a strengthening of the surface stratification.

3.4.1.2 Changes at depth

Because the Adriatic Sea is the main location for deep water formation, we investigate the hydrographic changes occurring in this basin as a consequence of the freshwater perturbation. Fig. 3.5 represents a transect of temperature, salinity and potential density anomalies zonally averaged over the Adriatic basin. The shallow northern sub-basin of the Adriatic (between $41.5^{\circ}N$ and $44^{\circ}N$) is filled with water up to 0.12 K warmer, whereas in the deeper southern sub-basin (between $39^{\circ}N$ and $41.5^{\circ}N$), the warm layer is restricted to the upper 100 meters and a small cooling is modelled at intermediate depths. The freshening of the Adriatic is homogeneous over the entire water column with negative anomalies up to 0.3 psu. This results in a relatively homogeneous reduction by roughly 0.2 kg m^{-3} of the water mass density in the basin.

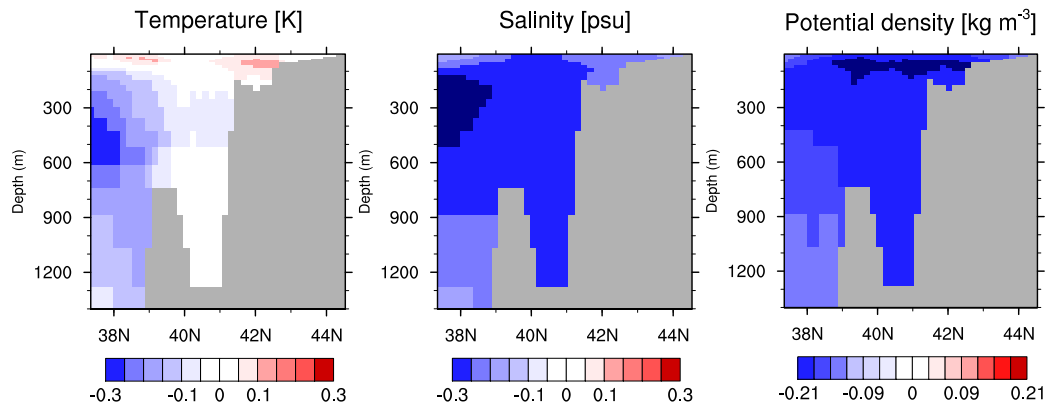


Figure 3.5: Zonally averaged transect over the Adriatic. Temperature, salinity and potential density anomalies (Nil-9000 vs. 9K-base) are represented, averaged over the years 400-499 of the experiment.

With respect to the hydrographic changes occurring in the main basin (here, we exclude both Aegean and Adriatic), the meridionally averaged west-east transect (Fig. 3.6) displays a strong west-east potential density anomalies gradient in the upper part of the water column. The largest negative salinity anomalies are found in the upper 100 meters of the western side of the Eastern Mediterranean, but excluding this feature, the strongest anomalies are found in average between 200 and 400 m depth and are fed by the fresher water flowing out the Adriatic and the Aegean at that depth. It seems that the perturbation has triggered the replacement of the warm and salty LIW with the formation of a new kind of water mass, which spreads in the eastern basin at intermediate depths, with cold and fresh hydrographic properties.

As seen in Fig. 3.2, the salinity changes at the surface happen within few decades. However, the salinity changes at greater depth are happening over a much different time scale. This is clearly depicted in Fig. 3.8, which displays the time evolution of salinity anomalies averaged over the eastern basin for different layers of the water column and for the entire duration of the experiment. Because the changes in density for the surface layers mainly happen during the first century, a zoom over this period is displayed in Fig. 3.7. It takes about 40 years to reach a stabilized salinity anomaly averaged

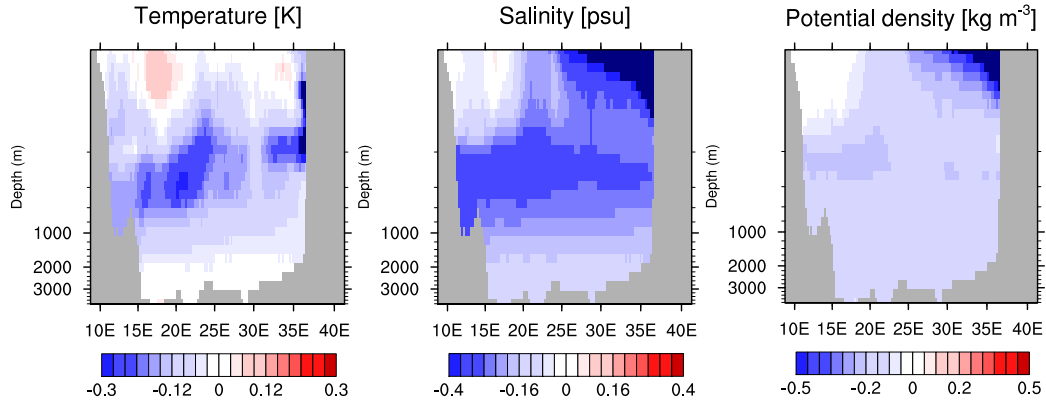


Figure 3.6: Meridionally averaged west-east transect of temperature, salinity and potential density anomalies (Nil-9000 vs. 9K-base), averaged over the years 400-499 of the experiment. The Aegean and the Adriatic are excluded. Note that the depth scale is non-linear.

over the eastern basin in the 0-32 m and 32-150 m layers. This lag is delayed to roughly 100 years for the intermediate layer 150-750 m. After 600 years of simulation, the averaged salt content of the layers 750-1000 m reaches a low-drifting value. The slope of the drift remains sharp for the layers 1000-1800 m and 1800 m-bottom and starts stabilizing after 1000 years.

This huge difference in the time scales of adjustment to the salinity anomalies between the surface/intermediate and the deep layers arises because the vertical circulation is restricted to the upper 800 m of the water column in the Nil-9000 experiment. This reduction of the vertical circulation cell, which becomes much shallower, occurs because the buoyancy loss of the surface water, which usually drives the winter convection, is lowered by the addition of freshwater. The freshening strengthens the stratification by creating a stronger density gradient in the upper water column. The convective events are thus reduced, and the deep circulation is strongly weakened. Due to the freshwater perturbation, the vertical circulation cell is active for a depth range between the surface and 800 m, where the salinity anomaly quickly stabilizes through advection. The spread of the salinity anomalies at greater depth is mainly driven by diffusive processes, because this water mass stagnates, and therefore needs a much longer time to adjust to the freshening.

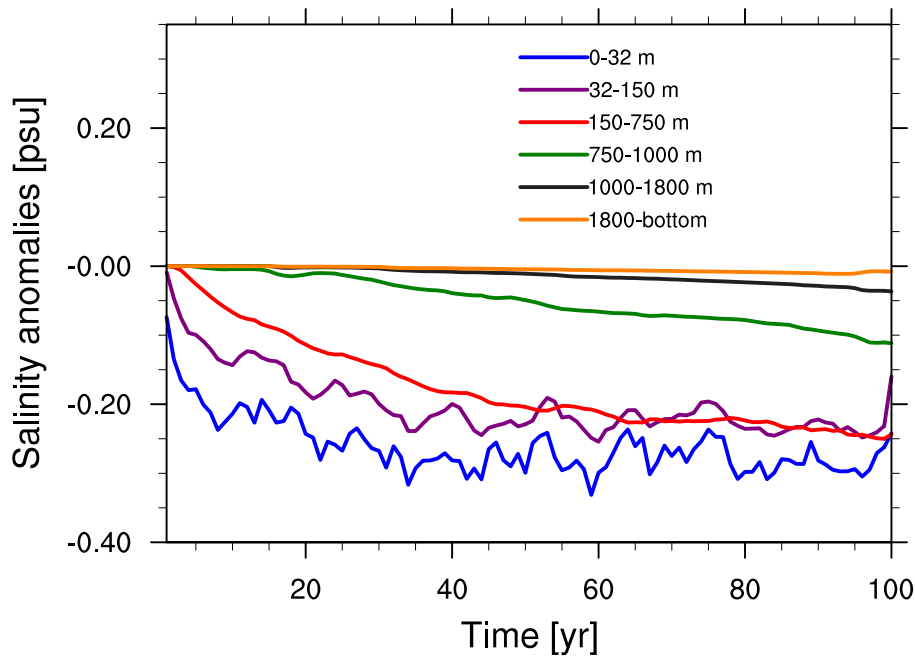


Figure 3.7: Time series of salinity anomalies (Nil-9000 vs. 9K-base) in chosen layers of the water column for the first 100 years of the perturbation.

We calculate the residence time of the water contained in the upper 800 m of the water column in the eastern basin, by dividing their volume with the transport of water flowing out at the Strait of Sicily. This water mass spends in average 30 years in the eastern basin. This order of magnitude is consistent with the time scale of adjustment to changes in salinity in the surface and intermediate layers, which we assess to be 40 and 100 years respectively.

After 17 centuries of perturbation, the eastern basin reaches an averaged salinity 0.3 psu lower than in the baseline simulation (Fig. 3.8). However, the water layer between 32 and 150 m of depth shows a different behaviour than the other layers with negative anomalies of 0.22 psu only. Fig. 3.9 depicts salinity anomaly profiles for different locations of the Eastern Mediterranean and reveals that a “jump“ of lower salinity anomalies is simulated in the profiles of the Levantine basin between 20 and 200 m of depth, depending on the location. The profile are relatively homogeneous in the Aegean and in the Adriatic, which are two basins where the mixing is more active through advection. In the Ionian basin, the surface salinity anomalies are the lowest,

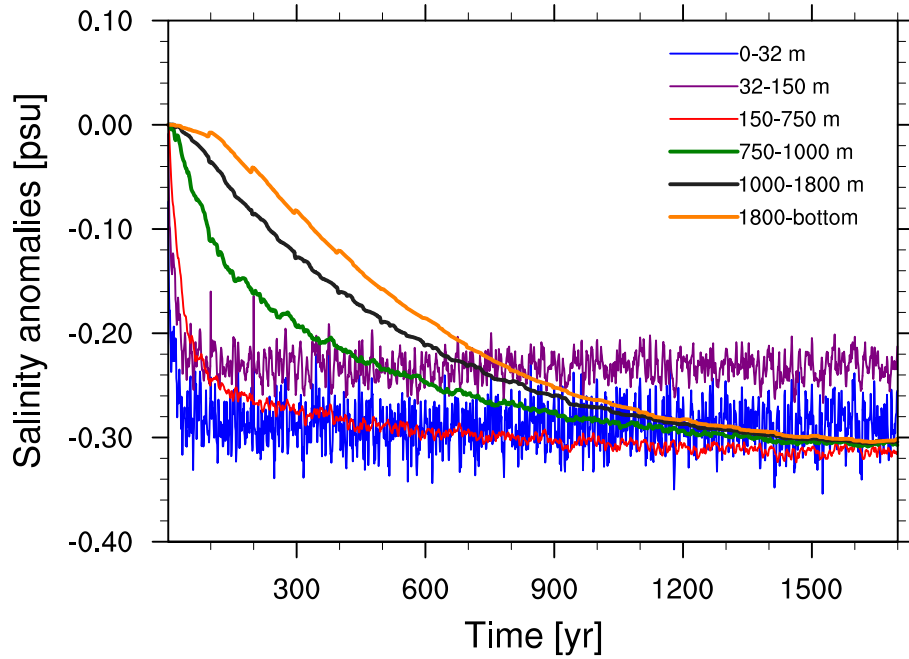


Figure 3.8: Time series of salinity anomalies (Nil-9000 vs. 9K-base) in chosen layers of the water column for the whole duration of the perturbation experiment.

because this basin is located the farthest from the location of the perturbation, along the main circulation path. So the fresher anomalies are already quite diluted when the “modified” fresher surface water reaches the Ionian basin. Moreover, the western side of the Ionian Sea is dominated by the intrusion of Atlantic water, whose salinity is not affected by the freshening from the Nile. Concerning the jump with lower salinity anomalies in the Levantine basin, this corresponds to a tongue of “less fresher water” compound of a mix of surface Ionian water and surface modified Atlantic water which slowly penetrates in the Levantine basin. This is well depicted in Fig. 3.10, which shows a vertical transect across the southern Ionian and Levantine basins. The surface water from the Ionian characterised by lower salinity anomalies enter the Levantine basin and sink below the lighter surface Levantine water along the way.

Nevertheless, the timing of the changes in salinity at depth happens to be very different between the sub-basins of the Eastern Mediterranean. It

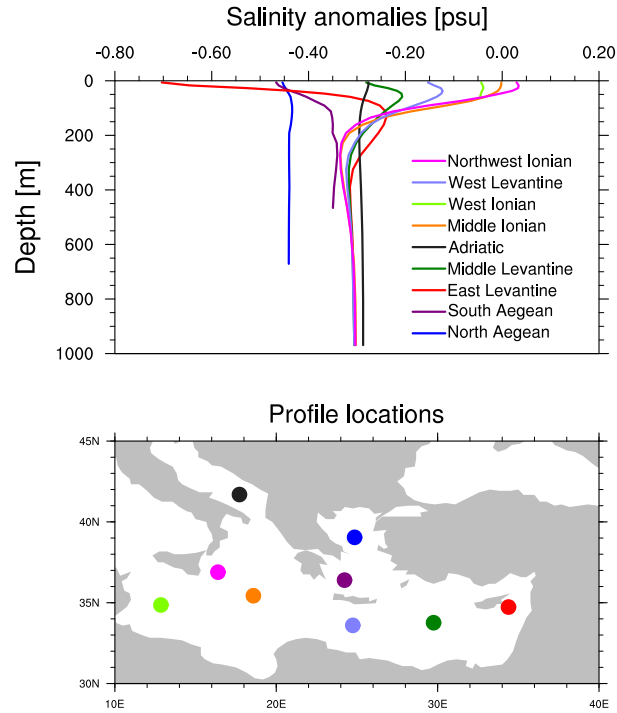


Figure 3.9: Salinity anomalies profiles (Nil-9000 vs. 9K-base) at different locations of the eastern basin, averaged over the years 1600-1699 of the experiments.

takes for example 20 years for the intermediate Aegean intermediate water (150-600 m) to reach a stable salinity, 200 years for the Adriatic intermediate water, and more than 500 years for both Ionian and Levantine intermediate layers. The basins with smaller volume and more active vertical circulation adapt quicker to the hydrographic changes.

3.4.2 Vertical stratification

The longest time scale of adjustment in the Eastern Mediterranean is that of the deeper layer salinity. The volume of eastern basin deep water is much larger than the volume of deep water formed each year. This reservoir effect strongly strengthens the stratification built after a rapid change in boundary conditions as it has been imposed in the Nil-9000 experiment. Because of their lower residence time, the density of surface water quickly reaches a

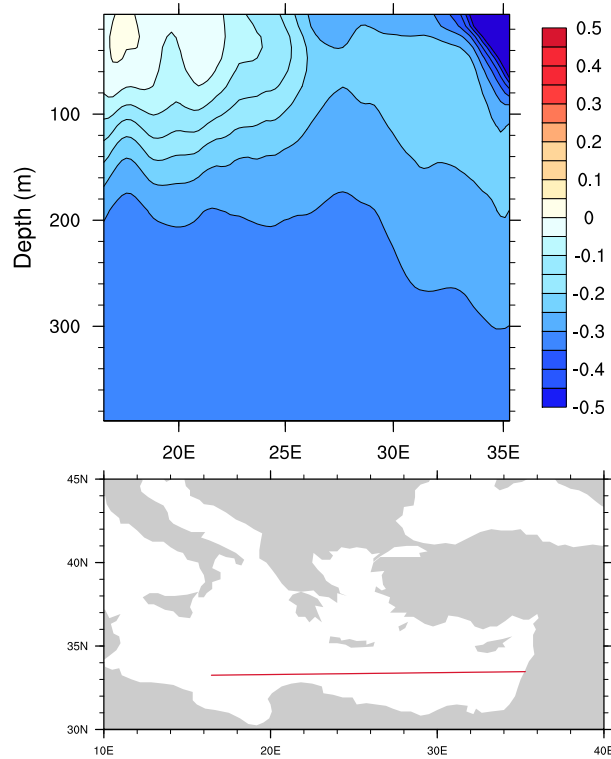


Figure 3.10: Horizontal transect of salinity anomalies (Nil-9000 vs. 9K-base) averaged over the time period 1600-1699.

lower equilibrium value, whereas the density of the deeper water layer still remains at the former higher density value. This provides a strengthening of the density gradient, thus the enhancement of the stratification.

To assess the impact of the freshwater perturbation on the vertical stratification of the water column, an Index of Stratification (IS) is calculated (in $\text{m}^2 \text{s}^{-2}$, see Beuvier et al., 2010; Herrmann et al., 2008; Somot, 2005; Lascaratos, 1993). This index has been used in previous studies to investigate the preconditioning of the convection by looking at the changes in the vertical stratification. It corresponds to the loss of buoyancy that must be provided to the stratified water to induce a convection event up to the bottom of the sea. The lower the index, the more likely is deep convection to occur, inducing thus the ventilation of deeper water. The Index of Stratification is calculated for the month of November (before the winter convection), for

each model grid point (i, j) using the following formula:

$$IS(i, j, h_{bot}) = \int_0^{h_{bot}(i, j)} N^2(i, j, z) z \, dz, \quad (3.1)$$

where z is the depth, h_{bot} is the depth at the bottom and N is the local Brunt-Vaisala frequency: $N^2 = \frac{g}{\rho} \frac{\partial \rho}{\partial z}$.

This calculation is performed for each grid point (i, j) characterised by its local maximal depth h_{bot} . A basin average of IS is made for the Aegean, the Levantine, the Ionian and the Adriatic basins. Fig. 3.11 displays the difference of this quantity between the Nil-9000 experiment and 9K-base.

The stratification index in the Adriatic remains identical to the one of the baseline simulation. In this basin, even if the surface freshening originated a strong surface stratification at the very beginning, preventing thus the deep convection, the intermediate/deep waters of the Adriatic are evacuated toward the Ionian through lateral advection as a compensation flow for the surface water coming from the Ionian into the Adriatic. So the deeper water is quickly replaced by fresher water from the surface. The vertical density gradient of the Adriatic is therefore much lower than in the other sub-basins and its hydrographic properties are much more homogeneous. For this reason, the winter convection can not be prevented for a long time. There is thus only a small reservoir effect in the Adriatic: all the water layer rapidly reach a similar salinity anomaly, making the stratification relatively identical to the one before the perturbation although the averaged salt content is lower. In the Aegean, the stratification shortly increases after the beginning of the perturbation, but within 20 years, the strong gradient created by the low surface salinity vanished rapidly through mixing. The Ionian basin and the Levantine basin both show a sharp increase of the stratification during the first century. The IS value reaches a maximum in the second century of the perturbation experiment, but it continuously decreases thereafter; the stratification index becomes stable after roughly 1000 years of perturbation for the Levantine and surprisingly, the stratification anomaly of the Ionian becomes negative after 900 years but the drift is still very small.

The three bottom panels of Fig. 3.11 represent a 2D view of the stratification anomalies (Nil-9000 vs. 9K-base) for three different time periods:

100-199 years when the stratification increase is the strongest, 400-499 years during the decrease phase, and 1600-1699 years which correspond to the end of the perturbation. The strong stratification (up to 70 % increase) that has built in the Ionian and the Levantine slowly weakens, and negative anomalies of IS slowly establish in western Ionian and spread toward the Levantine with the time. The stratification starts eroding because the eastern basin has reached a quasi-equilibrium state in terms of salt content, the deepest layers did slowly adjust to the changes in salinity in such a way that the difference in salinity anomalies between the surface and the deepest part has decreased, thus diminishing the density gradient initially created by the perturbation.

Negative anomalies of IS are modelled in the Ionian towards the end of the perturbation experiment because the deeper layer have reached a rather stable salinity anomaly of 0.3 psu which is greater than the anomaly of 0.05 psu reached in the surface layers. This reduced the density gradient compared to the 9K-base experiment, leading to a decrease of the stratification index.

3.4.3 Mixed layer depth and sources of dense water

We confirm that the formation of Levantine Intermediate Water (LIW) is extremely sensitive to enhanced Nile runoff (e.g. Myers, 2002). Whereas the deep water convection in the Adriatic basin is mainly driven by heat loss, the LIW formation is highly reactive to changes in salinity. Fig. 3.12 represents a zonally averaged transect of the mean salinity in the eastern basin. In the 9K-base experiment, the presence of LIW is noticed with a water mass of high salinity ($39.5\text{m}^3\text{s}^{-1}$) between 300 and 700 m of depth. This water mass is absent in the perturbation experiment Nil-9000.

In the baseline simulation, LIW is formed east from Crete, as depicted in Fig. 3.13, which displays a winter mixed layer deeper than 200 m in this area. This intermediate water formation is located directly on the path of the water freshened by the Nile runoff. In the perturbation experiment Nil-9000, the freshening from the Nile has been little diluted when the surface flow reaches the location where LIW would be formed (Fig. 3.13). The formation of intermediate water is thus prevented by the decrease in surface density. The intermediate water formation in the North Aegean is not affected by the

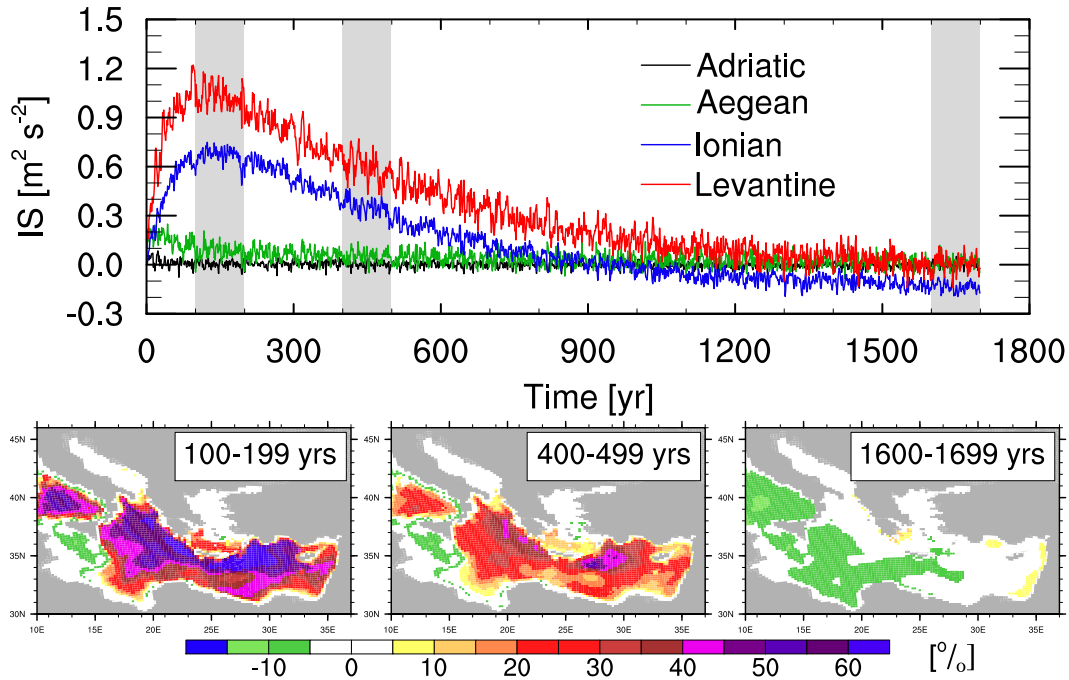


Figure 3.11: Time series of stratification index anomalies (Nil-9000 vs. 9K-base) in November for the Adriatic, the Aegean, the Ionian and the Levantine basins. The grey shading shows the position of each 2D bottom panel on the time series, where percentage of IS changes are represented.

perturbation, however, the pattern of winter mixed layer depth between 200 and 400 m is extending southward in the Ionian, because the surface water of the northwest Ionian does not experience a density loss (Fig. 3.4), thus the surface stratification does not increase.

In Fig. 3.14, we assess the volume of dense water formed in winter by multiplying the March mixed layer depth with the area of the cell. We consider the percentage of changes in the volume of dense water formed in the Adriatic, the Aegean and the Levantine Seas compared with the baseline. To filter out the strong interannual variability signal, we plot the 10-year running mean. The Adriatic basin, the main location for the deep water formation, forms 5% less deep water at the very beginning of the perturbation. However, after already 200 years, the volume of dense water formed in March becomes very similar to the baseline. In the Aegean, the volume of dense water

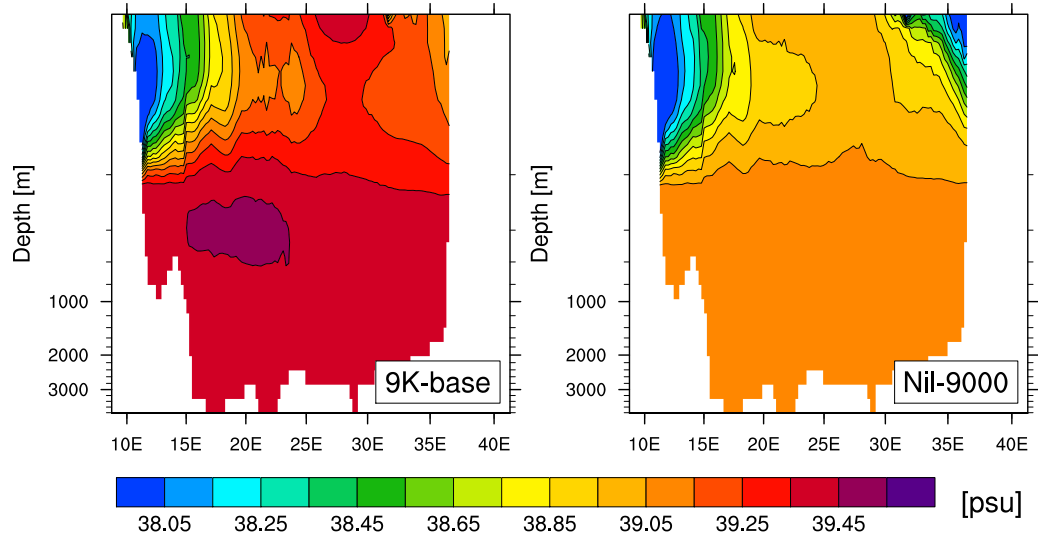


Figure 3.12: Zonally averaged transect of annual mean salinity [psu] averaged over the years 1300-1399 for 9K-base and Nil-9000. Because we aim to identify the presence/absence of LIW, the Aegean and the Adriatic were excluded before performing the zonal average. Note that the depth scale is non-linear.

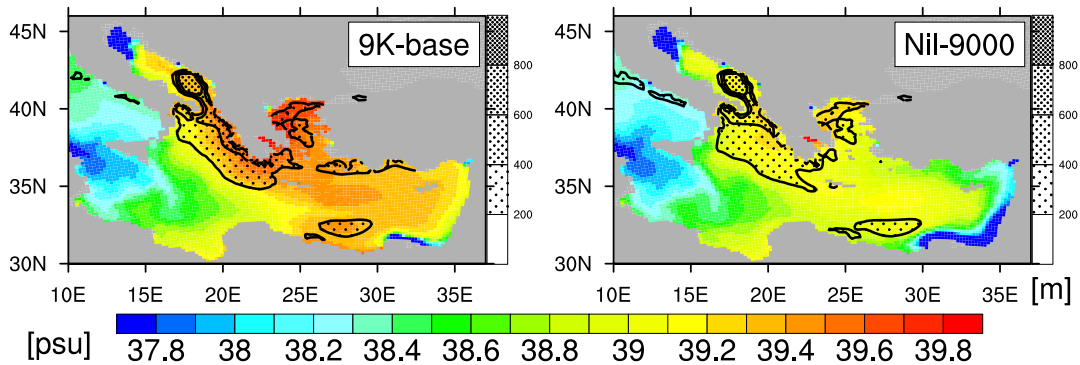


Figure 3.13: Surface salinity [psu] and March mixed layer depth [m] averaged over the years 1300-1399 of the experiment.

decreases and stabilizes with the value of -11%. Finally, the Levantine shows the strongest change with a stable decrease of -22%. This location is the closest of the origin of the perturbation, thus the most affected. Not shown here, the Ionian basin forms more dense water than in the baseline (increase

of 6%), as can be inferred from the extended winter mixed layer depth in this area (Fig. 3.13).

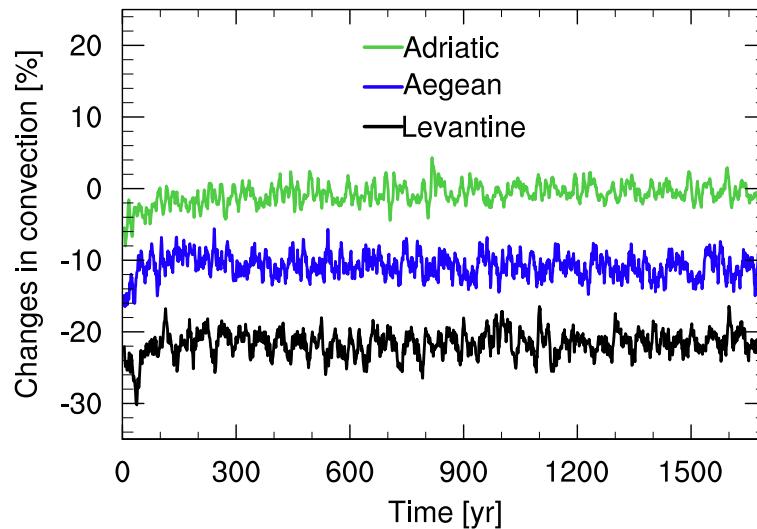


Figure 3.14: Time series of changes in convection (Nil-9000 vs. 9K-base) for the Adriatic, the Aegean and the Levantine Seas. The 10-year running mean is displayed.

As a conclusion, the freshwater perturbation induces a rearrangement of the water masses. The principal locations of deep/intermediate water formation remain the same: the Adriatic and the North Aegean. However, the warm and salty intermediate water stops forming in the North Levantine/southeast Aegean and is replaced by a new intermediate water formation stretched over the North Ionian (Fig. 3.13), where colder and fresher water sinks at a depth interval of 200-400 m (Fig. 3.6).

3.4.4 Zonal and meridional overturning circulation

The Mediterranean thermohaline circulation (MTHC) is driven by salinity and temperature differences that induce a vertical circulation in the basin. This vertical circulation cell is triggered by deep and intermediate water formation, which occurs in the Gulf of Lions for the Western Mediterranean, and in the Adriatic and Aegean basins for the Eastern Mediterranean. The formation of LIW also contributes to this vertical circulation. To understand

how the enhanced Nile outflow affects the circulation in the Mediterranean, we compute the overturning stream functions in Sv for different basins of the Mediterranean.

Whereas the meridional overturning stream function (MOF) is commonly used to assess the strength of the Atlantic thermohaline circulation, the zonal overturning stream function (ZOF) is rather calculated for the Mediterranean. The ZOF has been used by Myers and Haines (2002) in their study to assess the stability of the MTHC, and later by Somot et al. (2006) to study the changes of the MTHC under climate change scenarios. Following this method, we first calculate the zonal overturning stream function of the Mediterranean. The ZOF is a meridional integration from the south (y_S) to the north (y_N) of the zonal velocity $u(x, y, z)$, which is then integrated from the bottom of the sea $h_{bot}(x, y)$. This stream function is given by the following equation:

$$ZOF(x, z) = \int_{h_{bot}}^z \int_{y_S}^{y_N} u(x, y, z) \, dy \, dz. \quad (3.2)$$

Our model grid is slightly curvilinear (Fig. 2.1) making the term “zonal” not exactly appropriate because the integration is done over the y axis, which is slightly rotated. However, the comparison with ZOF calculated with vertical velocities (thus not affected by the small rotation of the coordinates) has shown that the results are not changed if calculated as displayed in Eq. (3.2).

Fig. 3.15 shows the ZOF for the baseline experiment and the Nil-9000 experiment. In the baseline, the MTHC is characterised by two main circulation cells. The first cell covers both the western and the eastern basins, and has a clockwise circulation with a main path of Atlantic surface water travelling toward the east, and Levantine intermediate water travelling from the east to the west. A maximum of 1.0 Sv is found at subsurface depth, between 100 and 200 m depth. Located in the eastern basin, the second cell shows a counterclockwise vertical circulation which is much weaker with a maximum of 0.2 Sv. This cell corresponds to the circulation of Eastern Mediterranean Deep Water toward the extreme east of the basin, this being compensated by a subsurface flow of Levantine Intermediate Water from the

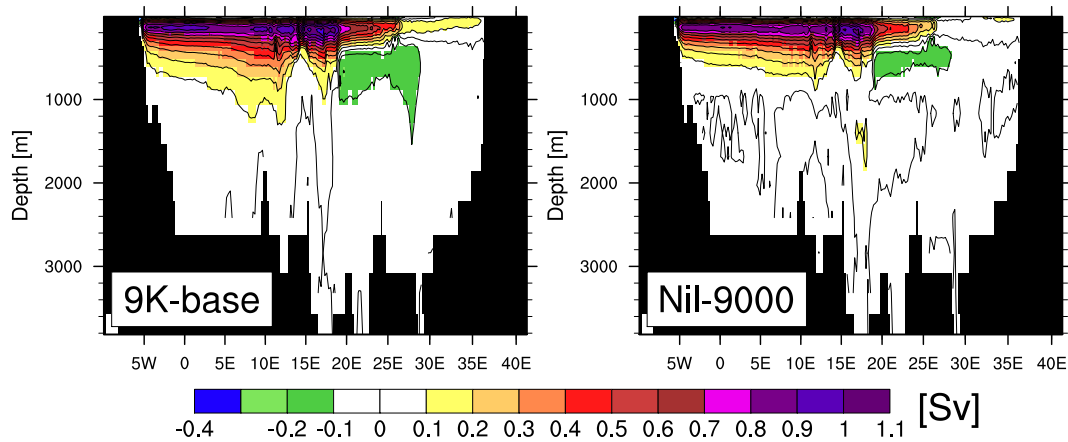


Figure 3.15: Zonal overturning stream function integrated over the entire Mediterranean basin. It has been calculated on the basis of mean velocity field of years 400-499. The left panel represents the baseline experiment, the right panel represents the Nil-9000 experiment.

northern Levantine toward the west.

However, the MTHC also has meridional components. It is for example useful to compute the MOF to assess the formation of Adriatic deep water and its penetration in the Ionian basin. This quantity is displayed in Fig. 3.16 and shows the formation of ADW in the South Adriatic (between $40^{\circ}N$ and $42^{\circ}N$) with a value of $0.35 Sv$. South of the Strait of Otranto (south of $40^{\circ}N$), another vertical circulation cell represents the cascading of ADW in the Ionian basin where it mixes and becomes EMDW. Another local MOF can be calculated for the Aegean Sea to define the formation of intermediate water in this region. Fig. 3.18 displays the MOF for the Aegean Sea. The formation of intermediate water is modeled in the Aegean basin with a transport of $0.15 Sv$ in the northern part (north of $38^{\circ}N$) and $0.3 Sv$ in the southern part (between $36^{\circ}N$ and $38^{\circ}N$).

How does the freshening from the additional Nile runoff affect the different branches of the Mediterranean thermohaline circulation? To answer this question, we compare the Nil-9000 perturbation experiment and the baseline after 450 years (averaged over the years 400-499), for the ZOF of the full basin (Fig. 3.15), the MOF of the Adriatic (Fig. 3.16) and the MOF of the Aegean (Fig. 3.18). In Nil-9000, the ZOF is weaker than in 9K-base, both deep ver-

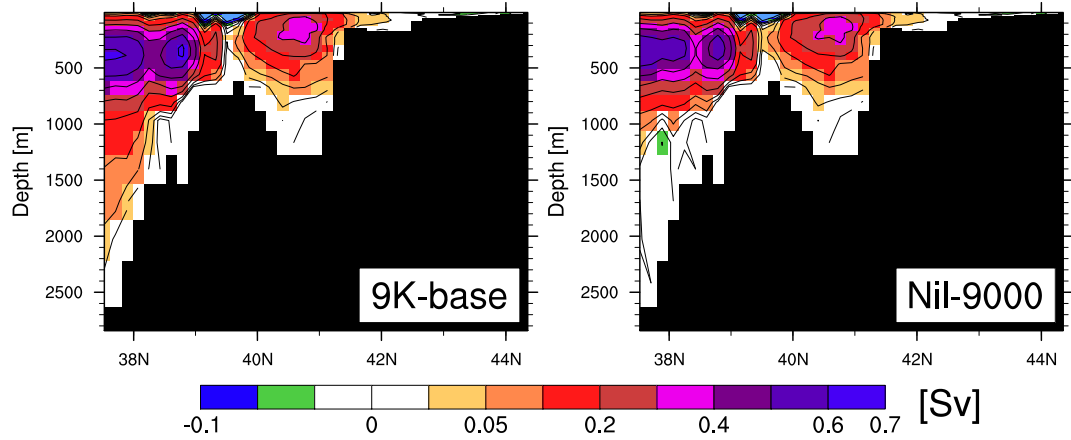


Figure 3.16: Meridional overturning stream function integrated over the Adriatic Sea and the northern part of the Ionian Sea. It has been calculated on the basis of mean velocity field of years 400-499. The left panel represents the baseline experiment, the right panel represents the Nil-9000 experiment.

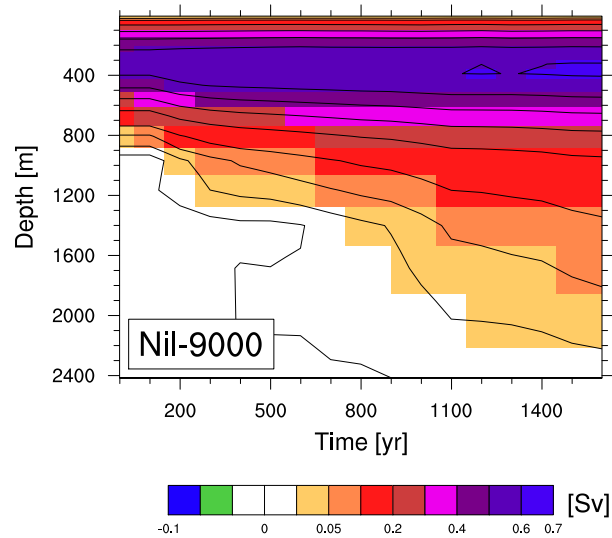


Figure 3.17: Time series based on the 100-year averaged of the meridional overturning stream function integrated over the Adriatic Sea and the northern part of the Ionian Sea, at $38.5^{\circ}N$, for the Nil-9000 experiment.

tical circulation cells become shallower showing a circulation restricted to the upper 800 meters. The eastern cell seems especially affected and remains at a maximum depth of 800 meter instead of 2000 meters as in 9K-base. The interruption of the LIW formation is depicted in the upper clockwise cell, which becomes limited to $25^{\circ}E$ eastward and displays a strength 0.2 Sv weaker. The MOF of the Adriatic basin remains unchanged in the southern Adriatic in case of additional Nile runoff, depicting that the convection still occurs. However, due to the absence of preconditioning from LIW import, the Adriatic deep water no longer sink to the bottom of the Ionian: the cascading of ADW south from Otranto is thus reduced to a maximum depth of 1000 m (vs. 2000 m in the baseline experiment) and the vertical circulation cell south of Otranto slightly weakens. This state is however transitional, Fig. 3.17 shows the slow recovery of the deep cascading through time, the vertical circulation cell compound of deep water flowing out of the Adriatic and surface water flowing into the basin deepens and strengthens, reaching values very close to the state of the baseline after 1600 years. Concerning the Aegean Sea, the vertical circulation cell of the northern part of the basin remains unchanged, whereas the one of the southern part slightly weakens with values of 0.25 Sv (Fig. 3.18), reflecting the reduced formation of Levantine Intermediate Water.

As it has been mentioned before, this general “weakening” and “shallowing” of the Mediterranean thermohaline circulation, due to the strengthening of the stratification is not maintained through time. The figures which have been presented in this subsection correspond to averaged values over the years 400-499 of the experiment. After 1700 years of experiment, the system has partially recovered. This can be inferred from Fig. 3.19, which shows that both main vertical circulation cells have started to become deeper, even if the strength of the transport remains similar to the time period 400-499 years, thus still weaker than the baseline.

3.4.5 Water aging

To assess the reduction in ventilation of the deep water, we incorporated an age tracer in the model, which indicates the apparent age of the water in each grid cell of the model. This tracer has a fixed concentration at the

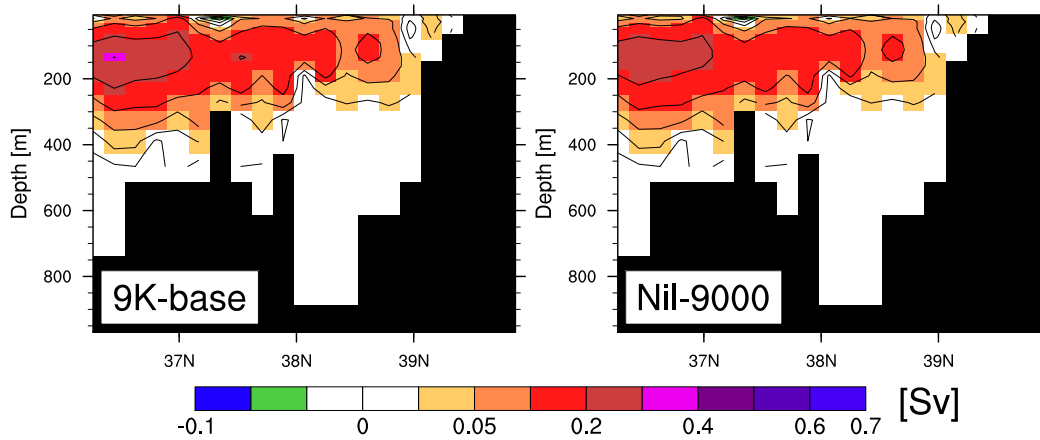


Figure 3.18: Meridional overturning stream function integrated over the Aegean Sea. It has been calculated on the basis of mean velocity field of years 400-499. The left panel represents the baseline experiment, the right panel represents the Nil-9000 experiment.

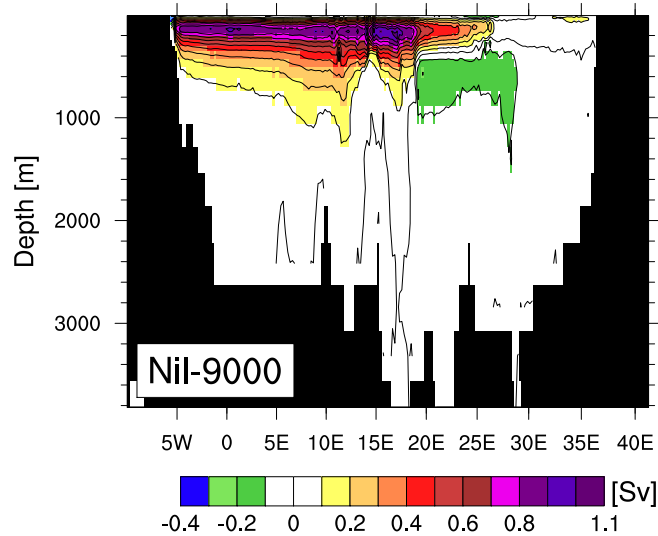


Figure 3.19: Zonal overturning stream function integrated over the entire Mediterranean basin for the Nil-9000 experiment. It has been calculated on the basis of mean velocity field of years 1600-1699.

surface, and decays below the first water layer with a 50-year e-folding time. It is advected and diffused in the same way as temperature and salinity. The

advantage of such a tracer is that no long spin-up is needed to reach a stable age of the water masses. It is however very sensitive: for example, when a big volume of old water is mixed with a very little volume of young water, the mean age of the water decreases considerably, preventing the water of reaching an age older than 200 years.

Fig. 3.20 represents the age of water averaged over the eastern basin for each model layer, and its evolution through the time of the experiment. The baseline experiment shows a maximum water age of 120 years at a depth between 2000 m and 3000 m. For the 9K-base, Fig. 3.20 shows relatively young water (< 10 years old) in the first 250 m of the water column, which is well mixed. Until 1200 m of depth, the water becomes gradually older up to 70 years old. Below that depth, a 100-year cycle is visible. This cycle corresponds to the 100-year atmospheric forcing repeated in a loop. In some years of the cycle, a strong cooling happens in winter leading to strong deep water convection in the Adriatic Sea, this explains the surge of younger water in the bottom layers of the eastern basin.

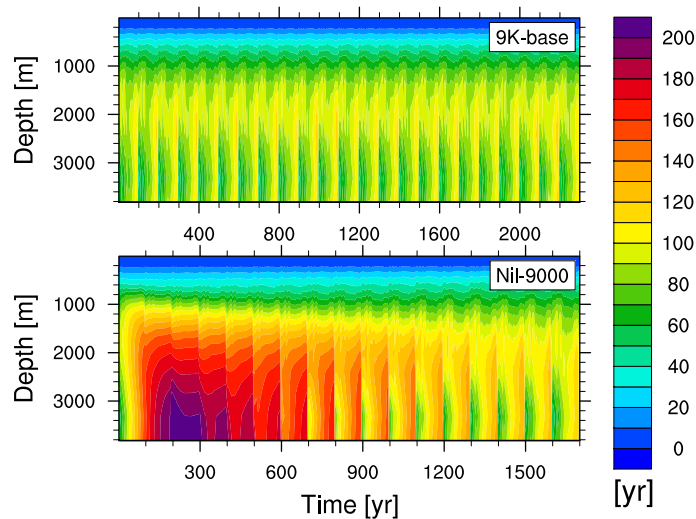


Figure 3.20: Time series of the age of water averaged over the Eastern Mediterranean for different depths. The top panel represents the 9K-base experiment, the bottom panel represents the Nil-9000 experiment.

In the Nil-9000, from the beginning of the experiment on, the water below 1000 m depth becomes older, reaching an age older than 200 years in the

deepest layers. During the first 300 years, a little jump is noticed with a periodicity of 100 years, showing that the young dense water created by some convective events tries to sink. However, at that time of the experiment, the stratification is still strong enough to prevent this intrusion. Later on, the stratification starts eroding through diffusion and mixing processes allowing the newly formed dense water to penetrate deeper (Fig. 3.20). At the end of the experiment, the water age of the deeper layer is relatively close to the one of the 9K-base experiment.

3.4.6 Strait dynamics

To better assess the processes involved in the sudden intrusion of dense water below 1000 m depth, we compare the potential density of the water outflowing from the convection sites with the potential density of the main eastern basin (Ionian/Levantine Seas) at 1000 m and 2000 m of depth. We thus consider the density of the deep water outflowing into the Ionian Sea from the Adriatic through the Strait of Otranto, and from the Aegean through the Strait of Antikithira (western strait of the Cretan Arc). We also consider the density of the deep water outflowing into the Levantine from the Strait of Kassos and the Strait of Karpathos (two straits on the eastern side of the Cretan Arc). Fig. 3.21 shows the evolution of the yearly averaged potential density at sill depth for the four straits, and at 1000 m and 2000 m in the Ionian and Levantine basins, both presenting the same density properties at those depths. In the 9K-base simulation, the potential density of the Cretan straits never exceeds the density of the main eastern basin (Ionian/Levantine) at 2000 m depth. However, once per 100-year cycle, the density at the sill of the Strait of Karpathos overtakes the density of the main eastern basin (Ionian and Levantine) at 1000 m depth. This means that the deepest water formed in the Aegean never reaches a density high enough to feed the very deep EMDW but rather remains at intermediate depths. The exception is one event in the 100-year cycle, where a strong cooling over the Aegean triggers the formation of water dense enough to penetrate below 1000 m in the Levantine. In contrast, the water outflowing from the Adriatic at depth of the Otranto sill shows a very strong interannual variability with a range of density fluctuations of 0.25 from 29.76 up to 30.02. The density threshold

of 29.89 at 1000 m depth in the Ionian Sea is thus often overtaken by the one of the deep water outflowing through Otranto. This is especially noticeable for three winters of the 100-year cycle: the winter between the years 17–18, and two successive cold winters between the years 96–97 and 97–98.

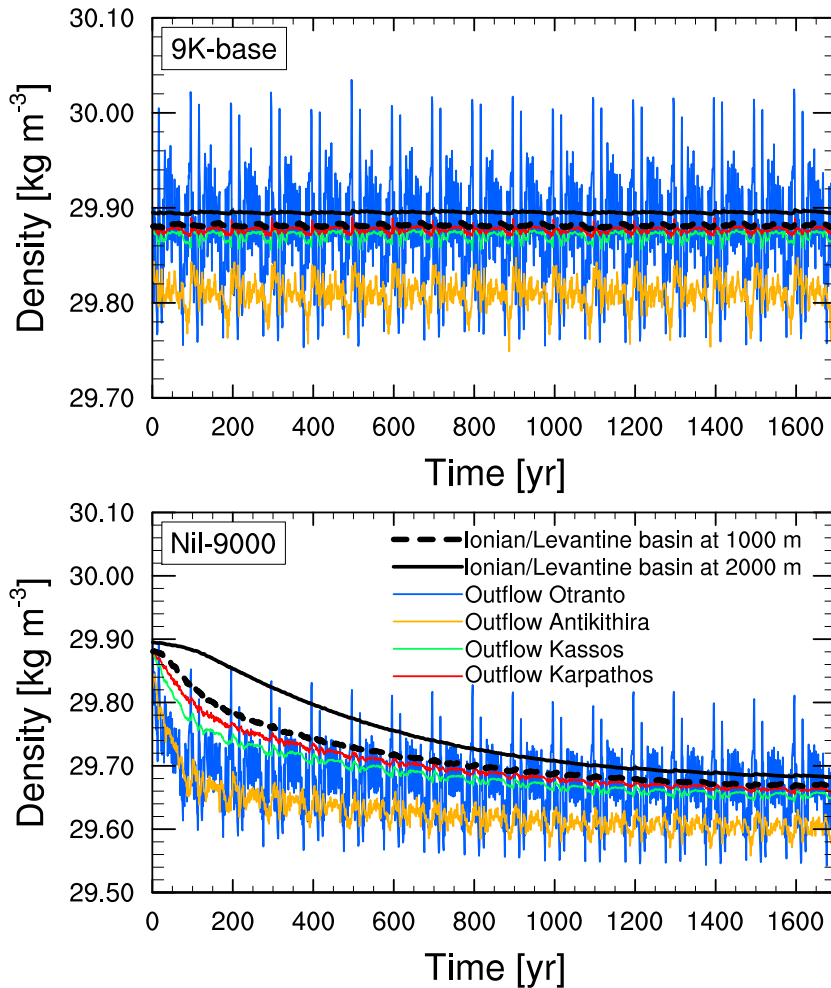


Figure 3.21: Time series of the annual mean potential density at sill depth for the Strait of Otranto, the Strait of Antikithira, the Strait of Kassos, the Strait of Karpathos; and averaged over the Ionian basin at 1000 m and 2000 m of depth. The top panel represents the baseline experiment, the bottom panel represents the Nil-9000 experiment.

In the Nil-9000 perturbation simulation, the density of the Otranto deep outflow slightly starts overtaking the threshold of density at 1000 m in the

Ionian at the end of the second century of the perturbation with the cold events 96–97 and 97–98. During the following centuries this becomes really obvious, not because the Adriatic deep water gains in density (this property is quickly stabilized in the Adriatic) but because the threshold in density of the Ionian Sea at 1000 m slowly decreases. The regular intrusion of younger water at greater depth displayed in Fig. 3.20 is thus mainly due to the two cold winters which create dense water able to sink at a depth greater than 1000 m in the Ionian basin. The stronger the density difference between the deep Adriatic outflow and the Ionian water at 1000 m, the deeper is the intrusion.

3.4.7 Impact of extreme winters

As analysed in the last section, the 100-year atmospheric forcing used to force the regional ocean model for the 9 ka BP time slice includes three strong winters, where the SST of the Adriatic can reach values up to 6 K colder than the seasonal mean. This extreme cooling induces a strong buoyancy loss and creates deep convection, which brings young water into the deep layers of the Eastern Mediterranean. To assess the importance of these extreme winter in the erosion process of the stratification built through freshening, we design an additional experiment, where the 100-year atmospheric forcing is reduced to 50-year, excluding the three severe winters. This new numerical simulation is called Nil-9000-no-cold-winter.

From Fig. 3.22, we can infer that in absence of the three severe winters, the stratification of the deep layers lasts much longer. It is clear that the periodic intrusion of younger water in Nil-9000-no-cold-winter is much more limited than in Nil-9000. As an example, without the severe winters, the occurrence of deep water with an apparent age younger than 100 years is delayed to 1300 years of experiment, whereas it already happened after 700 years in Nil-9000.

However, despite the absence of severe cold periods there will always be a winter, which manages to destratify the water column. It might happen later, in the context of milder winter, but the process occurs inevitably and the ventilation recovers in the latest part of the experiment, as displayed in Fig.

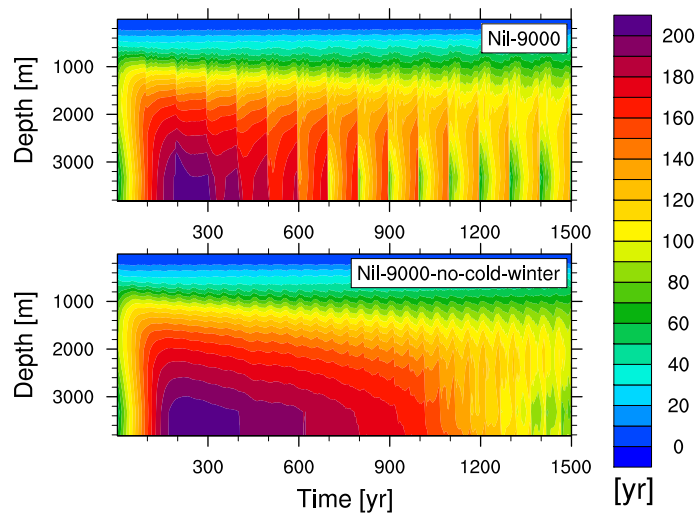


Figure 3.22: Time series of the age of water averaged over the Eastern Mediterranean for different depths. The top panel represents the Nil-9000 experiment, the bottom panel represents the Nil-9000-no-cold-winter experiment.

3.22. The vertical diffusivity and the background diffusion both play an important role in this mechanism. Whereas the surface density quickly reaches an equilibrium, these two parameterizations lead to the very slow spreading of the surface density decrease toward greater depth through diffusion.

As a conclusion, the occurrence of severe winter accelerates the process of ventilation recovery in the deep layers, but it is not the only mechanism responsible for this recovery. In the present context of non-transient climate (with a fixed time slice and a fixed perturbation), the re-establishment through time seems unavoidable.

3.5 Sensitivity to the magnitude of the perturbation

In the last section, we presented the sensitivity of the Eastern Mediterranean deep circulation to enhanced Nile runoff with an additional amount of freshwater of $9000 \text{ m}^3 \text{ s}^{-1}$. In this section, we investigate whether the

response of the system is linear to the magnitude of the prescribed perturbation. In other words, how sensitive is the vertical circulation to the magnitude of the perturbation? For this purpose, we compare three simulations with enhanced Nile runoff with different amount of additional freshwater: $3000 \text{ m}^3 \text{ s}^{-1}$, $6000 \text{ m}^3 \text{ s}^{-1}$ and $9000 \text{ m}^3 \text{ s}^{-1}$. These simulations are respectively referred to as Nil-3000, Nil-6000 and Nil-9000 and correspond to a rough increase of the Nile runoff by a factor of 1.6, 2.1 and 2.7 in comparison with the baseline simulation. In terms of freshwater budget, these perturbations represent an increase by 8%, 16% and 24% of P+R-E. Nil-3000 and Nil-6000 experiments have been run for 500 and 1000 years respectively.

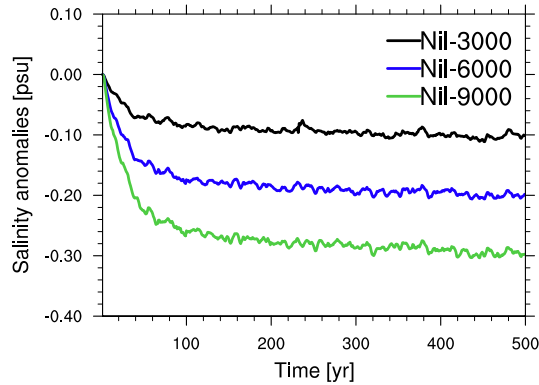


Figure 3.23: Time series of salinity anomalies for the layer 150-750 m for Nil-3000, Nil-6000 and Nil-9000; vs. 9K-base.

We infer from Fig. 3.23 that the averaged freshening of the Eastern Mediterranean is directly proportional to the magnitude of the perturbation, with negative anomalies of 0.1 psu, 0.2 psu and 0.3 psu in the 150-750 m layer, respectively for the simulations Nil-3000, Nil-6000 and Nil-9000.

Using the age tracer (Fig. 3.24), we find that a perturbation with an additional freshwater flux of $3000 \text{ m}^3 \text{ s}^{-1}$ does not provide a surface stratification, that is sufficient to prevent the deep water formation at the beginning of the perturbation. Although the deep water (below 2000 m) reaches an age of 150 years, the intrusion of young water (<100 years) is noticed from the beginning at the bottom of the water column at each 100-year cyclic period. The *IS* anomalies after 450 years of experiment (Fig. 3.25) barely exceed

10 % reflecting a small increase of the vertical stratification.

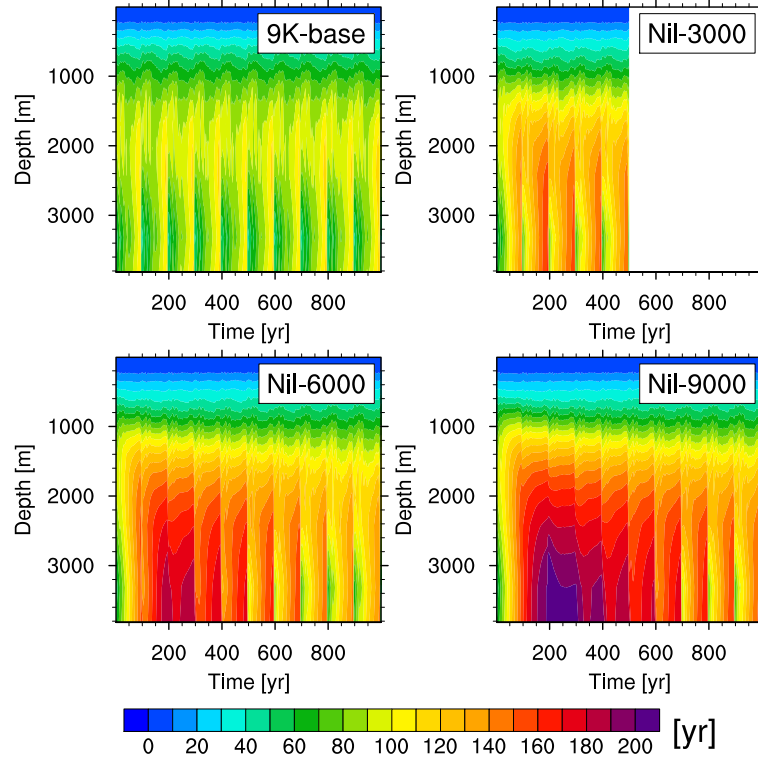


Figure 3.24: Time series of the age of water averaged over the Eastern Mediterranean for different depths. 9K-base, Nil-3000, Nil-6000 and Nil-9000 experiments are represented.

With $6000 \text{ m}^3 \text{ s}^{-1}$, the deep water reaches a maximum mean age above 180 years, the intrusion of young water in the deeper part is prevented only within the first 400 years. The *IS* anomalies show a maximum increase of the vertical stratification of 30 %, with the highest values displayed in the North Levantine and the North Ionian. The South Aegean and the Tyrrhenian Sea also experience an increase of the vertical stratification up to 20 %, while this was not the case with the perturbation of $3000 \text{ m}^3 \text{ s}^{-1}$.

As detailed in section 3.4, a perturbation of $9000 \text{ m}^3 \text{ s}^{-1}$ build stagnant deep water older than 200 years. The recovery of the ventilation starts later than in Nil-6000: young water starts reaching the bottom after 600 years. In this experiment, the vertical stratification increases by up to 45 % in the

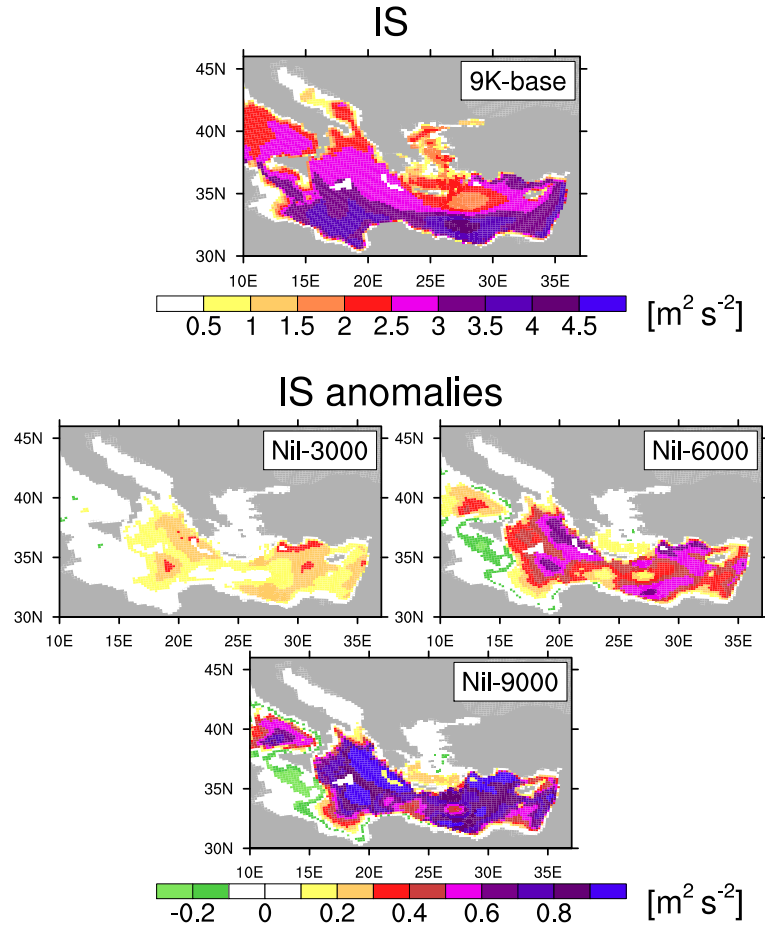


Figure 3.25: Index of stratification in November averaged over the years 400-499. Absolute values of IS are represented for 9K-base, anomalies of IS (vs. 9K-base) are represented for Nil-3000, Nil-6000 and Nil-9000.

main basin, however, a decreased of up to 10% is noticed in the west side of the Ionian basin. This decrease of the stratification is related to the positive surface salinity anomalies of this area (section 3.4.4), which induce a reduction of the density gradient in comparison with the baseline. The scaling of the IS anomalies confirms the linearity of the response to the magnitude of the freshwater perturbation.

We conclude that the vertical stratification of the Eastern Mediterranean shows a linear response to the magnitude of the freshwater perturbation for a defined location. In respect of the perturbation from the Nile runoff, we

are able to set a threshold of the amount of additional freshwater required to obtain a collapse of the deep circulation. We define this threshold between 3000 and $6000 \text{ m}^3 \text{ s}^{-1}$, this quantity provides a sufficient increase of the surface stratification to prevent the deep ventilation.

3.6 Sensitivity to the origin of the perturbation

In this section, we aim to investigate the importance of the location of the perturbation. At similar magnitude, is one perturbation more effective than another in preventing the deep ventilation? To answer this question, we compare four experiments, where an extra freshwater supply of $3000 \text{ m}^3 \text{ s}^{-1}$ is prescribed:

- Nil-3000: here, the additional freshwater is added into the runoff from the Nile. This experiment investigates the hypotheses raised by many previous studies (among many others, Rossignol-Strick, 1985, 1987), which postulate that the enhanced North African monsoon fed the Nile with a substantial amount of extra freshwater, thus triggering a decrease of the surface stratification.
- Po-3000: in this experiment, the water is prescribed to the Po runoff, accounting for an increased precipitation over the northern borderlands as suggested by Cramp et al. (1988); Rohling and Hilgen (1991); Schmiedl et al. (2010) and other studies. They argued that this would have lead to an increase of the water discharged by the northern rivers, thus contributing to the surface density decrease required to weaken the deep ventilation.
- Bos-3000: this perturbation investigates the possibility that the opening of the Bosphorus would supply the freshwater necessary to increase the vertical stratification and prevent the deep water formation. This is based on the study Lane-Serff et al. (1997), who established a relation between the postglacial connection of the Black Sea to the Mediterranean and the timing of sapropel formation.

- Prec-3000: here, the prescribed additional freshwater is homogeneously distributed over the Eastern Mediterranean Sea to test the suggestions of Rohling (1994) and Kallel et al. (1997a), who claim that the precipitation was generally increased during the last sapropel event.

All these simulations have been carried out for 500 years.

Concerning the opening of the Bosphorus, the magnitude of $3000 \text{ m}^3 \text{ s}^{-1}$ roughly corresponds to half of the present net water transport from the Black Sea into the Mediterranean (Peneva et al., 2001). For the Po, an additional runoff of $3000 \text{ m}^3 \text{ s}^{-1}$ relates to a threefold increase of the water discharge from the baseline. A $3000 \text{ m}^3 \text{ s}^{-1}$ increase of the Nile runoff account for an increase by a factor of roughly 1.6 in comparison with the baseline simulation for the HIM.

3.6.1 Surface stratification

Although the same amount of additional freshwater is prescribed in all four perturbations, they display different responses in terms of surface stratification. Fig. 3.26 depicts anomalies of SST, SSS and surface density for each perturbation. The area next to the origin of the perturbation is consistently affected by the strongest surface density loss. Negative anomalies up to 1.5 kg m^3 are thus simulated in the Aegean for Bos-3000, and in the Adriatic for Po-3000, due to the pronounced freshening in these locations. In contrast, the simulations with the enhanced Nile runoff and increased precipitation both display a freshening much more homogeneous. In each perturbation, the western part of the Ionian Sea display positive anomalies of SST and SSS. This response feature is interpreted as a typical response to freshwater perturbations. These anomalies are particularly pronounced in the Po-3000 experiment with a salinity bias up to 0.5 psu and a warming up to 0.3 K.

3.6.2 Vertical stratification

In order to investigate the establishment of the vertical stratification after a surface freshening from different origins, we look at *IS* anomalies (Fig. 3.27).

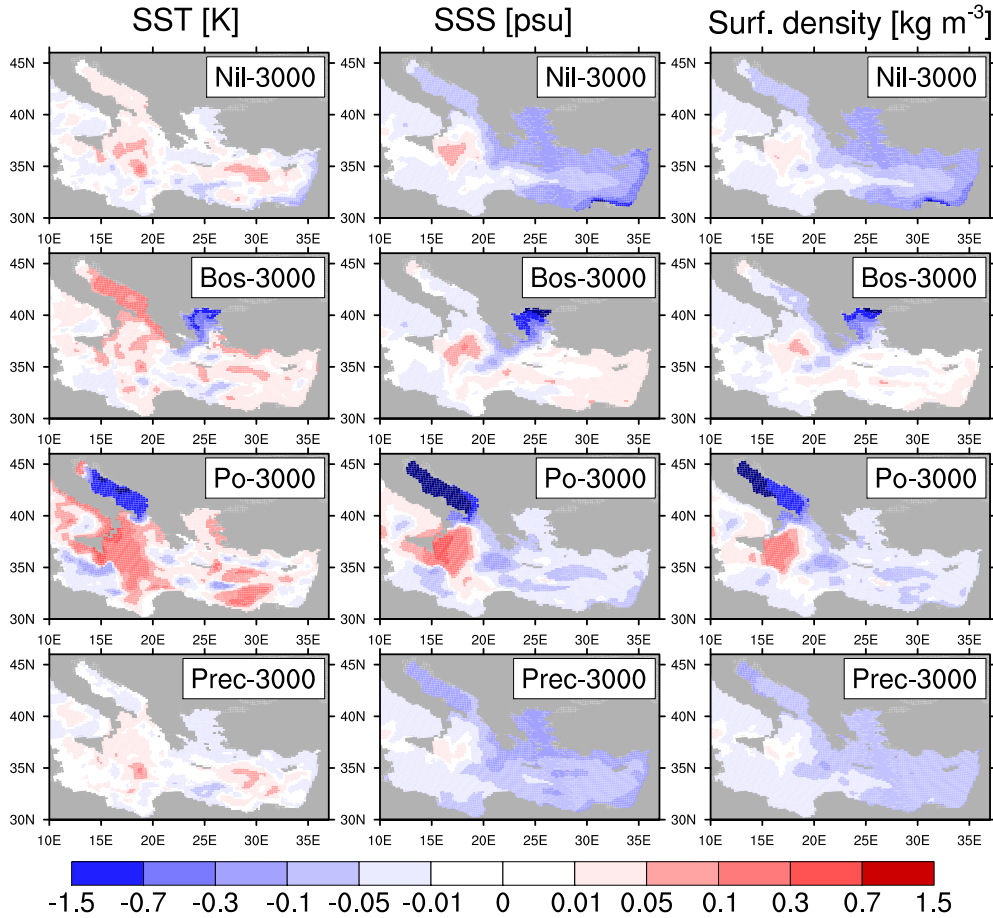


Figure 3.26: SST, SSS and potential density anomalies (vs. 9K-base) averaged over the years 400-499 for Nil-3000, Bos-3000, Po-3000 and Prec-3000.

Po-3000 generally displays the strongest anomalies of IS ; this response is expected because the perturbation is located next to the main location of deep water formation. Thus the fresh anomaly quickly spreads in the basin at intermediate depth through advection in the vertical circulation cell, which has become much shallower. Positive anomalies are recorded with increases of up to 30% in the Ionian and up to 40% in the Levantine. However, the Adriatic and the Aegean surprisingly display negative anomalies. This reduction of the vertical stratification is unexpected in regions located that close to the origin of the perturbation. The same happens for the Bos-3000 experiment: whereas the main eastern basin displays an increase of the

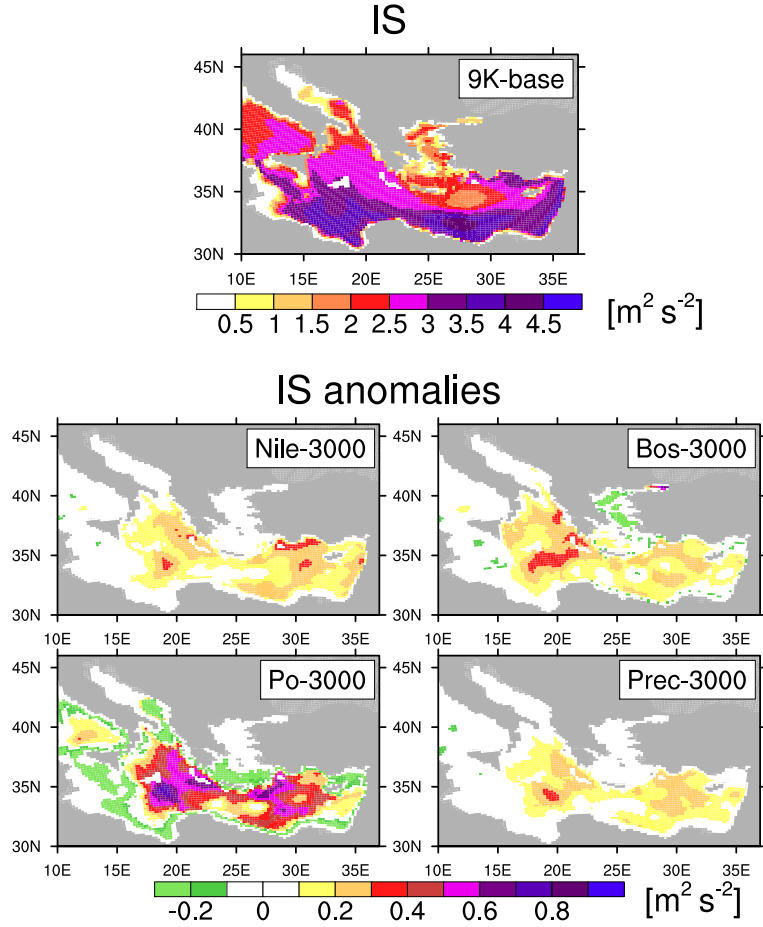


Figure 3.27: Index of stratification in November averaged over the years 400-499. Absolute values of IS are represented for 9K-base, anomalies of IS (vs. 9K-base) are represented for Nil-3000, Bos-3000, Po-3000 and Prec-3000.

vertical stratification above 10%, the stratification index of the Aegean Sea decreases. Nil-3000 and Prec-3000 both display a relatively small increase of the vertical stratification with values barely exceeding 10% in areas affected by the strongest bias.

To understand why a decrease of the vertical stratification is modelled in the sub-basin close to the origin of the freshwater perturbation in Bos-3000 and Po-3000, we compute a volumetric IS (IS_v), instead of integrating it through the vertical levels of the model as done before. IS_v is calculated for each model grid point (i, j, k) as follows:

$$IS_v(i, j, k) = g \frac{z(k)}{\rho(i, j, k)} \Delta\rho, \quad (3.3)$$

where $\Delta\rho = \rho(i, j, k - 1) - \rho(i, j, k)$.

Looking at anomalies of the IS_v provides information on the vertical structure of the increase/decrease of the stratification that is built due to the additional freshwater input.

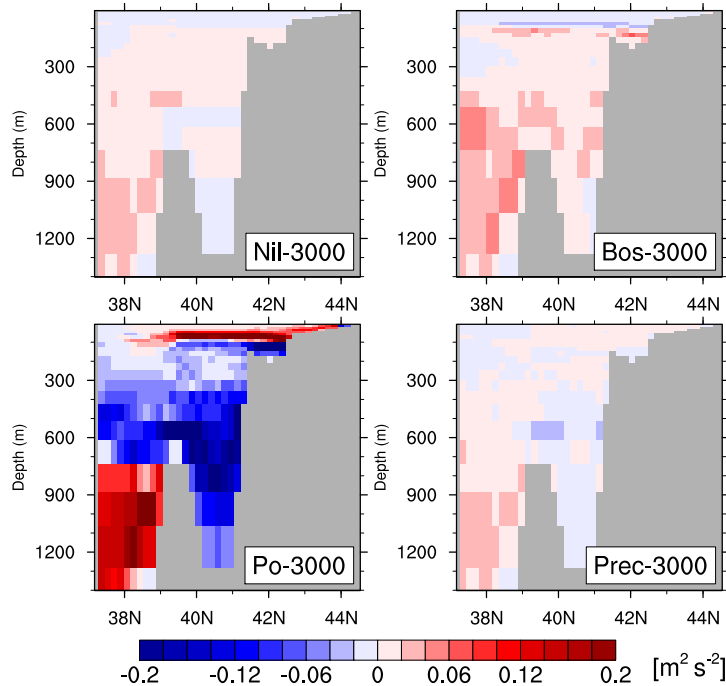


Figure 3.28: Zonally averaged transect over the Adriatic of IS_v anomalies (vs. 9K-base) for the years 400-499. Nil-3000, Bos-3000, Po-3000 and Prec-3000 experiments are represented.

This quantity is represented in a zonally averaged transect of the Adriatic (Fig. 3.28). In Po-3000, contrasting with the other experiments, the anomalies of IS_v depict a robust dipole with a high strengthening of the stratification in the first 100 m of the Adriatic basin, and a strong decrease simulated below this depth. As can be inferred from Fig. 3.29, we explain this feature by the fact that, despite the strong negative anomalies of the surface potential density, a minimum bias is displayed at a depth of 200 m. Below this depth the negative bias starts strengthening again. This leads to

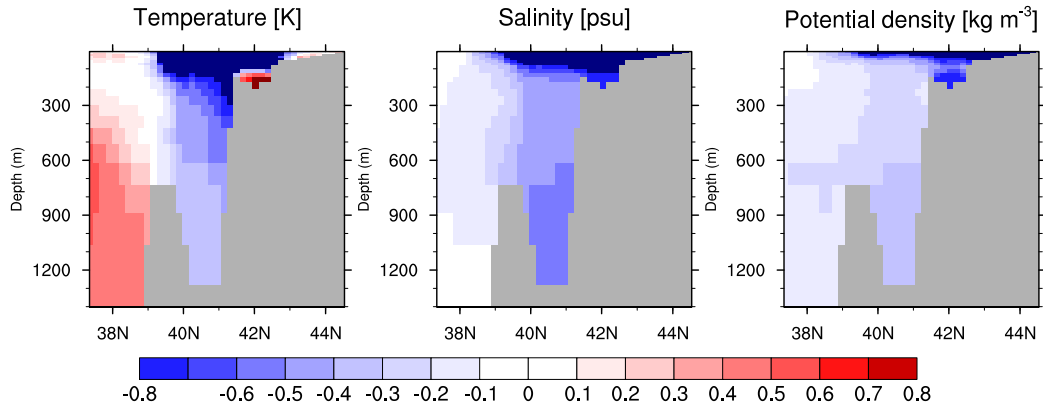


Figure 3.29: Zonally averaged transect over the Adriatic. Temperature, salinity and potential density anomalies (Po-3000 vs. 9K-base) are represented for the years 400-499.

a weaker vertical stratification below 200 m, thus to lower IS_v values. This pattern of the density anomalies is driven by both salinity and temperature (Fig. 3.29). The zonally averaged temperature transect of the Adriatic shows a strong cooling of up to -2 K at the surface, then the cooling decreases with the depth with values of -0.2 K at the bottom of the deep Adriatic basin. This vertical temperature structure provides a lower vertical density gradient from the surface to the depth. On the other hand, the salinity anomalies show a similar structure as the potential density, with a strong freshening at the surface and at depth, and a minimum bias at around 200 m depth. From 200 m toward greater depth, this provides a lower density gradient as well. The presence of less freshwater at intermediate depth in the Adriatic basin is related to the penetration of water from the Ionian.

In the Bos-3000 experiment, a very similar hydrographic structure of the water column is modelled in the Aegean basin, this basin being located nearby the freshwater perturbation. IS_v anomalies zonally averaged over the Aegean (Fig. 3.30) also display a strong stratification of the upper 100 m and negative values below. Explaining this pattern, a lower density gradient is also modelled below 100 m, with similar anomaly structures of temperature and salinity as found in the Adriatic for the Po-3000 experiment (Fig. 3.31).

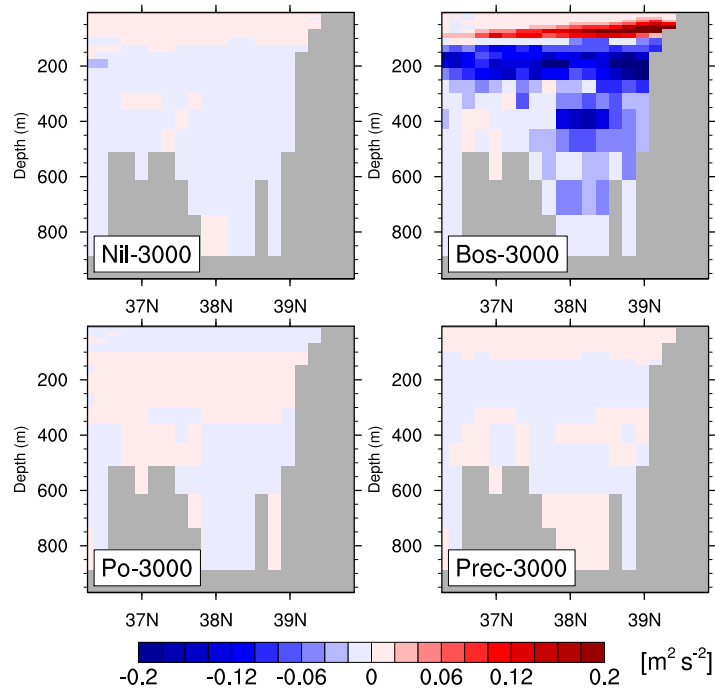


Figure 3.30: Zonally averaged transect over the Aegean of IS_v anomalies (vs. 9K-base) for the years 400-499. Nil-3000, Bos-3000, Po-3000 and Prec-3000 experiments are represented.

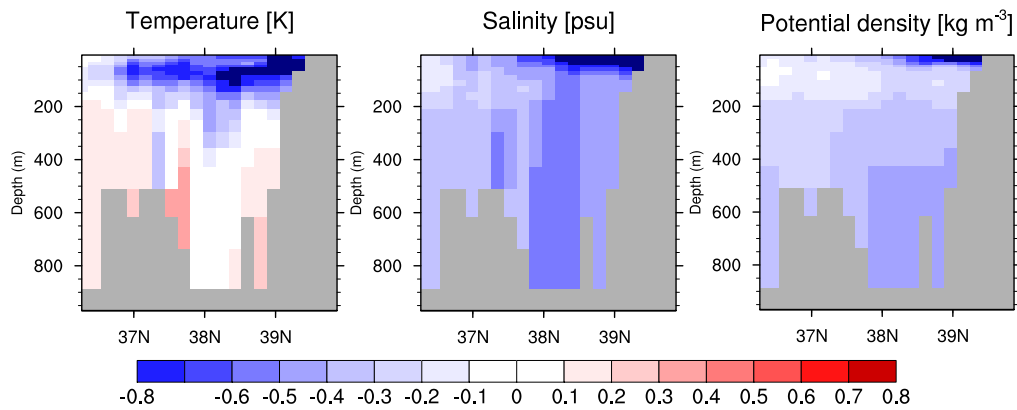


Figure 3.31: Zonally averaged transect over the Aegean. Temperature, salinity and potential density anomalies (Bos-3000 vs. 9K-base) are represented for the years 400-499.

3.6.3 Mixed layer depth and sources of dense water

In this section, we assess the changes in winter convection related to the changes in stratification induced by the freshwater perturbations. Fig. 3.32 displays anomalies of winter mixed layer depth. The perturbation of $3000 \text{ m}^3 \text{ s}^{-1}$, which originates in the Nile river does not show remarkable changes of the depth and location of the mixed layer, nor does the simulation with increased precipitation. However, the Po-3000 experiment exhibits a reduction of the winter mixed layer in the Adriatic, which becomes 500 m shallower, and an increase above 300 m in the North Ionian and above 100 m in the South Aegean/North Levantine. This suggests that the weakening of the deep water formation in the Adriatic results in a strengthening of the intermediate water source in the Ionian, as well as the Levantine Intermediate formation. In Bos-3000, the depth of the winter mixed layer is decreased by up to 200 m in the North Aegean, whereas an increase by up to 100 m is modelled in the North Ionian and the South Aegean. Additional freshwater input from the Black Sea or from the Po appear to play a predominant role in the deep/intermediate water formation. The extension of the deeper winter mixed layer depth pattern over the North Ionian is likely to be a typical response to an increased freshening of the Eastern Mediterranean, as it was also simulated in response to the perturbation from the Nile (section 3.4.3).

As a consequence of the changes in winter mixed layer depth, the volume of dense water formed is also modified. Fig. 3.33 displays time series of changes in convection in the four sub-basins of the eastern Mediterranean for all experiments with $3000 \text{ m}^3 \text{ s}^{-1}$ of additional freshwater. For comparison purposes, we added the results from the Nil-9000 experiment. In the Adriatic, the reduction of the depth of the winter mixed layer, due to the increased Po runoff, triggers a decrease by half of the volume of dense water formed. The strong interannual variability of the anomaly signal is a consequence of the 100-year cycle of the atmospheric forcing. The other perturbations do not trigger relevant changes in volume of dense water formed in the Adriatic. In the Aegean, Po-3000 and Bos-3000 both display an increase in the convection with respective mean changes of 9 % and 4 %. The signal from the Bosphorus perturbation should be interpreted cautiously though because the changes depicted here are averaged over the entire Aegean. However, in Fig. 3.32

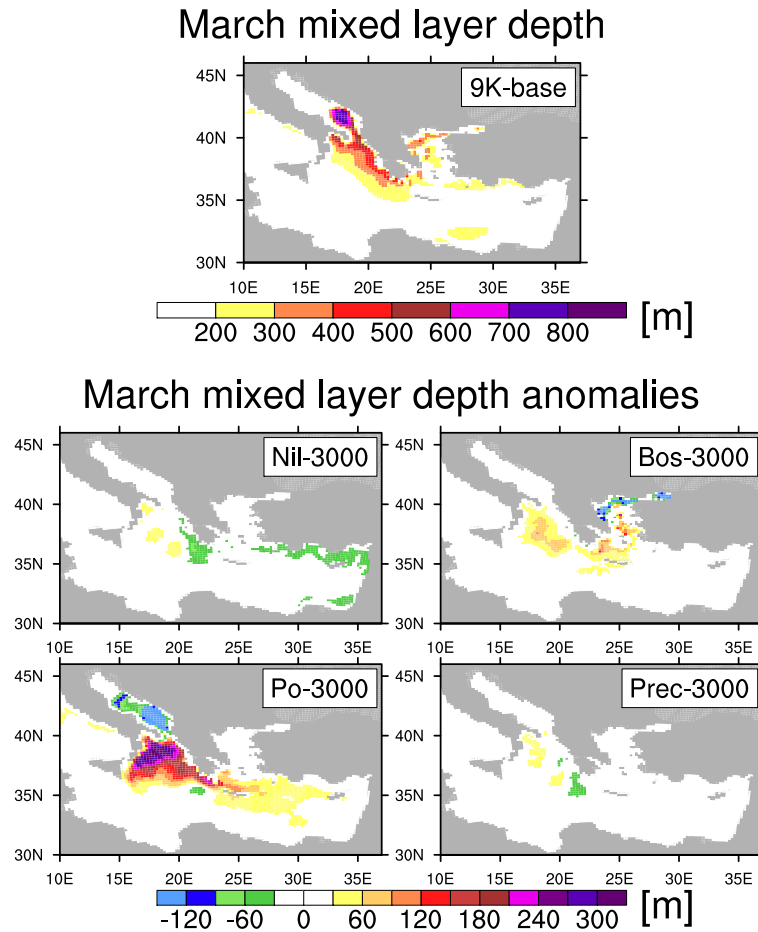


Figure 3.32: March mixed layer depth averaged over the years 400-499. Absolute values are represented for 9K-base, anomalies (vs. 9K-base) are represented for Nil-3000, Bos-3000, Po-3000 and Prec-3000.

it was shown that the changes within the Aegean basin are very regional in this simulation, with a switch of the dense water formation from the North Aegean to the South Aegean. Nil-3000 and Nil-9000 respectively display a mean decrease by 4 % and 11 % in the Aegean. The changes in the Levantine are similar than those of the Aegean, but the amplitude of the anomalies is twice as large. Finally, the Ionian basin displays the strongest changes in Po-3000, with a mean increase of 25 %. In general, the homogeneous increase in precipitation (Prec-3000) do not simulate significant changes in volume of deep water formed in any of the basins.

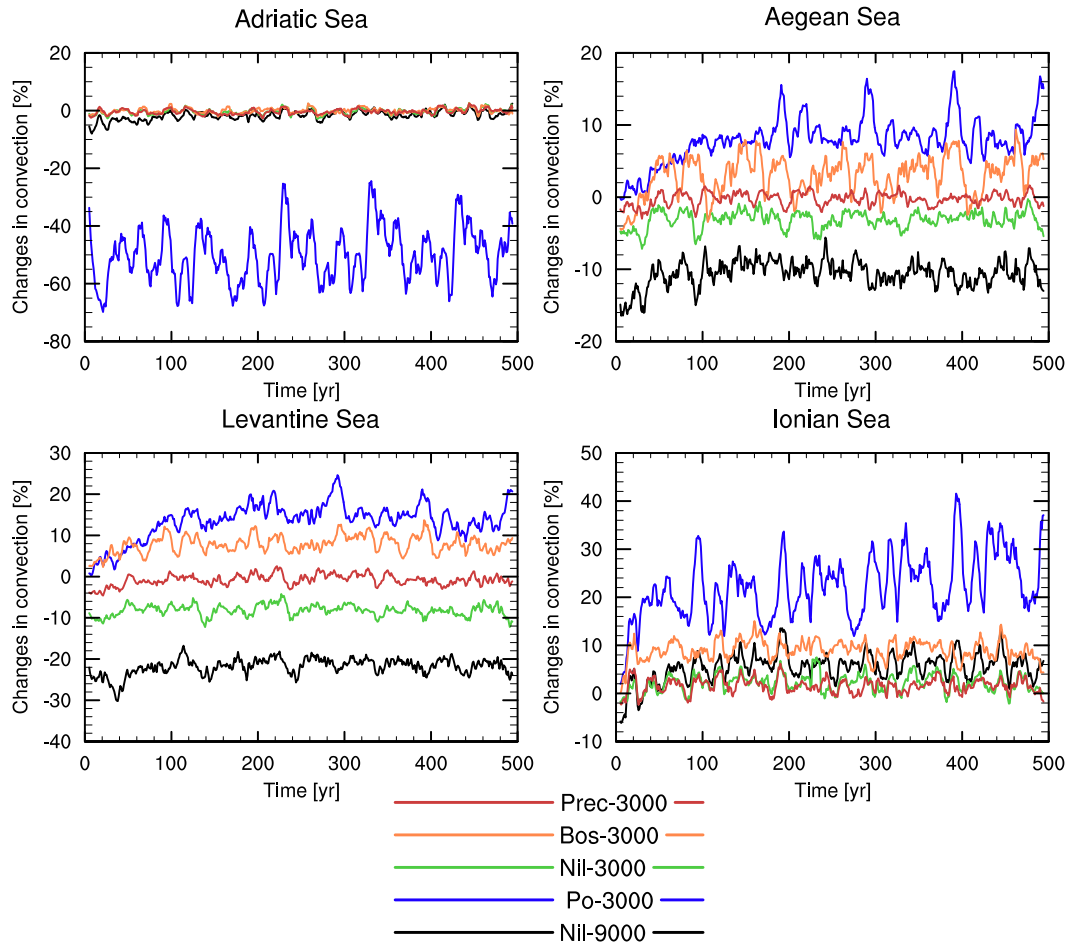


Figure 3.33: Time series of changes in convection (vs. 9K-base) for the Adriatic, the Aegean, the Levantine and the Ionian Seas. The 10-year running mean is represented for Prec-3000, Bos-3000, Nil-3000, Po-3000, and Nil-9000.

It becomes clear that a freshening from the north (e.g. Po or Bosphorus) tends to increase the intermediate water formation in the southern Aegean/northern Levantine, whereas a freshening from the south (e.g. Nile) rather reduces this formation. The freshening from the Po or Black Sea also triggers the extension of the intermediate dense water formation over northern Ionian as a replacement for the missing sources from the Adriatic or from the North Aegean, respectively for Po-3000 and Bos-3000. This read-

justment of the location of dense water formation ineluctably leads to a new distribution of the water masses in the basin because the hydrographic properties of the mediterranean water display strong regional contrasts. We thus expect the intermediate water masses to be particularly affected by hydrographic changes, when they are formed in a different sub-basin due to the fresh perturbation.

3.6.4 Water masses at intermediate depths

Remarkable differences between Po-3000 and the baseline experiment occur at intermediate depths (200-800 m). The decline of the formation of dense cold deep water in the Adriatic in the Po-3000 experiment and its replacement by a larger formation of intermediate warmer water in the northern Ionian and southern Aegean, lead to a general warming of the water in the main eastern basin, as displayed in the meridionally averaged transect of temperature anomalies of the Levantine and Ionian Seas in Fig. 3.34. The maximum warming affects the intermediate water layer with highest values (above 0.6 K) found at a depth of around 600 m, this water layer also displays the freshest bias.

In Bos-3000, a small warming of the main basin is also simulated at intermediate depths, though weaker, with a maximum of 0.2 K found between 200 and 400 m depth. In this experiment, the hydrographic properties of the intermediate water masses do not display strong changes, since the former and new locations of intermediate dense water formation present analog hydrographic properties. This is not the case in Po-3000, where a part of the dense water, that is formed in the Adriatic before the perturbation, is replaced by water formed in the northern Ionian. These two basins present different hydrographic characteristics, thus the intermediate water exhibits stronger anomalies in Po-3000 (Fig. 3.34).

3.6.5 Water aging

The time evolution of the age of water averaged over the Eastern Mediterranean (Fig. 3.35) displays a very similar response to the perturbations from the Nile, the Bosphorus and the increased precipitation. None of these per-

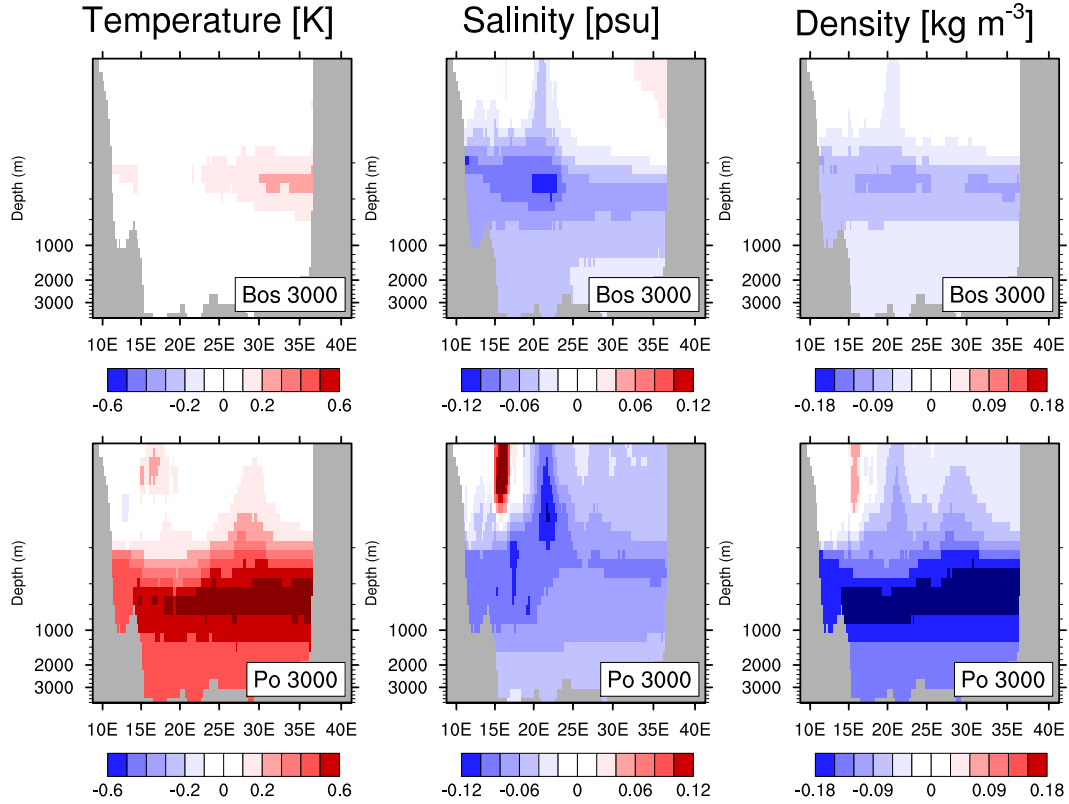


Figure 3.34: Meridionally averaged transect of temperature, salinity and density anomalies (vs. 9K-base) for Bos-3000 and Po-3000. Only the Ionian and the Levantine Seas are considered. Note that the depth scale is non-linear.

turbations allows a sustained shutdown of the deep ventilation for several centuries; indeed, young water are reaching the bottom in each 100-year cycle of the experiments. In contrast, the perturbation which originates from the Po river shows a strong response, with deep water stagnating already from the beginning without intrusion of young water at the bottom. As seen in section 3.6.3, the volume of young dense water formed in the Adriatic is reduced by half in Po-3000 (Fig. 3.33). This reduction is mainly caused by the surface freshening from the Po that prevents the new dense water formed to sink as deep as before the perturbation. This can be inferred from the winter mixed layer which becomes 500 m shallower in the Adriatic (Fig. 3.32). This explains the extremely strong stagnation that quickly builds after the start

of the perturbation. However, the strong vertical stratification slowly starts to erode after 3 centuries of perturbation, as for the Nil-9000 perturbation.

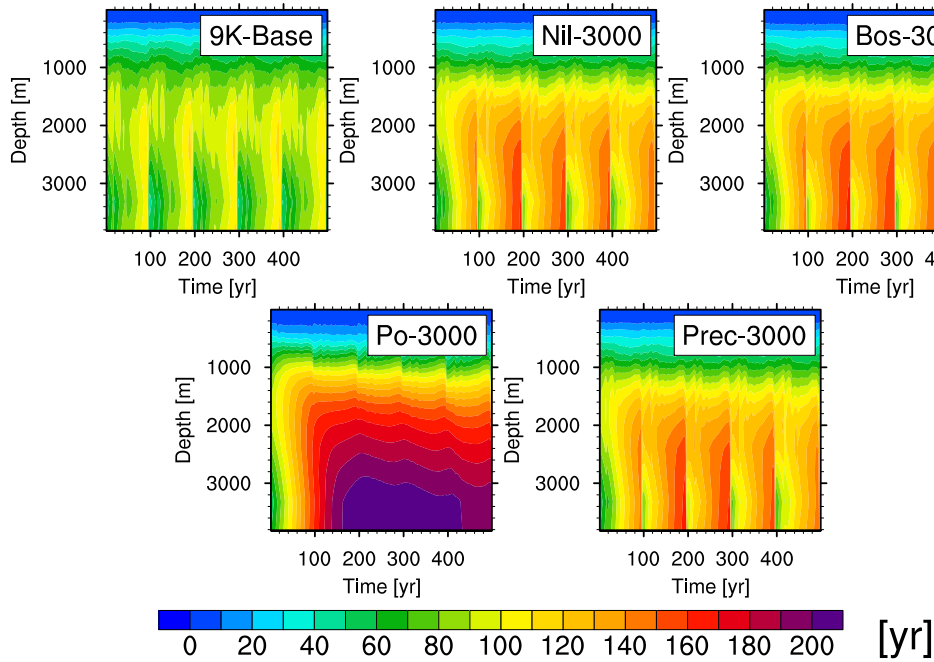


Figure 3.35: Time series of the age of water averaged over the Eastern Mediterranean for different depths. 9K-base, Nil-3000, Bos-3000, Po-3000 and Prec-3000 are represented.

It is clear that the origin of the perturbation plays an important role in the establishment and duration of the deep water stagnation. If an additional freshwater input from the Black Sea, the Nile or the precipitation display a similar and rather weak response; the deep circulation of the Eastern Mediterranean has shown to be extremely sensitive to a freshwater perturbation from the Po, the additional freshwater directly disturbing the main source of dense water which is the Adriatic basin. A perturbation from the Po (Po-3000) is more effective to prevent the deep ventilation than a perturbation three times larger from the Nile (Nil-9000).

3.7 Transient perturbation: a prerequisite to maintain the stagnation

From the former sections, we conclude that a recovery of the deep ventilation seems ineluctable. However, the time scale of the recovery depends on both the origin and the magnitude of the perturbation, the latter inducing a very linear response. All the perturbations which have been described so far have the common characteristic that they are fixed and permanent perturbations. Moreover, we use a 100-year daily atmospheric forcing which corresponds to the fixed time slice of 9 ka BP and does not reflect a transitional state. However, the transition into the sapropel time might have been a period characterised by transient climate. To consider this aspect, we perform a perturbation which is gradually changing over time.

It has been discussed in the literature that sea level rise and Atlantic freshening, both caused by the deglaciation, could potentially induce the development of a stable stratification, thus the reduction of the deep ventilation (e.g. Rohling, 1994; Béthoux and Pierre, 1999). The ice sheets started to decay at the end of the Last Glacial Maximum (LGM, 21 000 years BP) until the mid-Holocene (6000 years BP), which suggests that their impact on the Mediterranean stratification at the beginning of the Holocene is non-negligible. Based on this assumption, we prescribe a gradual freshening on the hydrographic properties of the incoming Atlantic water, at the western margin of the model. Such a freshwater perturbation experiment mimics the effect of sea level rise and global surface water salinity decrease, both caused by the melting of the decaying ice sheets over Greenland.

In the Atl-fresh simulation, a freshening of 0.014 psu per century is prescribed. We carry out the experiment for 3400 years. Depending on the scenario, this can correspond to a release of melted freshwater of either 0.05 Sv or 0.3 Sv. The first holds if this freshwater is only mixed in the upper 700 meters of the ocean and the second holds if a mixing over the entire ocean is considered. We start with a mean salinity of 39.1 psu and reach a mean value of 38.5 psu at the end of the perturbation experiment. Additionally, we perform a perturbation experiment which combines a strong perturbation (Nil-9000) with a gradual Atlantic freshening of 0.014 psu per century. This

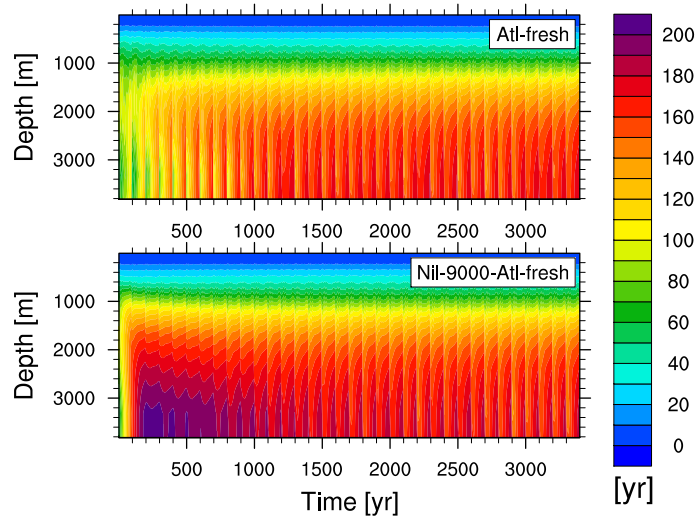


Figure 3.36: Time series of the age of water averaged over the Eastern Mediterranean for different depths. The experiments Atl-fresh and Nil-9000-Atl-fresh are represented.

experiment is named Nil-9000-Atl-fresh.

Fig. 3.36 depicts the time evolution of the age of water averaged over the eastern basin as a function of depth. Contrasting with the previous experiments with a fixed prescribed amount of additional freshwater, the experiment with the freshening only (Atl-fresh) shows a very slow establishment of the poor ventilation in the deep layers. This simulation needs a time of 1500 years to reach a stable state (Fig. 3.37) with deep water (>2000 m) between 140 and 180 years old. In contrast, the combined experiment starts with a strong stagnation of the deep water, mainly triggered by the prescribed $9000 \text{ m}^3 \text{ s}^{-1}$ from the Nile. The associated gradual freshening strengthens the stagnation as suggests the comparison with Nil-9000 "alone" (section 3.4.5, Fig. 3.20), and also prevents the full erosion of the stratification. After 3000 years of perturbation, both simulations reach an equivalent state (Fig. 3.37). This underlines the necessity of a gradual decrease in surface density to achieve a long-lasting weakening of the deep ventilation. Such a state can not be reached with a fixed perturbation.

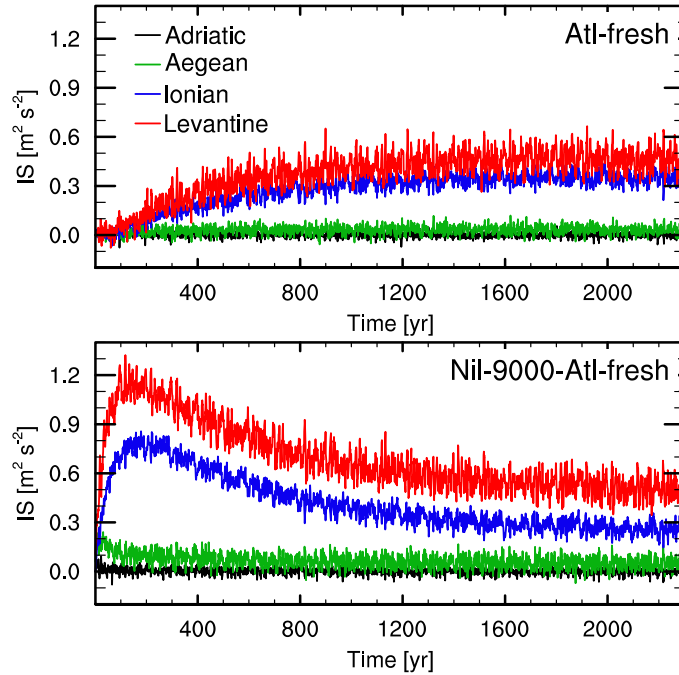


Figure 3.37: Time series of stratification index anomalies (vs. 9K-base) in November for the Adriatic, the Aegean, the Ionian and the Levantine basins. The experiments Atl-fresh and Nil-9000-Atl-fresh are represented.

3.8 Synthesis and implications

In this chapter, we investigate some of the mechanisms controlling the formation of the sapropel S1. We focus on the “physical” scenario, which considers that an increase in freshwater supply led to a strengthening of the surface stratification and thus a decrease of the deep water ventilation. For this purpose, we carry out various experiments with additional freshwater input and analyse the sensitivity of the Eastern Mediterranean deep water ventilation to the resulting surface freshening. Our analysis concentrates on the changes in (i) the vertical stratification, (ii) the winter mixed layer depth as a proxy for dense water convection, (iii) the overturning circulation, and (iv) the apparent age of the water.

The results from our experiments provide a good insight into various mechanisms, which could have led to the stagnation of the deep water layers.

Whereas an increase in freshwater input from the Nile runoff is often considered as crucial for sapropel formation (e.g. Rossignol-Strick, 1985, 1987), our experiments show that such a perturbation has a smaller effect on the vertical stratification than, e.g. an extra freshwater supply from the Po river. In general, the horizontal circulation is not strongly affected by the freshwater perturbations, as it is largely wind-driven; however, changes in the vertical circulation are simulated with an active cell becoming much shallower, due to the increase of the vertical stratification.

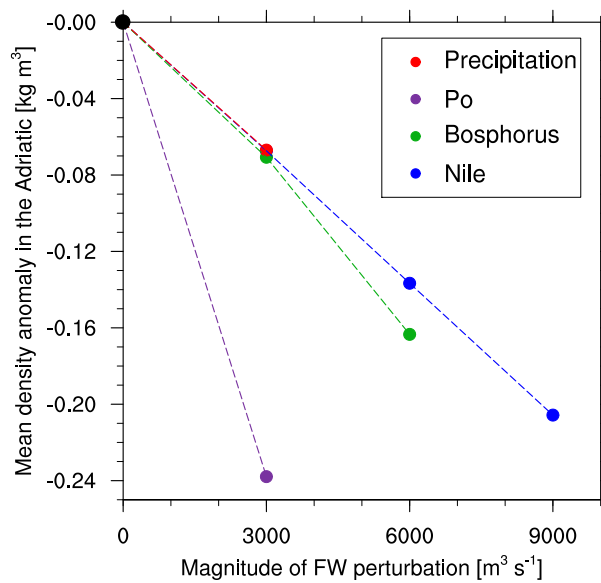


Figure 3.38: Relation between the mean density anomaly in the southern basin of the Adriatic between 150 and 500 m of depth, and the magnitude of freshwater input, for each experiment.

As a summary of the results from the various perturbation experiments, Fig. 3.38 synthesizes the relation between the magnitude of the perturbation for different origins and the mean density change averaged in a box of the southern basin of the Adriatic, roughly between 150 and 500 m of depth. We choose the Adriatic because it is the main area of dense water formation, which drives the deep ventilation. The results clearly show that the increased precipitation, the enhanced Nile runoff and the opening of the Bosphorus have a comparable effect on the density, at intermediate depths in the Adriatic, for a magnitude of $3000 \text{ m}^3 \text{ s}^{-1}$. However, for a doubling

of the freshwater input to $6000 \text{ m}^3 \text{ s}^{-1}$, the perturbation from the Bosphorus induces stronger negative density anomalies of the Adriatic intermediate layers than a perturbation from the Nile. Whereas the response is almost linear with respect to the magnitude of the perturbation for the enhanced Nile runoff, this is not true for the Bosphorus input, whose response increases in a non-linear way. An extra discharge from the Po river is more than four times as effective in diminishing the density, it even surpasses the three times larger perturbation from the Nile.

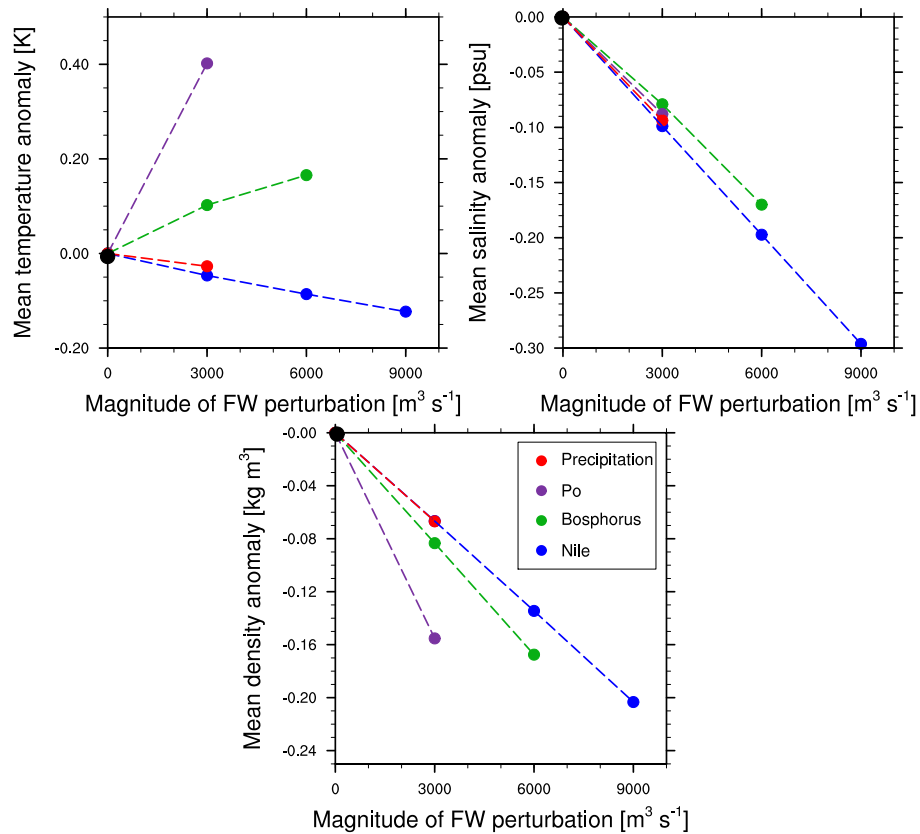


Figure 3.39: Relation between the mean temperature, salinity and density anomalies at the Strait of Sicily between 200 and 400 m of depth, and the magnitude of freshwater input, for each experiment.

The hydrographic properties of the water flowing from the eastern basin to the western basin through the Strait of Sicily are substantially modified by the addition of freshwater (Fig. 3.39). In the baseline, the warm and salty

LIW flows into the western basin through the Strait of Sicily. However, this water mass has shown to be highly sensitive to freshwater perturbations: the LIW production weakens with increased freshwater supply from the south (e.g. the Nile) and strengthens when the extra freshwater supply comes from the north, this latter response being especially true for the Po perturbation. As expected, this is reflected in the properties of the water, which penetrates into the western part of the Mediterranean. Fig. 3.39 shows that this water is warmer for perturbations from the north (Po and Bosphorus, the Po experiment displaying a strong warming of 0.4 K), this warming is explained by the increase of intermediate formation in the North Ionian, South Aegean and North Levantine. For perturbations from the south (Nile) or homogeneously distributed over the eastern basin (increased precipitation), the intermediate water is colder, because less water is formed in the warm Levantine basin. These temperature changes thus reflect the different regions of intermediate water formation. In contrast to the temperature signal, the changes in salinity only show little dependence on the input location. In all the perturbation experiments, the water transferred to the western basin is fresher with negative anomalies between 0.08 and 0.1 psu; the freshening is linear to the rate of the perturbation. The changes in salinity and temperature lead to a density decrease of up to 0.20 kg m^{-3} . This might have consequences on the ventilation of the western basin, by leading to a decrease of the deep water formation in the Gulf of Lion, where the presence of salty LIW preconditions the winter convection in the baseline.

The mean age of the deep water averaged over the third century is associated to the magnitude of the freshwater perturbation in Fig. 3.40. Even if the age tracer implemented in the model has the shortcoming to be limited to a maximum age of 200 years, thus limiting the interpretation of this quantity; it is obvious that the perturbation from the Po is by far the most effective to produce stagnant deep water. However, after one to two thousands of years, depending on the perturbation, a state with complete ventilation of the deep water is reached, as in the baseline simulation.

Fig. 3.41 relates the maximum depth of the deep eastern counter-clockwise cell (considering the 0.1 Sv isoline) to the magnitude of the perturbation for each experiment. All the applied perturbations lead to a considerable de-

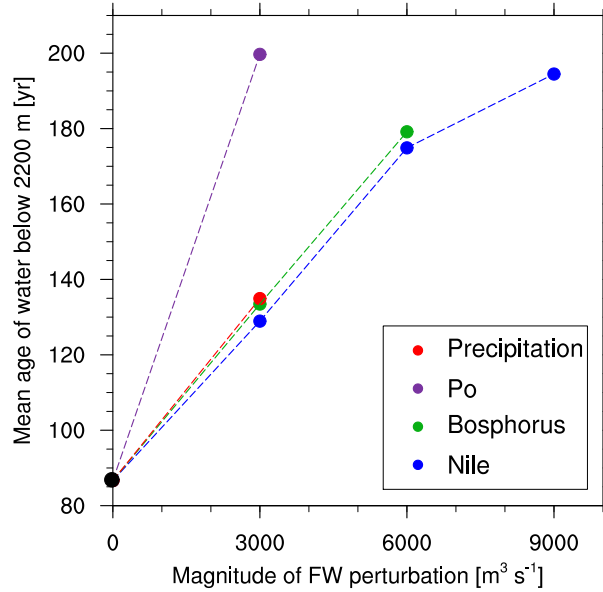


Figure 3.40: Relation between the maximum apparent age of deep water averaged over the third century of the perturbation, and the magnitude of freshwater input, for each experiment.

crease of the depth of the eastern vertical circulation cell. This reflects an active circulation, limited to the upper part of the water column, with a maximum depth between 700 m to 850 m depending on the perturbation, versus 1550 m in the baseline, which reflects a well-ventilated state. When the magnitude of the perturbation increases, the vertical circulation cell becomes shallower. However, this response appears to be non-linear, because the depth of the Strait of Sicily acts as natural boundary, in such a way that the overturning cell can not become shallower than that depth. The lowest perturbation of $3000 \text{ m}^3 \text{ s}^{-1}$ triggers a strong decrease of the depth of the active cell, but greater magnitudes only slightly strengthen the decrease simulated with $3000 \text{ m}^3 \text{ s}^{-1}$. From Fig. 3.41, we could infer that the Po is less effective than the other perturbations in weakening the deep ventilation. However, a 2D picture of the zonal overturning stream function reveals that the cell is restricted to a very narrow part of the extreme eastern Levantine in that experiment and represents the increase of the LIW formation as a compensation for the decrease of deep water formation in the Adriatic. For

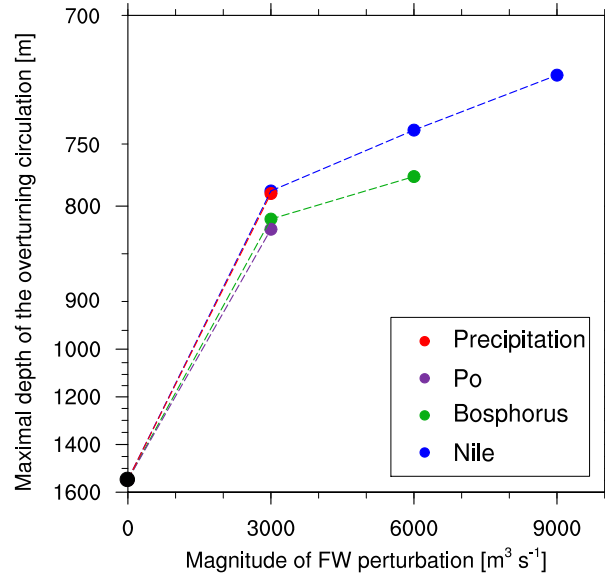


Figure 3.41: Relation between the maximum depth of the overturning circulation in the eastern basin (considering the 0.1 Sv isoline) averaged over the fifth century of the perturbation, and the magnitude of freshwater input, for each experiment.

the other perturbations, the cell is slightly shallower but still present over a wide part of the eastern basin.

3.9 Discussion

3.9.1 Limitations

In our study, we mainly investigate the sensitivity of the deep ventilation to the magnitude and the location of the perturbation. However, the timing of the changes in freshwater fluxes may also play an important role. The enhanced discharge from the northern rivers (e.g. the Po) or the outflow from the Bosphorus are thought to display a strong seasonal cycle with a maximum in autumn and winter, whereas the Nile discharge is expected to display a stronger increase during summer, coinciding with the monsoon season. This aspect has not been considered in our approach. It might not influence our results in the case of the Nile perturbation, because the

spread of the freshening to the regions of convection already takes some years. However, in the case of the Po, to account for the seasonal cycle while prescribing the extra freshwater could strengthen the response even further, because the perturbation originates very close to the main convective area. A stronger additional runoff in winter, when the convection occurs, is thus thought to amplify the decrease in dense water formation.

The occurrence and persistence of the sapropel S1 in the geological records suggests that the stagnation of deep water was maintained for at least 3000 years. However, our perturbation experiments with a fixed amount of additional freshwater supply simulate an unavoidable recovery of the deep water ventilation. The depth of the interface between stagnant deep water and active upper circulation (initially restricted to ~ 800 m after the perturbation) deepens through time, because diffusion and mixing erode the vertical stratification. In contrast, the perturbations with a permanent gradual increase of the freshening (here, the gradual freshening of Atlantic water) do simulate a sustained deep water stagnation. This raises the importance of considering a transient perturbation as a necessary condition to maintain a reduced vertical circulation. This also points out the importance of the parameterization of the vertical mixing the ocean model, because it directly influences the time scale for the recovery of the deep ventilation. Meijer and Dijkstra (2009) found that a reduction of the vertical mixing of water properties was needed to keep persistent conditions favorable for sapropel formation. We believe that the mixing parameterization used in our ocean model induces a somewhat too strong mixing, which does not allow the persistence of the stagnation over a long time period, for the size of freshwater perturbations that is prescribed in our experiments. However, the changes of surface salinity recorded by proxy data for the sapropel S1 period are around 3 psu (section 3.9.2.1). To obtain such a strong decrease, a much higher magnitude of freshwater perturbation is required (see section 3.9.2.1). With such a huge perturbation, we argue that our ocean vertical mixing parameterization would not be an obstacle to the persistence of the stagnation over a long time period.

3.9.2 Comparison to previous studies

3.9.2.1 Comparison to observations

One way to assess the plausibility of the perturbation we prescribe is to compare the changes in surface salinity found in our simulations with reconstructions from marine sedimentary records. In most studies, a surface salinity reduction at the time of sapropel S1 is reported, with a typical decrease between 1 and 3 psu. A decrease of up to 4 psu is suggested by Kallel et al. (1997a), with an absence of gradient (salinity almost uniform with an average of 36 psu). Thunell and Williams (1989) estimated a decrease around 2.9 psu in the Eastern Mediterranean with a mean value of 35.9 psu and postulated a reversal of the thermohaline circulation with lower surface salinity (36.5 psu) in the western basin. Rohling and De Rijk (1999) claimed that the surface salinity gradient was decreased by half at the time of sapropel S1. Finally, Emeis et al. (2000) reported a reduction in surface salinity by roughly 2 psu in the Levantine and very minor reductions in the Ionian.

Table 3.2: Summary of the experiments performed showing the changes excess evaporation, in surface salinity and basin averaged salinity for the Eastern Mediterranean, averaged over the years 400-499.

Experiment	Decrease in excess Evaporation (vs. 9K-base) %	Surface Salinity psu	Surface Salinity Anomaly (vs. 9K-base) psu	Basin averaged Salinity psu	Basin averaged Salinity Anomaly (vs. 9K-base) psu
9K-base		39.00		39.12	
Po-3000	8	38.79	-0.21	39.05	-0.07
Nil-3000	8	38.90	-0.1	39.05	-0.07
Nil-6000	16	38.79	-0.21	38.98	-0.14
Nil-9000	24	38.68	-0.32	38.91	-0.21
Bos-3000	8	38.95	-0.05	39.07	-0.05
Bos-6000	16	38.87	-0.13	39.0	-0.12
Prec-3000	8	38.92	-0.08	39.05	-0.07
Atl-fresh		38.90	-0.10	39.06	-0.06
Nil-9000-Atl-fresh		38.58	-0.42	38.86	-0.26

Table 3.2 summarizes the changes in surface and basin averaged salinity for the eastern basin simulated in each perturbation experiment. In general, the paleoreconstructions propose a surface salinity decrease much stronger than in our experiments, where mean surface salinity anomalies between 0.08 and 0.42 psu are simulated. This inconsistency could be partly related to errors in the interpretation of oxygen isotope composition in terms of salinity, which involve a high uncertainty (e.g. Rohling, 1999, 2000). In order to explain why none of our perturbation experiments can reach such a strong surface salinity decrease, we compare the changes in the water budget (E-P-R) triggered by the perturbations with the changes in E-P-R suggested by other studies. In our work, the highest perturbation applied ($9000 \text{ m}^3 \text{ s}^{-1}$) only makes the excess evaporation to drop from 72 cm y^{-1} in the baseline to 55 cm y^{-1} . However, the model experiments from Myers (2002) have shown that decreases in excess evaporation by 60 % and 80 % respectively lead to a mean surface salinity of 37.8 psu and 37.3 psu in the Eastern Mediterranean. Rohling (1999) used a box model to represent the long-term average changes in salinity and $\delta^{18}\text{O}$. Assuming a relative humidity of $r = 0.8$, he calculated an averaged salinity of 37.1 psu associated with a decrease by 65 % of excess evaporation during the sapropel S1 period. In order to obtain a decrease of E-P-R between 60 % and 80 % in our strongest simulation (Nil-9000), we would need an extra freshwater supply between $16000 \text{ m}^3 \text{ s}^{-1}$ and $21400 \text{ m}^3 \text{ s}^{-1}$ in addition to the $9000 \text{ m}^3 \text{ s}^{-1}$ added to the Nile runoff. Even combining $6000 \text{ m}^3 \text{ s}^{-1}$ from the Bosphorus, $3000 \text{ m}^3 \text{ s}^{-1}$ from the precipitation, $3000 \text{ m}^3 \text{ s}^{-1}$ from the Po, this would still leave a consequent amount of freshwater input unexplained. Except for the increase in Po runoff, we have not taken into account enhanced runoff from local rivers bordering the northern part of the Mediterranean, as could result from enhanced precipitation over the northern borderlands (e.g. Rohling and Hilgen, 1991; Schmiedl et al., 2010). This could provide a contribution to the expected freshwater budget, but can only partly explain the missing freshwater supply. A substantial freshwater source still remains unclarified.

Concerning the west-east surface salinity gradient, the changes simulated in our model are very small in the eastern basin compared to those suggested by the reconstructions. The strongest decrease of this gradient is found in

Nil-9000 with a value of 1.4 psu (vs. 1.7 psu in the baseline).

3.9.2.2 Comparison to previous model studies

In this section, we address the comparison of our work with previous model studies. Myers (2002) and Myers and Haines (2002) found that a small decrease of 8% in excess evaporation leads to a decrease of the strength of the thermohaline circulation, and that a 20% decrease leads to the stagnation of the deep water (pre-requisite for the sapropel formation) with an active vertical circulation restricted to the upper 500 m. In our study, a decrease by 8% (all experiments with $3000 \text{ m}^3 \text{ s}^{-1}$ of additional freshwater) leads to the limitation of the thermohaline circulation to the upper 800 m (Fig. 3.41). This corresponds to about the half of the depth of the deep eastern vertical circulation cell in the baseline. A decrease by 24% of the excess evaporation in our experiment Nil-9000 does also trigger a collapse of the deep circulation, with ventilation confined to the upper 720 m. Confirming what has been stated in the studies from Emeis et al. (2000); Myers (2002) and Myers and Haines (2002), we find that the LIW formation is very sensitive to freshwater input from the Nile. The simulated decrease in LIW formation, due to enhanced Nile runoff, partly affects the preconditioning of deep water formation, because less salt is laterally advected from the Levantine to the northern basins. This confirms the statement from Myers (2002).

Meijer and Tuentner (2007) found that an extra discharge from the north or an increased P-E field is equally or more effective in diminishing the deep water formation than an additional Nile runoff. However, their study presents the shortcoming not to have the same rate of changes, which makes their results dependent on both the location and the amount of the perturbation. Using the same magnitude of extra freshwater supply, we confirm that an additional discharge from the northern rivers (here, the Po) is far more effective than supplies from other origins. An increase in P-E is as effective as an increase in Nile runoff or the opening of the Bosphorus in enhancing the vertical stratification, thus in weakening the deep ventilation. Mangini and Schlosser (1986) suggested that a 0.2 psu decrease in the Adriatic would make the water formed in the Adriatic overflowing the deep Ionian water. Myers (2002) found that a 0.35 psu decrease in the Adriatic is required to

stop the deep convection. Our perturbation experiment with enhanced Po runoff triggers a salinity decrease of 1.5 psu in the Adriatic, and can strongly reduce both depth and strength of dense deep water convection in the basin. The strength of the overturning circulation in the Adriatic drops from 0.35 Sv (baseline) to less than 0.05 Sv in the experiment with increased Po runoff. In our other perturbations, the salinity decrease in the Adriatic is smaller than 0.2 psu, the strength and depth of the overturning circulation in the Adriatic are not affected. Even so, the water formed is lighter and thus overflows the dense deep Ionian water at the beginning of the experiments.

Emeis et al. (2000) proposed that water formation may have shifted westward ~ 2000 years before the onset of the sapropel S1, and then only collapsed, when a significant density decrease occurred in the Ionian and the Adriatic (maybe associated with warming). This transition state with a shift of the water formation to the Ionian could correspond to the circulation state depicted in most of our experiments, which are characterised by an intensification and expansion of the winter mixed layer pattern in the northern Ionian. This increase of convection in the Ionian appears as a compensation for the reduction of LIW formation (in Nile experiments), Adriatic deep water formation (in Po experiment), and intermediate water formation in the North Aegean (in Bosphorus experiments). We stated before that the amount of prescribed freshwater perturbation is much too small to induce the typical surface salinity decrease recorded by marine proxy data, and the associated restriction of the vertical circulation, with depth limits quoted at 300 m in the open eastern basin (Rohling and Gieskes, 1989) and 125 m in the Aegean Sea (Perissoratis and Piper, 1992). We believe that our experiments reflect the transition state suggested by Emeis et al. (2000): a substantial density decrease provokes a rearrangement of the water masses and the limitation of the vertical circulation to the upper ~ 800 m. However, the simulated decrease in surface density is not strong enough to reduce the ventilation to the very top of the water column (300 m in the open eastern basin), as suggested by the literature.

Consistently with the study of Meijer and Tuenter (2007), we find the response of the surface salinity to be non-uniform over the basin (even with a uniform distribution of the additional freshwater as in Prec-3000). As in

their study, our experiments simulate positive anomalies in the central Ionian. This is also consistent with the study of Emeis et al. (2000), who found minor/absent surface salinity anomalies in the Ionian at the time of sapropels S1. As proposed by Meijer and Tüenter (2007), we also mainly attribute the positive surface salinity anomalies of the Ionian to a shift southward of the Atlantic Jet (section 3.4.1.1).

3.10 Summary and conclusion

In this chapter, we address the question about the mechanisms, that could have lead to the sapropel S1 formation in the Eastern Mediterranean. We focus on the hypothesis that a surface density decrease strengthened the vertical stratification, thus preventing the ventilation of the deep water layers. We use a regional ocean model, forced by atmospheric data derived from global simulations for the 9 ka BP time slice and perform a baseline simulation. From this baseline, we carry out various freshwater perturbation experiments, with freshwater input from various origins and magnitudes. We consider extra freshwater supplies from enhanced Nile and Po runoff, from the opening of the Strait of the Bosphorus, from increased precipitation and from a gradual freshening of the Atlantic water. We discuss the plausibility of each perturbation to trigger the stagnation of the deep water and analyse the mechanisms behind.

We find that all the freshwater perturbations trigger a weakening of the overturning circulation of the Eastern Mediterranean. The counterclockwise eastern cell becomes much shallower and reflects a ventilation restricted in average to the upper 800 m of the water column, compared to 1600 m in the baseline. In general, the intermediate water formation in the Ionian increases to compensate the reduction of deep/intermediate water formation in other locations. Depending on the origin of the perturbation, the location affected by the reduction of deep/intermediate water formation differs.

The deep ventilation response is very sensitive to the origin of the perturbation. An additional source of freshwater from the Po triggers the strongest and longest-lasting stagnation, whereas the same amount of freshwater input from the Black Sea, the Nile or the precipitation exhibits a much weaker re-

sponse. Such a perturbation induces a rearrangement of the Eastern Mediterranean water masses, especially affecting the intermediate water which becomes warmer, because it is partly formed in another sub-basin with different hydrographic properties.

The general mechanisms behind the establishment of the stratification are the following. The freshwater perturbation provides a strong density decrease at the surface. The surface and intermediate water quickly adjust to the decrease in density, whereas the deeper layers still remain at the old density. This enhances the vertical gradient of density and provides a stronger vertical stratification. The new formed dense water is not dense enough to penetrate below the deep water in the Ionian and Levantine basins, whose hydrographic properties barely changed after the perturbation.

However, if the vertical stratification quickly establishes after a rapid change in boundary conditions, it starts eroding after three centuries of perturbation. The diffusion of the fresh anomalies to greater depths leads to the slow weakening of the stratification. When the deep layers have completely adjusted to the freshening, the deep vertical circulation recovers and reach the well-ventilated state, which is displayed in the baseline.

In summary, the adjustment of the changes occurring in the Eastern Mediterranean due to external freshwater perturbations are happening over two very different time scales. A short time scale, dependent on the flushing time of the basin: this time scale is valid for the adjustment of the upper layers, where the shallow intermediate circulation is active. A long time scale, which is dependent on the vertical mixing: this time scale acts to adjust the changes in the stagnant deep layers.

Another important finding was that a gradual permanent perturbation is required to maintain the stagnation over thousands of year, as proxies suggested for the sapropel S1. A sudden and fixed perturbation allows to kick off the quick development of the deep stagnation but a gradual decrease in surface density is necessary to maintain such a state.

Finally, none of the perturbation tested in our study has a magnitude sufficient to induce the strong surface salinity changes suggested by the paleo-reconstructions. Even when all the perturbation are combined, a consequent amount of extra freshwater input remains unexplained.

Our study show that the perturbation suggested in the literature can trigger a weakening of the vertical circulation and the stagnation of the deep water, but are not sufficient to explain the salinity decrease recorded by proxy data.

3.11 Outlook

In our study, the freshwater perturbations were all started from a baseline experiment representing a well-ventilated state, in order to test which freshwater inputs could have triggered a stagnation of deep waters. However, $\delta^{13}\text{C}$ and $\delta^{18}\text{O}$ values of epibenthic foraminifera in sediment cores from the Eastern Mediterranean suggest that a stagnating deep water circulation might have started already at around 14 ka BP (Schmiedl, personal communication). It can thus be postulated that during the Early Holocene, the Eastern Mediterranean basin was filled with deep water of high density remaining from the glacial conditions, when the water was colder and saltier, thus denser. In order to consider this assumption, another approach would be to start the freshwater perturbations from a baseline, where the deep water partly reflects glacial conditions and already stagnates. We can expect that the strong contrast between the very dense deep water remaining from the glacial period and the surface water affected by a strong density decrease from the freshwater perturbations might create an exceptional stratification, which is strong enough to sustain for several millennia.

The biogeochemistry of the Mediterranean is also an important aspect, which should be investigated. The coupling of the regional ocean model to an ocean biogeochemistry model is necessary to assess the time scale needed to reach oxygen depletion in the deep layers of the basin, after the establishment of the stagnation. The time delay between the shutdown of deep water ventilation and the establishment of anoxia is still debated in the literature (e.g. Rohling, 1994; Casford et al., 2003). The coupling of the physical and biogeochemical processes of the ocean would also allow to test the plausibility of the “biogeochemical hypothesis”, which states that higher export production could have trigger the formation of sapropel S1.

Chapter 4

Summary and Conclusion

The aim of the present study is to assess the sensitivity of the Eastern Mediterranean Sea to high- and low-latitude climate forcings at times of climate extremes in the Holocene. The focus lies on the Holocene Insolation Maximum (HIM, 9 ka BP), a time period with warm summers. The HIM coincides with the onset of formation of the sapropel S1, whose occurrence suggests abrupt changes in circulation. A regional ocean model set up for the Mediterranean is used to investigate this time period. We validate and analyse the hydrographic changes simulated by the model with paleo-reconstructions. Through freshwater perturbation experiments, we investigate the plausible mechanisms leading to the stagnation of the deep water in the Eastern Mediterranean, as it was postulated for the sapropel S1 period.

Main findings

To conclude this thesis, we summarize the main results of our study and attempt to answer the research questions raised in the introduction.

- **Is it possible to simulate states of the Mediterranean ocean climate adequately, using an atmospheric forcing derived from global simulations with a coarse resolution Earth system model?**

We have modelled the upper ocean climate of the Eastern Mediterranean for the present-day and the Early Holocene (9 ka BP) with a regional ocean gen-

eral circulation model forced by daily atmospheric data derived from global simulations with an Earth system model. The results from the present-day simulation match well with observations and climatologies. We conclude that the approach to force the regional ocean model with atmospheric input derived from ESM simulations leads to satisfactory results, allowing a relatively accurate representation of the main spatial features characteristic of the Mediterranean.

- **Can we simulate an Early Holocene ocean climate of the Eastern Mediterranean, which is consistent with the geological records?**

Yes. We carried out two experiments to simulate the Early Holocene ocean climate: 9K1 with changes in solar forcing only, and 9K2 with changes in solar forcing, atmospheric pCO₂ and topography (presence of major ice sheets). We use SSTs reconstructed from planktonic foraminifera assemblages to validate our simulations. As a novel approach, we propose a reinterpretation of the reconstruction, to consider the conditions throughout the upper water column rather than at a single depth. We claim that such a depth-integrated approach is more adequate for surface temperature comparison purposes in a situation where the upper ocean structure in the past was different from today. In this case, the depth-integrated interpretation of the proxy data strongly improves the agreement between modelled and reconstructed temperature signal with the subsurface summer warming being recorded by both model and proxies. From the model/proxy comparison, we infer that the simulation 9K2 represents an upper-ocean climate that is more realistic than the 9K1 simulation, which simulates in general a too warm climate, due to the fact that the forcing used for this simulation does neither include the cooling effect from the melting glaciers nor from the lower pCO₂. We believe that the dipole in summer temperature anomalies identified in the Levantine by both simulations and reconstructions is a general feature of time periods with enhanced summer insolation. Such a characteristic response is thus expected for other time periods like e.g. the Eemian.

- **What causes the pronounced spatial temperature patterns recorded by reconstructions for the HIM?**

Both modelled and reconstructed temperature integrated over the upper 30 m of the water column display a summer warming with well-defined spatial patterns, in particular a subsurface warming in the Cretan and western Levantine areas. The drivers of this pronounced warming are found to be a combination of (i) enhanced downwelling (due to stronger Ekman transport) and wind mixing, both caused by strengthened Etesian winds, and (ii) an enhanced vertical temperature gradient due to the stronger seasonal cycle in the northern hemisphere. Together, these processes induce a stronger heat transfer from the surface to the subsurface during late summer in the western Levantine and are responsible for the anomalous heat accumulation simulated in this region, a process never identified before, but potentially characteristic of time slices with enhanced insolation.

- **Which perturbations of fresh water fluxes are required in order to generate a stagnation of deep waters in the Eastern Mediterranean?**

We find that all the freshwater perturbations (enhanced Po and Nile runoff, increased precipitation, sudden opening of the Bosphorus, and freshening of the Atlantic water) trigger a weakening of the overturning circulation of the Eastern Mediterranean. The deep eastern cell becomes much shallower and reflects a ventilation restricted to the upper 800 m of the water column, compared to 1600 m in the baseline. We find that the deep ventilation response is very sensitive to the origin of the perturbation. An additional source of freshwater from the Po triggers the strongest and longest-lasting stagnation, whereas the same amount of freshwater input from the Black Sea, the Nile or the precipitation triggers a much weaker response.

- **What are the mechanisms governing the establishment of deep water stagnation?**

The freshwater perturbation provides a strong density decrease at the surface. The surface and intermediate waters quickly adjust to the decrease in density

within a short time scale that is related to the flushing time of the eastern basin (few decades). However, the deeper water first remains at the old density, because the changes in the deep layers happen within a much longer time scale (several centuries to millennia), which is set by the vertical mixing time scale, directly depending on the vertical mixing parameterization in the model. This enhances the vertical gradient of density and provides a stronger vertical stratification. The dense water newly formed at the surface through buoyancy loss is not dense enough to penetrate below the older deep water in the Ionian and Levantine basins, whose hydrographic properties have barely changed after the perturbation.

In general, the freshwater perturbations induce a reorganization of the water masses in the Eastern Mediterranean: the intermediate water formation in the Ionian increases to compensate the reduction of (i) the LIW formation (in Nile experiments), (ii) the Adriatic deep water formation (in Po experiment), and (iii) the intermediate water formation in the North Aegean (in Bosphorus experiments). These changes particularly affect the properties of the intermediate waters, which are partly formed in another sub-basin, with different hydrographic properties. The LIW formation is also sensitive to additional freshwater supply. LIW production weakens with increased freshwater supply from the south (e.g. the Nile) and strengthens when the extra freshwater supply comes from the north, this latter response being especially true for the Po perturbation.

- **Can we simulate a stagnation of Eastern Mediterranean deep water, which lasts for several millennia?**

Yes, but only with a perturbation that becomes gradually stronger. A sudden and fixed perturbation allows to kick off the quick development of the deep stagnation. However, the vertical mixing slowly erodes the strong vertical stratification, which was built after the rapid change in boundary conditions. A gradual surface freshening prevents the erosion of the strong vertical stratification. This permanent decrease in surface density can be provided by the continuously changing hydrographic properties of the Atlantic water, resulting from the deglaciation of the Laurentide ice sheet. Such a permanent decrease in surface density is required to maintain the stagnation over thousands of years, as suggested by the geological records for the sapropel S1.

List of Figures

2.1	Topography changes between 9K and CTRL. The superimposed dots represent 1 of each 10 grid box center of the model in each direction.	16
2.2	Sub-basins of the Mediterranean: Gulf of Lion (GL), Alboran Sea (ALB), Tyrrhenian Sea (TYR), Adriatic Sea (ADR), Ionian Sea (ION), Aegean Sea (AEG), Levantine Sea (LEV). The Atlantic box (ATL) and the Black Sea (BS) are shown as well. The main straits are marked with a red star.	20
2.3	Modelled March mixed layer depth (colours) and near-surface currents field (arrows) at 27 m depth for CTRL. Only a subset of vectors has been plotted. The mixed layer depth is reached when the density difference between this depth and the surface exceeds 0.125. Note that such a calculation can only give an approximative estimate of the depth of the mixed layer.	21
2.4	Annual, winter (JFM) and summer (JAS) SSTs at 6 m for CTRL (left), World Ocean Data 1998 climatology (middle) and MEDATLAS climatology (right).	23
2.5	Annual mean SSS deviations at 6 m, CTRL vs. World Ocean Data 1998 climatology (left) and CTRL vs. MEDATLAS climatology (right).	24
2.6	Anomalies of 2-m temperature for winter (JFM) and summer (JAS) from global simulations, 9K1 vs. CTRL (left) and 9K2 vs. CTRL (right).	27
2.7	Annual mean anomalies of P-E, P and E from global simulations, 9K1 vs. CTRL (left) and 9K2 vs. CTRL (right).	29

-
- 2.8 Annual mean SSS (CTRL, top) and SSS anomalies vs. CTRL (9K1, middle; 9K2, bottom) at 6 m depth (colours). March mixed layer depth is overlaid as fill patterns. 30
- 2.9 Anomalies in monthly seasonal cycle of upper ocean temperature averaged over the Eastern Mediterranean, 9K1 vs. CTRL (left) and 9K2 vs. CTRL (right); isolines represent the absolute values in °C for 9K1 (left) and 9K2 (right). 34
- 2.10 Anomalies of summer (JAS) temperature at different levels, 9K1 vs. CTRL (left column) and 9K2 vs. CTRL (right column). 35
- 2.11 Summer (JAS) temperature difference between 6 m and 27 m for CTRL and MEDATLAS climatology. 36
- 2.12 Monthly climatology of wind components averaged over the Aegean/West Levantine regions for CTRL (black), 9K1 (blue) and 9K2 (red). Left panel shows 10-m wind speed cubed, the cubed value is considered because it is proportional to mixing strength. Right panel shows both west-east and north-south wind stress components. The shading represents the time period, when modelled Etesian winds are active. 36
- 2.13 Mean summer (JAS) wind stress for CTRL. 37
- 2.14 Temperature change through vertical advection averaged between 12 and 42 m (colours) and vertical velocities (fill patterns, positive values for upward velocities) in July for CTRL. 38
- 2.15 Difference between the net atmospheric heat input and changes in ocean heat content from May 1st until September 30th. Left panel shows CTRL. Right panel shows differences between net atmospheric heat input from ERA-Interim Reanalysis (averaged over 1989/2005) and changes in ocean heat content from MEDATLAS climatology. Positive values indicate that the atmospheric input is higher than the temperature change in the water column, reflecting an export of heat from this region. Negative values reflect an heat accumulation. . . . 39
- 2.16 Annual mean net heat flux at the surface for CTRL. 39

- 2.17 Anomalies of temperature for different model layers for summer (JAS). The columns show the isolated effect of insolation forcing (9K2-W0 vs. CTRL), enhanced Etesian winds on CTRL climate (CTRL-W9 vs. CTRL) and on 9K2 climate (9K2 vs. 9K2-W0), as well as the total effect of both factors (9K2 vs. CTRL). 40
- 2.18 Comparison of modelled SST with SST reconstructed from proxy data (Kucera et al. (in prep.)) for 9K1 (left) and 9K2 (right). Annual mean, winter (JFM) and summer (JAS) are considered. 44
- 2.19 Annual, winter (JFM) and summer (JAS) SST, reconstructed from proxy data (dots, Kucera et al. (in prep.)) vs. modelled one (background colour) for 9K1 (left) and 9K2 (right). 1st row displays annual SST, 2nd row displays winter SST, 3rd row displays summer SST. 45
- 2.20 Annual, winter (JFM) and summer (JAS) SST anomalies, reconstructed from proxy data (dots, Kucera et al. (in prep.)) vs. modelled one (background colour) for 9K1 vs. 0K (left) and 9K2 vs. 0K (right). 1st row displays annual SST anomalies, 2nd row displays winter SST anomalies, 3rd row displays summer SST anomalies. 47
- 2.21 Comparison of modelled T_{0-30} with T_{0-30} reconstructed from proxy data (Kucera et al. (in prep.)) for 9K1 (left) and 9K2 (right). Annual mean, winter (JFM) and summer (JAS) are considered. 49
- 2.22 Annual and summer (JAS) T_{0-30} , calculated from SST reconstructions from proxy data (triangles, Kucera et al. (in prep.)) vs. modelled one (background colour) for 9K1 (left) and 9K2 (right). 1st row displays annual T_{0-30} , 2nd row displays summer T_{0-30} 50

2.23	Annual and summer (JAS) T_{0-30} anomalies, calculated from SST reconstructions from proxy data (triangles, Kucera et al. (in prep.)) vs. modelled one (background colour) for 9K1 vs. 0K (left) and 9K2 vs. 0K (right). 1 st row displays annual T_{0-30} anomalies, 2 nd row displays summer T_{0-30} anomalies. . .	51
3.1	Monthly climatology of the freshwater fluxes anomalies, Nile-9000 vs. CTRL in mm d^{-1}	62
3.2	Yearly mean surface salinity anomalies (Nile-9000 vs. 9K-base) of the first six years of the perturbation experiment. . .	63
3.3	Anomalies (Nile-9000 vs. 9K-base) of the surface salinity (colours) and the near-surface circulation field (arrows) at 27 m depth averaged over 1-99 years, 100-199 years and 1600-1699 years after the start of the perturbation. Only a subset of vectors has been plotted.	64
3.4	SST, SSS and surface potential density anomalies (Nile-9000 vs. 9K-base) averaged over the years 400-499. The near-surface circulation field at 27 m depth for Nile-9000 is overlaid as arrows on the SST anomalies. Only a subset of vectors has been plotted.	65
3.5	Zonally averaged transect over the Adriatic. Temperature, salinity and potential density anomalies (Nile-9000 vs. 9K-base) are represented, averaged over the years 400-499 of the experiment.	67
3.6	Meridionally averaged west-east transect of temperature, salinity and potential density anomalies (Nile-9000 vs. 9K-base), averaged over the years 400-499 of the experiment. The Aegean and the Adriatic are excluded. Note that the depth scale is non-linear.	68
3.7	Time series of salinity anomalies (Nile-9000 vs. 9K-base) in chosen layers of the water column for the first 100 years of the perturbation.	69
3.8	Time series of salinity anomalies (Nile-9000 vs. 9K-base) in chosen layers of the water column for the whole duration of the perturbation experiment.	70

3.9	Salinity anomalies profiles (Nil-9000 vs. 9K-base) at different locations of the eastern basin, averaged over the years 1600-1699 of the experiments.	71
3.10	Horizontal transect of salinity anomalies (Nil-9000 vs. 9K-base) averaged over the time period 1600-1699.	72
3.11	Time series of stratification index anomalies (Nil-9000 vs. 9K-base) in November for the Adriatic, the Aegean, the Ionian and the Levantine basins. The grey shading shows the position of each 2D bottom panel on the time series, where percentage of <i>IS</i> changes are represented.	75
3.12	Zonally averaged transect of annual mean salinity [psu] averaged over the years 1300-1399 for 9K-base and Nil-9000. Because we aim to identify the presence/absence of LIW, the Aegean and the Adriatic were excluded before performing the zonal average. Note that the depth scale is non-linear.	76
3.13	Surface salinity [psu] and March mixed layer depth [m] averaged over the years 1300-1399 of the experiment.	76
3.14	Time series of changes in convection (Nil-9000 vs. 9K-base) for the Adriatic, the Aegean and the Levantine Seas. The 10-year running mean is displayed.	77
3.15	Zonal overturning stream function integrated over the entire Mediterranean basin. It has been calculated on the basis of mean velocity field of years 400-499. The left panel represents the baseline experiment, the right panel represents the Nil-9000 experiment.	79
3.16	Meridional overturning stream function integrated over the Adriatic Sea and the northern part of the Ionian Sea. It has been calculated on the basis of mean velocity field of years 400-499. The left panel represents the baseline experiment, the right panel represents the Nil-9000 experiment.	80
3.17	Time series based on the 100-year averaged of the meridional overturning stream function integrated over the Adriatic Sea and the northern part of the Ionian Sea, at $38.5^{\circ}N$, for the Nil-9000 experiment.	80

3.18	Meridional overturning stream function integrated over the Aegean Sea. It has been calculated on the basis of mean velocity field of years 400-499. The left panel represents the baseline experiment, the right panel represents the Nil-9000 experiment.	82
3.19	Zonal overturning stream function integrated over the entire Mediterranean basin for the Nil-9000 experiment. It has been calculated on the basis of mean velocity field of years 1600-1699.	82
3.20	Time series of the age of water averaged over the Eastern Mediterranean for different depths. The top panel represents the 9K-base experiment, the bottom panel represents the Nil-9000 experiment.	83
3.21	Time series of the annual mean potential density at sill depth for the Strait of Otranto, the Strait of Antikithira, the Strait of Kassos, the Strait of Karpathos; and averaged over the Ionian basin at 1000 m and 2000 m of depth. The top panel represents the baseline experiment, the bottom panel represents the Nil-9000 experiment.	85
3.22	Time series of the age of water averaged over the Eastern Mediterranean for different depths. The top panel represents the Nil-9000 experiment, the bottom panel represents the Nil-9000-no-cold-winter experiment.	87
3.23	Time series of salinity anomalies for the layer 150-750 m for Nil-3000, Nil-6000 and Nil-9000; vs. 9K-base.	88
3.24	Time series of the age of water averaged over the Eastern Mediterranean for different depths. 9K-base, Nil-3000, Nil-6000 and Nil-9000 experiments are represented.	89
3.25	Index of stratification in November averaged over the years 400-499. Absolute values of IS are represented for 9K-base, anomalies of IS (vs. 9K-base) are represented for Nil-3000, Nil-6000 and Nil-9000.	90
3.26	SST, SSS and potential density anomalies (vs. 9K-base) averaged over the years 400-499 for Nil-3000, Bos-3000, Po-3000 and Prec-3000.	93

-
- 3.27 Index of stratification in November averaged over the years 400-499. Absolute values of IS are represented for 9K-base, anomalies of IS (vs. 9K-base) are represented for Nil-3000, Bos-3000, Po-3000 and Prec-3000. 94
- 3.28 Zonally averaged transect over the Adriatic of IS_v anomalies (vs. 9K-base) for the years 400-499. Nil-3000, Bos-3000, Po-3000 and Prec-3000 experiments are represented. 95
- 3.29 Zonally averaged transect over the Adriatic. Temperature, salinity and potential density anomalies (Po-3000 vs. 9K-base) are represented for the years 400-499. 96
- 3.30 Zonally averaged transect over the Aegean of IS_v anomalies (vs. 9K-base) for the years 400-499. Nil-3000, Bos-3000, Po-3000 and Prec-3000 experiments are represented. 97
- 3.31 Zonally averaged transect over the Aegean. Temperature, salinity and potential density anomalies (Bos-3000 vs. 9K-base) are represented for the years 400-499. 97
- 3.32 March mixed layer depth averaged over the years 400-499. Absolute values are represented for 9K-base, anomalies (vs. 9K-base) are represented for Nil-3000, Bos-3000, Po-3000 and Prec-3000. 99
- 3.33 Time series of changes in convection (vs. 9K-base) for the Adriatic, the Aegean, the Levantine and the Ionian Seas. The 10-year running mean is represented for Prec-3000, Bos-3000, Nil-3000, Po-3000, and Nil-9000. 100
- 3.34 Meridionally averaged transect of temperature, salinity and density anomalies (vs. 9K-base) for Bos-3000 and Po-3000. Only the Ionian and the Levantine Seas are considered. Note that the depth scale is non-linear. 102
- 3.35 Time series of the age of water averaged over the Eastern Mediterranean for different depths. 9K-base, Nil-3000, Bos-3000, Po-3000 and Prec-3000 are represented. 103
- 3.36 Time series of the age of water averaged over the Eastern Mediterranean for different depths. The experiments Atl-fresh and Nil-9000-Atl-fresh are represented. 105

-
- 3.37 Time series of stratification index anomalies (vs. 9K-base) in November for the Adriatic, the Aegean, the Ionian and the Levantine basins. The experiments Atl-fresh and Nil-9000-Atl-fresh are represented. 106
- 3.38 Relation between the mean density anomaly in the southern basin of the Adriatic between 150 and 500 m of depth, and the magnitude of freshwater input, for each experiment. 107
- 3.39 Relation between the mean temperature, salinity and density anomalies at the Strait of Sicily between 200 and 400 m of depth, and the magnitude of freshwater input, for each experiment. 108
- 3.40 Relation between the maximum apparent age of deep water averaged over the third century of the perturbation, and the magnitude of freshwater input, for each experiment. 110
- 3.41 Relation between the maximum depth of the overturning circulation in the eastern basin (considering the 0.1 Sv isoline) averaged over the fifth century of the perturbation, and the magnitude of freshwater input, for each experiment. 111

List of Tables

2.1	Fresh water budget for the Mediterranean and the Eastern Mediterranean for CTRL, 9K1 and 9K2.	26
2.2	Index of Stratification (IS , in $m^2.s^{-2}$).	32
2.3	Mean error and mean biases.	52
3.1	Description of the experiments.	59
3.2	Summary of the experiments performed showing the changes excess evaporation, in surface salinity and basin averaged salinity for the Eastern Mediterranean, averaged over the years 400-499.	114

Bibliography

- Aksu, A. E., Hiscott, R. N., Yasar, D., Isler, F. I., and Marsh, S.: Seismic stratigraphy of Late Quaternary deposits from the southwestern Black Sea shelf: evidence for non-catastrophic variations in sea-level during the last similar to 10,000 yr, *Marine Geology*, 190, 61–94, 2002.
- Andersson, A., Bakan, S., Fennig, K., Grassl, H., Klepp, C., and Schulz, J.: Hamburg Ocean Atmosphere Parameters and Fluxes from Satellite Data - HOAPS-3 - monthly mean., World Data Center for Climate, doi:10.1594/WDCC/HOAPS3_MONTHLY, 2007.
- Arakawa, A. and Lamb, V. R.: Computational design of the basic dynamical processes of the UCLA general circulation model, *Methods Comput. Phys.*, 17, 173–265, 1977.
- Astraldi, M., Gasparini, G. P., Sparnocchia, S., Moretti, M., and Sansone, E.: The characteristics of the water masses and the water transport in the Sicily Strait at long time scales, *Bulletin de l'Institut Oceanographique (Monaco)*, pp. 95–115, 1996.
- Baschek, B., Send, U., Lafuente, J. G., and Candela, J.: Transport estimates in the Strait of Gibraltar with a tidal inverse model, *Journal Of Geophysical Research-Oceans*, 106, 31 033–31 044, 2001.
- Bé, A. W. H., Jongebloed, W. L., and McIntyre, A.: X-ray microscopy of Recent planktonic Foraminifera., *J. Paleont.*, 43, 1384–1396, 1977.
- Berrisford, P., Dee, D., Fielding, K., Fuentes, M., Kallberg, P., Kobayashi, S., and Uppala, S.: The ERA-Interim Archive. ERA Report Series No. 1, Tech. rep., ECMWF: Reading, UK (available from www.ecmwf.int/publications), 2009.

- Béthoux, J. P.: Budgets Of The Mediterranean Sea - Their Dependence On The Local Climate And On The Characteristics Of The Atlantic Waters, *Oceanologica Acta*, 2, 157–163, 1979.
- Béthoux, J.-P. and Pierre, C.: Mediterranean functioning and sapropel formation: respective influences of climate and hydrological changes in the Atlantic and the Mediterranean, *Mar. Geol.*, 153, 29–39, 1999.
- Beuvier, J., Sevault, F., Herrmann, M., Kontoyiannis, H., Ludwig, W., Rixen, M., Stanev, E., Béranger, K., and Somot, S.: Modeling the Mediterranean Sea interannual variability during 1961-2000: Focus on the Eastern Mediterranean Transient, *Journal Of Geophysical Research-Oceans*, 115, C08 017, doi:10.1029/2009JC005950, 2010.
- Bigg, G. R.: An Ocean General-Circulation Model View Of The Glacial Mediterranean Thermohaline Circulation, *Paleoceanography*, 9, 705–722, 1994.
- Braconnot, P., Otto-Bliesner, B., Harrison, S., Joussaume, S., Peterchmitt, J. Y., Abe-Ouchi, A., Crucifix, M., Driesschaert, E., Fichefet, T., Hewitt, C. D., Kageyama, M., Kitoh, A., Laine, A., Loutre, M. F., Marti, O., Merkel, U., Ramstein, G., Valdes, P., Weber, S. L., Yu, Y., and Zhao, Y.: Results of PMIP2 coupled simulations of the Mid-Holocene and Last Glacial Maximum - Part 1: experiments and large-scale features RID B-2378-2009, *Climate Of The Past*, 3, 261–277, 2007.
- Brody, L. R. and Nestor, M. J. R.: Regional forecasts for the Mediterranean basin, Tech. Rep. 80-10, Naval Environmental Prediction Research Facility, Monterey, California, USA, 1985.
- Bryden, H. L. and Kinder, T. H.: Steady 2-Layer Exchange Through The Strait Of Gibraltar, *Deep-Sea Research Part A-Oceanographic Research Papers*, 38, S445–S463, 1991.
- Bryden, H. L., Candela, J., and Kinder, T. H.: Exchange Through The Strait Of Gibraltar, *Progress In Oceanography*, 33, 201–248, 1994.

- Casford, J. S. L., Rohling, E. J., Abu-Zied, R. H., Fontanier, C., Jorissen, F. J., Leng, M. J., Schmiedl, G., and Thomson, J.: A dynamic concept for eastern Mediterranean circulation and oxygenation during sapropel formation RID A-6984-2008 RID B-9736-2008, *Palaeogeography Palaeoclimatology Palaeoecology*, 190, 103–119, 2003.
- Cramp, A. and O’Sullivan, G.: Neogene sapropels in the Mediterranean: a review, *Marine Geology*, 153, 11–28, 1999.
- Cramp, A., Collins, M., and West, R.: Late Pleistocene Holocene Sedimentation In The Nw Aegean Sea - A Paleoclimatic Paleoceanographic Reconstruction, *Palaeogeography Palaeoclimatology Palaeoecology*, 68, 61–77, 1988.
- da Silva, A., Young, C., and Levitus, S.: Atlas of surface marine data, Vol. 1-5, NOAA Atlas NESDIS, U.S. Department of Commerce, NOAA, NESDIS, 1994.
- D’Ortenzio, F., Iudicone, D., de Boyer Montegut, C., Testor, P., Antoine, D., Marullo, S., Santoleri, R., and Madec, G.: Seasonal variability of the mixed layer depth in the Mediterranean Sea as derived from in situ profiles, *Geophys. Res. Lett.*, 32, L12 605, doi:10.1029/2005GL022463, 2005.
- Ducassou, E., Mulder, T., Migeon, S., Gonthier, E., Murat, A., Revel, M., Capotondi, L., Bernasconi, S. M., Mascle, J., and Zaragosi, S.: Nile floods recorded in deep Mediterranean sediments, *Quaternary Research*, 70, 382–391, 2008.
- Emeis, K. C., Struck, U., Schulz, H. M., Rosenberg, R., Bernasconi, S., Erlenkeuser, H., Sakamoto, T., and Martinez-Ruiz, F.: Temperature and salinity variations of Mediterranean Sea surface waters over the last 16,000 years from records of planktonic stable oxygen isotopes and alkenone unsaturation ratios, *Palaeogeography Palaeoclimatology Palaeoecology*, 158, 259–280, 2000.
- Emeis, K. C., Schulz, H., Struck, U., Rossignol-Strick, M., Erlenkeuser, H., Howell, M. W., Kroon, D., Mackensen, A., Ishizuka, S., Oba, T., Sakamoto, T., and Koizumi, I.: Eastern Mediterranean surface water temperatures

- and delta O-18 composition during deposition of sapropels in the late Quaternary, *Paleoceanography*, 18, 1005, 2003.
- Fairbanks, R. G.: A 17,000-Year Glacio-Eustatic Sea-Level Record - Influence Of Glacial Melting Rates On The Younger Dryas Event And Deep-Ocean Circulation, *Nature*, 342, 637–642, 1989.
- Freydier, R., Michard, A., De Lange, G., and Thomson, J.: Nd isotopic compositions of Eastern Mediterranean sediments: tracers of the Nile influence during sapropel S1 formation?, *Marine Geology*, 177, 45–62, 2001.
- Garzoli, S. and Maillard, C.: Winter Circulation In The Sicily And Sardinia Straits Region, *Deep-Sea Research Part A-Oceanographic Research Papers*, 26, 933–954, 1979.
- Giorgi, F.: Climate change hot-spots, *Geophysical Research Letters*, 33, L08 707, 2006.
- Hayes, A., Kucera, M., Kallel, N., Sbaifi, L., and Rohling, E. J.: Glacial Mediterranean sea surface temperatures based on planktonic foraminiferal assemblages, *Quaternary Science Reviews*, 24, 999–1016, 2005.
- Herrmann, M., Somot, S., Sevault, F., Estournel, C., and Deque, M.: Modeling the deep convection in the northwestern Mediterranean Sea using an eddy-permitting and an eddy-resolving model: Case study of winter 1986-1987, *Journal Of Geophysical Research-Oceans*, 113, C04 011, doi:10.1029/2006JC003991, 2008.
- Huber, B. T., McLoed, K. G., and Wing, S. L.: Warm climates in earth history, Cambridge University Press, 2000.
- Kallel, N., Paterne, M., Duplessy, J. C., VergnaudGrazzini, C., Pujol, C., Labeyrie, L., Arnold, M., Fontugne, M., and Pierre, C.: Enhanced rainfall in the Mediterranean region during the last sapropel event, *Oceanologica Acta*, 20, 697–712, 1997a.
- Kallel, N., Paterne, M., Labeyrie, L., Duplessy, J. C., and Arnold, M.: Temperature and salinity records of the Tyrrhenian Sea during the last

- 18,000 years, *Palaeogeography Palaeoclimatology Palaeoecology*, 135, 97–108, 1997b.
- Kalnay, E., Kanamitsu, M., Kistler, R., Collins, W., Deaven, D., Gandin, L., Iredell, M., Saha, S., White, G., Woollen, J., Zhu, Y., Chelliah, M., Ebisuzaki, W., Higgins, W., Janowiak, J., Mo, K. C., Ropelewski, C., Wang, J., Leetmaa, A., Reynolds, R., Jenne, R., and Joseph, D.: The NCEP/NCAR 40-year reanalysis project, *Bulletin Of The American Meteorological Society*, 77, 437–471, 1996.
- Kucera, M., Rohling, E. J., Hayes, A., Hopper, L. G. S., Kallel, N., Buongiorno Nardelli, B., Adloff, F., and Mikolajewicz, U.: Sea surface temperature of the Mediterranean Sea during the early Holocene insolation maximum, *Climate Of The Past*, in prep.
- Kullenberg, B.: On the salinity of water contained in marine sediments, *Goeteborgs K. Vetensk. Vitterhets Samh. Handl*, 6, 3–37, 1952.
- Lane-Serff, G. F., Rohling, E. J., Bryden, H. L., and Charnock, H.: Post-glacial connection of the Black Sea to the Mediterranean and its relation to the timing of sapropel formation, *Paleoceanography*, 12, 169–174, 1997.
- Lascaratos, A.: Estimation Of Deep And Intermediate Water Mass Formation Rates In The Mediterranean-Sea, *Deep-Sea Research Part Ii-Topical Studies In Oceanography*, 40, 1327–1332, 1993.
- Levitus, S.: *Climatological Atlas of the World Ocean*, NOAA/ERL GFDL, Professional Paper 13, Princeton, N.J., 173 pp. (NTISPB83-184093), 1982.
- Levitus, S., Boyer, T. P., Conkwright, M., Johnson, D., OBrian, T., Antonov, J., Stephens, C., and Gelfield, R.: Introduction. *World Ocean Database 1998*. Vol. 1, NOAA Atlas NESDIS 18, 346 pp., 1998.
- Ludwig, W., Dumont, E., Meybeck, M., and Heussner, S.: River discharges of water and nutrients to the Mediterranean and Black Sea: Major drivers for ecosystem changes during past and future decades?, *Progress In Oceanography*, 80, 199–217, 2009.

- Mangini, A. and Schlosser, P.: The Formation Of Eastern Mediterranean Sapropels, *Marine Geology*, 72, 115–124, 1986.
- Marsland, S. J., Haak, H., Jungclaus, J. H., Latif, M., and Roske, F.: The Max-Planck-Institute global ocean/sea ice model with orthogonal curvilinear coordinates, *Ocean Modelling*, 5, 91–127, 2003.
- Matthiesen, S. and Haines, K.: A hydraulic box model study of the Mediterranean response to postglacial sea-level rise, *Paleoceanography*, 18, 1084, 2003.
- MEDAR-Group: MEDATLAS 2002 Database, Cruise Inventory, observed and analyzed data of temperature and bio-chemical parameters, IFREMER Edition (4 CDROM), 2002.
- Meijer, P. T. and Dijkstra, H. A.: The response of Mediterranean thermohaline circulation to climate change: a minimal model, *Climate Of The Past*, 5, 713–720, 2009.
- Meijer, P. T. and Tüenter, E.: The effect of precession-induced changes in the Mediterranean freshwater budget on circulation at shallow and intermediate depth, *Journal Of Marine Systems*, 68, 349–365, 2007.
- Mercone, D., Thomson, J., Croudace, I. W., Siani, G., Paterne, M., and Troelstra, S.: Duration of S1, the most recent sapropel in the eastern Mediterranean Sea, as indicated by accelerator mass spectrometry radiocarbon and geochemical evidence, *Paleoceanography*, 15, 336–347, 2000.
- Meteorological-Office: *Weather in the Mediterranean. Vol. I. General Meteorology.*, H.M.S.O. London. Second edition, 1962.
- Mikolajewicz, U.: Modeling Mediterranean ocean climate of the Last Glacial Maximum, *Climate Of The Past*, 7, 161–180, doi:10.5194/cp-7-161-2011, 2011.
- Mikolajewicz, U., Groger, M., Maier-Reimer, E., Schurgers, G., Vizcaino, M., and Winguth, A. M. E.: Long-term effects of anthropogenic CO₂ emissions simulated with a complex earth system model, *Climate Dynamics*, 28, 599–631, 2007.

- Myers, P. G.: Flux-forced simulations of the paleocirculation of the Mediterranean, *Paleoceanography*, 17, 1009, doi:10.1029/2000PA000613, 2002.
- Myers, P. G. and Haines, K.: Stability of the Mediterranean's thermohaline circulation under modified surface evaporative fluxes, *Journal of Geophysical Research*, 107, 7–1–10, 2002.
- Myers, P. G. and Rohling, E. J.: Modeling a 200-yr interruption of the Holocene Sapropel S-1, *Quaternary Research*, 53, 98–104, 2002.
- Myers, P. G., Haines, K., and Rohling, E. J.: Modeling the paleocirculation of the Mediterranean: The last glacial maximum and the Holocene with emphasis on the formation of sapropel S-1, *Paleoceanography*, 13, 586–606, 1998.
- Olausson, E.: Studies in deep-sea cores, Rep. Swed. Deep-Sea Exped, 1947-1948, 8, 337–391, 1961.
- Pacanowski, R. C. and Philander, S. G. H.: Parameterization Of Vertical Mixing In Numerical-Models Of Tropical Oceans, *Journal Of Physical Oceanography*, 11, 1443–1451, 1981.
- Peltier, W. R.: Global glacial isostasy and the surface of the ice-age earth: The ice-5G (VM2) model and grace, *Annual Review Of Earth And Planetary Sciences*, 32, 111–149, 2004.
- Peneva, E., Stanev, E., Belokopytov, V., and Le Traon, P. Y.: Water transport in the Bosphorus Straits estimated from hydro-meteorological and altimeter data: seasonal to decadal variability, *Journal Of Marine Systems*, 31, 21–33, 2001.
- Perissoratis, C. and Piper, D. J. W.: Age, Regional Variation, And Shallowest Occurrence Of S1 Sapropel In The Northern Aegean Sea, *Geo-Marine Letters*, 12, 49–53, 1992.
- Pinardi, N. and Masetti, E.: Variability of the large scale general circulation of the Mediterranean Sea from observations and modelling: a review, *Palaeogeography Palaeoclimatology Palaeoecology*, 158, 153–174, 2000.

- Roeckner, E., Buml, G., Bonaventura, L., Brokopf, R., Esch, M., Giorgetta, M., Hagemann, S., Kirchner, I., Manzini, L. K. E., Rhodin, A., Schlese, U., Schulzweida, U., and Tompkins, A.: The atmospheric general circulation model ECHAM5, Tech. Rep. 349, Max Planck Institute for Meteorology, Hamburg, 2003.
- Rohling, E. J.: Review And New Aspects Concerning The Formation Of Eastern Mediterranean Sapropels, *Marine Geology*, 122, 1–28, 1994.
- Rohling, E. J.: Environmental control on Mediterranean salinity and delta O-18 RID B-9736-2008, *Paleoceanography*, 14, 706–715, 1999.
- Rohling, E. J.: Paleosalinity: confidence limits and future applications RID B-9736-2008, *Marine Geology*, 163, 1–11, 2000.
- Rohling, E. J. and De Rijk, S.: Holocene climate optimum and last glacial maximum in the Mediterranean: the marine oxygen isotope record (vol 153, pg 57, 1999) RID B-9736-2008, *Marine Geology*, 161, 385–387, 1999.
- Rohling, E. J. and Gieskes, W. W. C.: Late Quaternary changes in Mediterranean intermediate water density and formation rate., *Paleoceanography*, 4, 531–545, 1989.
- Rohling, E. J. and Hilgen, F. J.: The Eastern Mediterranean Climate At Times Of Sapropel Formation - A Review, *Geologie En Mijnbouw*, 70, 253–264, 1991.
- Rosignol-Strick, M.: African Monsoons, An Immediate Climate Response To Orbital Insolation, *Nature*, 304, 46–49, 1983.
- Rosignol-Strick, M.: Mediterranean Quaternary Sapropels, An Immediate Response Of The African Monsoon To Variation Of Insolation, *Palaeogeography Palaeoclimatology Palaeoecology*, 49, 237–263, 1985.
- Rosignol-Strick, M.: Rainy periods and bottom water stagnation initiating brine accumulation and metal concentrations. I. The Late Quaternary, *Paleoceanography*, 2, 333–60, 1987.

- Rossignol-Strick, M., Nesteroff, W., Olive, P., and Vergnaud-Grazzini, C.: After The Deluge - Mediterranean Stagnation And Sapropel Formation, *Nature*, 295, 105–110, 1982.
- Ryan, W. B. F., Pitman, W. C., Major, C. O., Shimkus, K., Moskalenko, V., Jones, G. A., Dimitrov, P., Gorur, N., Sakinc, M., and Yuce, H.: An abrupt drowning of the Black Sea shelf, *Marine Geology*, 138, 119–126, 1997.
- Schiebel, R. and Hemleben, C.: Modern planktic foraminifera, *Palaeontologische Zeitschrift*, 79, 135–148, 2005.
- Schmiedl, G., Kuhnt, T., Ehrmann, W., Emeis, K. C., Hamann, Y., Kotthoff, U., Dulski, P., and Pross, J.: Climatic forcing of eastern Mediterranean deep-water formation and benthic ecosystems during the past 22 000 years, *Quaternary Science Reviews*, 29, 3006–3020, 2010.
- Simmons, A. S., Uppala, D. D., and Kobayashi, S.: ERA-interim: new ECMWF reanalysis products from 1989 onwards, *ECMWF News*, 110, 2935, 2007.
- Somot, S.: Modélisation climatique du bassin méditerranéen: variabilité et scénarios de changement climatique, Ph.D. thesis, Universit de Toulouse III, 2005.
- Somot, S., Sevault, F., and Deque, M.: Transient climate change scenario simulation of the Mediterranean Sea for the twenty-first century using a high-resolution ocean circulation model, *Climate Dynamics*, 27, 851–879, 2006.
- Soulet, G., Menot, G., Lericolais, G., and Bard, E.: A revised calendar age for the last reconnection of the Black Sea to the global ocean, *Quaternary Science Reviews*, 30, 1019–1026, 2011.
- Sperling, M., Schmiedl, G., Hemleben, C., Emeis, K. C., Erlenkeuser, H., and Grootes, P. M.: Black Sea impact on the formation of eastern Mediterranean sapropel S1? Evidence from the Marmara Sea, *Palaeogeography Palaeoclimatology Palaeoecology*, 190, 9–21, 2003.

- Stanev, E. V. and Peneva, E. L.: Regional sea level response to global climatic change: Black Sea examples, *Global Planet. Changes*, 32, 3347, 2002.
- Thunell, R. C. and Williams, D. F.: Glacial-Holocene Salinity Changes In The Mediterranean-Sea - Hydrographic And Depositional Effects, *Nature*, 338, 493–496, 1989.
- Tsimplis, M. N. and Bryden, H. L.: Estimation of the transports through the Strait of Gibraltar, *Deep-Sea Research Part I-Oceanographic Research Papers*, 47, 2219–2242, 2000.
- Tuenter, E.: Modeling orbital induced variations in circum-Mediterranean climate, Ph.D. thesis, Universiteit Utrecht, Utrecht, 2004.
- von Storch, H. and Zwiers, F.: *Statistical analysis in climate research*, Cambridge University Press, Cambridge, 1999.
- Vörösmarty, C., Fekete, B., and Tucker, B.: Global River Discharge, 1807-1991, Version. 1.1 RivDIS Data set., Available on-line [<http://www.daac.ornl.gov>] from Oak Ridge National Laboratory Distributed Active Archive Center, Oak Ridge, Tennessee, U.S.A., 1998.

Acknowledgement

My first thanks goes to Uwe Mikolajewicz, my supervisor. Thank you very much Uwe for your patience, your support, your guidance, and thank you for sharing your science all along these three and half years. Thank you also for your reassuring trust, whenever I needed it. I really learned a lot while working under your supervision.

Then I would like to thank Ernst Maier-Reimer, my co-advisor and Gerhard Schmiedl, my panel chair, for their great advice and support all along this PhD. Thanks also to Kay Emeis for the fruitful discussions in our Interdynamik meetings.

I wish to thank Michal Kucera for providing the SST paleo-reconstruction of the HIM, and for the interesting discussions we shared through emails.

A special thanks to the IMPRS, particularly Antje and Conni, for their support and advice, as well as to my fellow PhD-students and Post-docs: Mario, Steffen, Nils, Korbinian, Florian R., Aiko, Malte, Werner, Peter, Chao, Laura, Eleftheria, Florian Z., Rosi, Jaison, Julia, Juliane, Chris, Kevin... and all the others... A very big thank you to Freja of course!!

I also want to thank people from the "Ocean Physics" group: Alberto, Alfredo, Matthias, Christian and Dimitry, all addicts to our OPIUMS sessions (Ocean Physics Interactive Unofficial Meeting Seminars).

Thanks also to Helmuth Haak for his help with the MPIOM code.

Big thanks to Freja, Alberto, Steffen and Laura for proofreading and revision comments!

A special thanks to Samuel Somot and his team from Météo-France/CNRM. I really enjoyed working with them, and I learned a lot during the three months I spent in their institute.

I also want to thank the DFG and the ESF-MedCLIVAR Research Program for their financial support, the German Climate Computation Centre (DKRZ) for the computing facilities, and the members of Central IT Services (CIS) for their technical support.

I do not forget the "Fast-Fast" running team, and the climbing crew! Thanks for getting me out of the office and out onto the pavement or on the wall.

A huge “Merci” goes to my family, for their immense support.

Last but not least, I thank Steffen for believing in me.

